

MICROCOPY RESOLUTION TEST CHART
NATIONAL BUREAU OF STANDARDS-1963-A

AD-A184 870

DTIC FILE COPY

2

NAVAL POSTGRADUATE SCHOOL

Monterey, California



DTIC
ELECTE
SEP 30 1987
S D D

THESIS

CERENKOV RADIATION FIELD ANALYSIS
DUE TO A PASSING ELECTRON BEAM

by

Byron K. Price

June 1987

Thesis Advisor

J. R. Neighbours

Approved for public release; distribution is unlimited.

ADA184870

SECURITY CLASSIFICATION OF THIS PAGE

REPORT DOCUMENTATION PAGE

1a REPORT SECURITY CLASSIFICATION UNCLASSIFIED		1b RESTRICTIVE MARKINGS	
2a SECURITY CLASSIFICATION AUTHORITY		3 DISTRIBUTION/AVAILABILITY OF REPORT Approved for public release; distribution is unlimited	
2b DECLASSIFICATION/DOWNGRADING SCHEDULE			
4 PERFORMING ORGANIZATION REPORT NUMBER(S)		5 MONITORING ORGANIZATION REPORT NUMBER(S)	
6a NAME OF PERFORMING ORGANIZATION Naval Postgraduate School	6b OFFICE SYMBOL (if applicable) 61	7a NAME OF MONITORING ORGANIZATION Naval Postgraduate School	
6c ADDRESS (City, State, and ZIP Code) Monterey, California 93943-5000		7b ADDRESS (City, State, and ZIP Code) Monterey, California 93943-5000	
8a NAME OF FUNDING/SPONSORING ORGANIZATION	8b OFFICE SYMBOL (if applicable)	9 PROCUREMENT INSTRUMENT IDENTIFICATION NUMBER	
8c ADDRESS (City, State, and ZIP Code)		10 SOURCE OF FUNDING NUMBERS	
		PROGRAM ELEMENT NO	PROJECT NO
		TASK NO	WORK UNIT ACCESSION NO
11 TITLE (Include Security Classification) CERENKOV RADIATION FIELD ANALYSIS DUE TO A PASSING ELECTRON BEAM			
12 PERSONAL AUTHOR(S) Price, Byron, Kevin			
13a TYPE OF REPORT Master's Thesis	13b TIME COVERED FROM _____ TO _____	14 DATE OF REPORT (Year, Month, Day) 1987 June	15 PAGE COUNT 115
16 SUPPLEMENTARY NOTATION			
17 COSATI CODES		18 SUBJECT TERMS (Continue on reverse if necessary and identify by block number) Cerenkov Radiation, S-Z Plane, Cerenkov Pulse Shapes	
FIELD	GROUP		
19 ABSTRACT (Continue on reverse if necessary and identify by block number) This paper is a continuation of a preliminary study which investigated the magnetic field radiated from a charge bunch traveling over a finite path. One of the recommendations of the preliminary study was to investigate how the magnitude and shape of the radiated field depends on the location of the observer relative to certain time boundaries defined by relationships between the arrival times of different parts of a pulse. This recommendation was followed by studying the signals radiated from charge bunches with two different ratios of rise time to path length. Within the Cerenkov cone and near a time boundary, the observed pulses are shaped like spikes. The time boundaries were found to be hyperbolas in the plane defined by the direction of travel of the charge bunch and the direction of propagation of radiation.			
20 DISTRIBUTION/AVAILABILITY OF ABSTRACT <input checked="" type="checkbox"/> UNCLASSIFIED/UNLIMITED <input type="checkbox"/> SAME AS RPT <input type="checkbox"/> DTIC USERS		21 ABSTRACT SECURITY CLASSIFICATION unclassified	
22a NAME OF RESPONSIBLE INDIVIDUAL John R. Neighbours		22b TELEPHONE (include Area Code) (408) 646-2922	22c OFFICE SYMBOL 61 Nb

Approved for public release; distribution is unlimited.

Cerenkov Radiation Field Analysis
Due to a Passing Electron Beam

by

Byron K. Price
Lieutenant, United States Navy
B.S., University of Kentucky, 1980

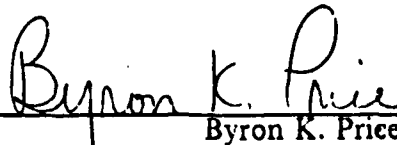
Submitted in partial fulfillment of the
requirements for the degree of

MASTER OF SCIENCE IN ENGINEERING SCIENCE

from the

NAVAL POSTGRADUATE SCHOOL
June 1987


Author:



Byron K. Price

Approved by:


J.R. Neighbors, Thesis Advisor


F.R. Buskirk, Second Reader


K. E. Woehler, Chairman,
Department of Physics


G. E. Schacher,
Dean of Science and Engineering

ABSTRACT

This paper is a continuation of a preliminary study which investigated the magnetic field radiated from a charge bunch traveling over a finite path. One of the recommendations of the preliminary study was to investigate how the magnitude and shape of the radiated field depends on the location of the observer relative to certain time boundaries defined by relationships between the arrival times of different parts of a pulse. This recommendation was followed by studying the signals radiated from charge bunches with two different ratios of rise time to path length. Within the Cerenkov cone and near a time boundary, the observed pulses are shaped like spikes. The time boundaries were found to be hyperbolas in the plane defined by the direction of travel of the charge bunch and the direction of propagation of radiation.



Accession For	
NTIS GRA&I	<input checked="" type="checkbox"/>
DTIC TAB	<input type="checkbox"/>
Unannounced	<input type="checkbox"/>
Justification	
By _____	
Dist. Statement / _____	
Additional Copies	
Dist	Statement
A-1	

TABLE OF CONTENTS

I.	INTRODUCTION	9
A.	BACKGROUND	9
B.	OBJECTIVES	9
II.	THEORY AND EQUATIONS	11
A.	RADIATION FIELDS	11
B.	FINITE BEAM PATHS	16
1.	Possible Observing Positions $P(z,s)$	16
2.	Limits of Integration	19
3.	Normalized Coordinates	23
III.	ANALYSIS OF THE S-Z PLANE	30
A.	S/L VERSES Z/L	30
B.	HYPERBOLAS IN THE S-Z PLANE	31
C.	CERENKOV PULSE SHAPES	33
IV.	CONCLUSIONS	93
A.	BACKGROUND	93
B.	OBSERVATIONS	93
1.	General Trends	93
2.	Specific Analysis	95
C.	SUMMARY	95
	APPENDIX A: CERENKOV PULSE PROGRAM	103
	APPENDIX B: S-Z PLANE PROGRAM	111
	LIST OF REFERENCES	113
	INITIAL DISTRIBUTION LIST	114

LIST OF TABLES

1. LIMITS OF INTEGRATION: PATH TO THE RIGHT 28
2. LIMITS OF INTEGRATION: PATH TO THE LEFT 29
3. LIMITS OF INTEGRATION: CENTERED 29

LIST OF FIGURES

2.1	$\rho(z,t) = \rho_0(z - vt)$: Charge Density	13
2.2	The Function $u(z')$ and $\rho'_0(u)$	14
2.3	Function $u(z')$ and Three Finite Paths	16
2.4	Path to the Right	17
2.5	Path to the Left	18
2.6	Path Centered About the Minimum	19
2.7	Path to the Right: $t_c > t_b$	20
2.8	$t_c > t_b$: $t_a < t < t_b$	21
2.9	$t_c > t_b$: $t_b < t < t_c$	22
2.10	$t_c > t_b$: $t_c < t < t_d$	23
2.11	Path to the Right: $t_c < t_b$	24
2.12	Path to the Right: $t_b = t_c$	25
2.13	Path to the Left: $t_a > t_d$	25
2.14	Path to the Left: $t_a < t_d$	25
2.15	Path to the Left: $t_a = t_d$	26
2.16	Centered About the Minimum	26
2.17	$t_1 < t < t_2$	27
2.18	$t_2 < t < t_3$	27
3.1	The S-Z Plane	36
3.2	The S-Z Plane	37
3.3	From Figure 3.1: Pulse 1	38
3.4	From Figure 3.1: Pulse 2	39
3.5	From Figure 3.1: Pulse 3	40
3.6	From Figure 3.1: Pulse 4	41
3.7	From Figure 3.1: Pulse 5	42
3.8	From Figure 3.1: Pulse 6	43
3.9	From Figure 3.1: Pulse 7	44
3.10	From Figure 3.1: Pulse 8	45

3.11	From Figure 3.1: Pulse 9	46
3.12	From Figure 3.1: Pulse 10	47
3.13	From Figure 3.1: Pulse 11	48
3.14	From Figure 3.2: Pulse 12	49
3.15	From Figure 3.2: Pulse 13	50
3.16	From Figure 3.2: Pulse 14	51
3.17	From Figure 3.2: Pulse 15	52
3.18	From Figure 3.2: Pulse 16	53
3.19	From Figure 3.2: Pulse 17	54
3.20	From Figure 3.2: Pulse 18	55
3.21	The S-Z Plane	56
3.22	The S-Z Plane	57
3.23	From Figure 3.21: Pulse 19	58
3.24	From Figure 3.21: Pulse 20	59
3.25	From Figure 3.21: Pulse 21	60
3.26	From Figure 3.21: Pulse 22	61
3.27	From Figure 3.21: Pulse 23	62
3.28	From Figure 3.21: Pulse 24	63
3.29	From Figure 3.21: Pulse 25	64
3.30	From Figure 3.21: Pulse 26	65
3.31	From Figure 3.21: Pulse 27	66
3.32	From Figure 3.21: Pulse 28	67
3.33	From Figure 3.21: Pulse 29	68
3.34	From Figure 3.21: Pulse 30	69
3.35	From Figure 3.22: Pulse 31	70
3.36	From Figure 3.22: Pulse 32	71
3.37	From Figure 3.22: Pulse 33	72
3.38	From Figure 3.22: Pulse 34	73
3.39	From Figure 3.22: Pulse 35	74
3.40	From Figure 3.22: Pulse 36	75
3.41	From Figure 3.22: Pulse 37	76
3.42	Equal Distance Points-Close Field	77
3.43	Equal Distance Points-Far Field	78

3.44	From Figure 3.42: Pulse 38	79
3.45	From Figure 3.42: Pulse 39	80
3.46	From Figure 3.42: Pulse 40	81
3.47	From Figure 3.42: Pulse 41	82
3.48	From Figure 3.42: Pulse 42	83
3.49	From Figure 3.43: Pulse 43	84
3.50	From Figure 3.43: Pulse 44	85
3.51	From Figure 3.43: Pulse 45	86
3.52	From Figure 3.43: Pulse 46	87
3.53	From Figure 3.43: Pulse 47	88
3.54	From Figure 3.43: Pulse 48	89
3.55	From Figure 3.43: Pulse 49	90
3.56	From Figure 3.43: Pulse 50	91
3.57	From Figure 3.43: Pulse 51	92
4.1	Pulse Shapes of Figure 3.1	97
4.2	Pulse Shapes of Figure 3.2	98
4.3	Pulse Shapes of Figure 3.21	99
4.4	Pulse Shapes of Figure 3.22	100
4.5	Peak Magnitude vs. Angle (φ)	101
4.6	Pulse Width vs. Angle (φ)	102

I. INTRODUCTION

A. BACKGROUND

The topic of time development for Cerenkov radiation was introduced by Buskirk and Neighbours in [Ref. 1] where the concept was applied to an electron beam with a ramp-front function. Later in [Ref. 2], which was a preliminary study, magnetic fields were calculated and plotted with respect to time for various locations relative to the beam. The values of β' and the index of refraction n , were chosen in order to study the relationship between the time regions relative to the beam and the shape of the radiated magnetic field curves. The value β' is equal to v/c , where c is the velocity of light in the medium. From this preliminary study, one of the recommendations was to investigate how the magnitude and shape of the radiated field depends on the location of the observer relative to certain time boundaries defined by relationships between the arrival times of different parts of a pulse.

The B field calculations in [Ref. 2: pp. 70-79] are theoretical and have assumed a linear ramp-front charge profile, a one dimensional current distribution, and a rigid charge shape. In other words, the radiation is produced by a bunch of electrons of negligible transverse dimension with a longitudinal distribution which does not change as the bunch travels along the z axis. The radiated power is proportional to the square of the charge per unit length and therefore to the square of the beam current. The expressions for B and E in [Ref. 1: p. 3751] are valid and the evaluation is therefore coherent only insofar as the bunch is not distorted either by the reaction of the radiation or by the instabilities associated with very high current beams, [Ref. 1: p. 3753]. So far none of the calculations have been compared to experimental results due to the shortage of suitable data.

Present technology is such that this structure is not observable in the Cerenkov radiation from S or L band linacs because of their relatively high fundamental frequency. However, other accelerators with their longer electron bunch structure and higher currents, should produce observable Cerenkov signals in air for energies greater than about 25 MeV. [Ref. 1: p. 3753]

B. OBJECTIVES

The main objective of this work is to investigate the magnitudes, shapes, and pulse widths of the radiated fields as a function of position in the radiation plane. More specifically, this thesis follows the recommendation to investigate the influence of the time boundaries in this plane. These time boundaries are known to depend on the arrival times of signals from different parts of the charge distribution.

The secondary objectives of this thesis are a result of the main objective. In order to calculate the B field as a function of time, the FORTRAN program of [Ref. 2: pp. 70-79] needs to be written in a structured format and transferred to the NPS main frame computer. Appendix A contains this program called "CERENKV" which is written using the WF77 version of FORTRAN. This program evaluates the integral which yields the magnitude of the Cerenkov pulse at a given time after an electron beam is discharged into a medium from an accelerator. The last objective provides yet another tool needed for studying the characteristics of the radiated magnetic field. This is a FORTRAN program that will generate the data for the time boundaries which plot the S/L versus the Z/L (S-Z plane) graph. In the next chapter, S is defined as the radius vector and Z is the horizontal distance measured from the beam discharge point along the beam path length L . The program is found in Appendix B and is available on the NPS main frame under the filename "TIME".

II. THEORY AND EQUATIONS

A. RADIATION FIELDS

The potentials from a moving charge distribution were determined in [Ref. 1: p. 3750]. The fields (in cgs units) from these potentials are given by Equations 2.1 and 2.2.

$$\mathbf{B} = \nabla \times \mathbf{A} \quad (2.1)$$

$$\mathbf{E} = -\nabla\Phi - (1/c_0)(\partial\mathbf{A}/\partial t) \quad (2.2)$$

The magnetic field \mathbf{B} , may be calculated from Equation 2.1 and since \mathbf{A} has only a z component, this approach is easier than finding \mathbf{E} . A similar derivation can be made in order to find the magnitude of the \mathbf{E} field. It is also true that, in the Cerenkov case, $E/B = c_0$, which, for plane waves, is the usual relation between the electric and magnetic fields. [Ref. 1: p. 3752].

In [Ref. 1: p. 3750], it was assumed that a charge density function ρ_v and a current density $\mathbf{j} = \rho_v \mathbf{v}$ moved with velocity v in the plus z direction. The charge and current are assumed to be concentrated along the z axis such that

$$\rho_0(\mathbf{r},t) = \rho(z,t)\delta(x)\delta(y). \quad (2.3)$$

The charge is assumed to move with no change in shape so that the z and t dependence of the charge is $\rho(z,t) = \rho_0(z-vt)$. The usual charge and current densities are represented by ρ_v and \mathbf{j}_v , while ρ and ρ_0 are charge per unit length. The velocity of light is c and c_0 in the medium and free space respectively.

The potentials are found by taking the usual retarded solutions to the wave equations; which become under the assumption of a line distribution of charge (Equation 2.3),

$$\mathbf{A}(\mathbf{r},t) = (v/c_0) \int (1/R)\rho(\mathbf{r}',t')dz'. \quad (2.4)$$

where $R = r - r'$ and t' , the retarded time, is given as $t' = t - |r - r'|/c$. Introducing a new variable, $u(z') = z' - vt'$ into Equation 2.4 gives

$$A(r,t) = (v/c_0) \int (1/R) \rho_0(u) dz'. \quad (2.5)$$

Since the charge is confined to the z' axis, the new variable $u(z')$ can be written more explicitly as

$$u(z') = z' - vt + (v/c)[x^2 + y^2 + (z - z')^2]^{1/2}. \quad (2.6)$$

The potential A , has only a z component, and the \mathbf{B} field has only x and y components, $B_x = \partial A_z / \partial y$ and $B_y = -\partial A_z / \partial x$. Carrying out the differentiation for the x component gives

$$B_x = v/c_0 \int (\partial R^{-1} / \partial y) \rho_0(u) dz' + v/c_0 \int R^{-1} (\partial \rho_0(u) / \partial y) dz'. \quad (2.7)$$

For radiation, the first integral, falling off as R^{-2} at large distances, will be neglected and only the second term is considered further. From Equation 2.6, it is seen that u is a function of x and y so that the second integral can be written

$$B_x = v^2/cc_0 \int (y/R^2) \rho'_0(u) dz', \quad (2.8)$$

where $\rho'_0(u)$ is the derivative of ρ_0 with respect to its argument u . The corresponding expression for B_y has y replaced by $-x$. These two components combined give the total magnetic radiation field \mathbf{B} . In the cylindrical coordinates (s, θ, z) , where s is the radius vector, $s = (x^2 + y^2)^{1/2}$, \mathbf{B} is tangential (i.e., in the θ direction) with a magnitude given by

$$B = (v^2/cc_0) \int (s/R^2) \rho'_m(u) dz'. \quad (2.9)$$

Writing Equation 2.9 with the finite limits z'_i and z'_f with $v^2/cc_0 = n\beta^2$ and assuming $\rho'(u) = \rho_m = \text{constant}$, the new expression for B is written as

$$B = n\beta^2 \rho'_m \int (s/R^2) dz'. \quad (2.10)$$

Here, $s = (x^2 + y^2)^{1/2}$ and $R^2 = s^2 + (z - z')^2$ or $R^2 = s^2 + w^2$, where $w = (z - z')$.

Prior to evaluating Equation 2.10, it is necessary to consider the dependence of u on z' as well as ρ'_0 on u . As previously stated, the charge density function, $\rho(z,t)$ moves with velocity v in the plus z direction without changing shape. This charge density motion makes up the beam current profile. The upper drawing in Figure 2.1 illustrates the charge density, $\rho(z,t)$. The rise in the charge density is approximated to be linear until it reaches a maximum constant value and then declines linearly to zero. The time it takes for the charge to reach this plateau is referred to as the rise time. Multiplying the rise time by v yields the value $\Delta u = (u_1 - u_2)$ which is used later in this paper. The lower drawing is the derivative of the charge density function which is the constant, ρ'_m in Equation 2.10.

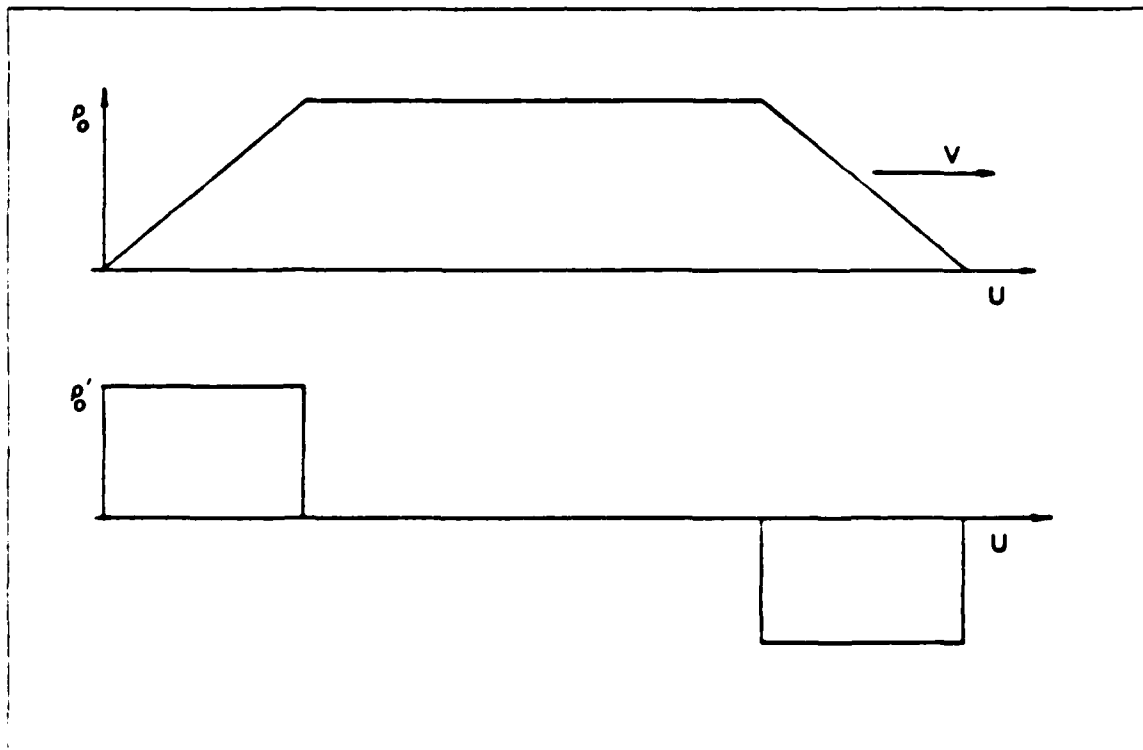


Figure 2.1. $\rho(z,t) = \rho(u - vt)$ Charge Density

Since $u(z')$ and $\rho'_0(u)$ are coupled together by a common axis u , they were closely compared side by side in [Ref. 1: p. 3751]. Figure 2.2 illustrates this comparison and aids as a supplement for the discussion which follows. The first two terms in Equation 2.6 are a straight line with unit slope and an intercept which changes with time, while

the third term is a hyperbola opening in the $+u$ direction with asymptotic slopes of $\pm v/c$. The sum of these two curves is $u(z')$. The limiting slopes are $1 \pm v/c$. Here, $1 + v/c$ is approximately 2, while $1 - v/c$ is close to zero. In the Cerenkov case, $1 - v/c < 0$ and all the curves for $u(z')$ for any time t , have a minimum. With $v > c$, the resultant $u(z')$ is a curve whose ends both point upward as shown. As time increases, the entire curve will translate downward to smaller u values as a result of the negative term $(-vt)$ in Equation 2.6. For the purposes of this paper, the u_1 value will be the zero starting point and the u_2 value will be a negative value when entering data in the program of Appendix A.

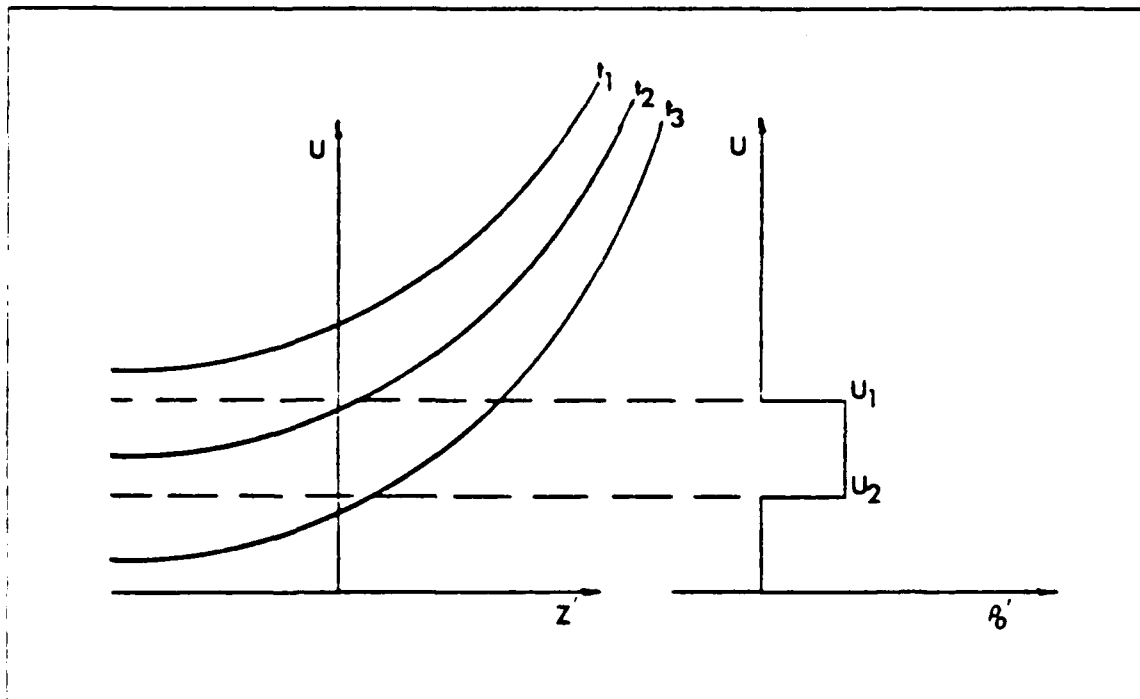


Figure 2.2 The Function $u(z')$ and $\rho'_o(u)$.

Only changing currents (those with a nonzero ρ'_o) will contribute to the magnetic radiation field from Equation 2.10. Again, since the end of the current pulse increases linearly upward, the derivative $\rho'_o(u)$ will be a constant valued squared pulse of magnitude ρ'_m and is also shown in Figure 2.2. The corresponding negative $\rho'_o(u)$ pulse occurring at the tail of a current pulse is not shown and its effect is considered separately. At a time t , where the $u(z')$ curve is tangent to the upper portion of the $\rho'_o(u)$ pulse, the B pulse begins. The value of the integral in Equation 2.10 increases as

$u(z')$ continues its constant downward motion with increasing time until it becomes tangent with the lower part of the $\rho_o(u)$ pulse. At this time the nonzero part of the integral has the largest extent. At later times, the integral will break up into two regions of the z' axis and if $\rho'_o(u)$ is constant, the value of the integral decreases with increasing time because the extent of the integral in the two regions continues to decrease as a result of the upward turn of $u(z')$. The preceding discussion applies to z' ranging from $-\infty$ to $+\infty$ with u_1 and u_2 serving as the upper and lower bounds in the integration process, [Ref. 1: p. 3751].

The time structure (shape) of the resulting B pulse can be determined by integrating Equation 2.10 directly, [Ref. 1: p. 3751]. This is where the limits of integration must be defined explicitly. The limits in the preceding paragraph are found with relative ease if the bounds of u_1 and u_2 extend indefinitely along the z' axis and are the only bounds to consider. However, this is not the case considered in this paper. Along with the bounds considered above, there is a definite set of boundaries that exist as a result of using a finite beam path length. Figure 2.3 shows the three examples of where the finite path may fall in the $u-z$ plane. These three cases will be discussed in more detail in the next subsection and the limits of integration will be found for each of the three cases. Before proceeding however, it is a good time to evaluate the integral in Equation 2.10.

Evaluating the integral in Equation 2.10 is easy as long as ρ'_o is flat (or constant). This assumption was made earlier in Figure 2.1. Using the expression $w = (z - z')$ in Equation 2.10 and integrating with respect to w , the final expression for B is found in Equation 2.11.

$$B = n\beta^2\rho'_m [\arctan(w_1/s) - \arctan(w_2/s)] \quad (2.11)$$

With the expression for B now available, the next step is to find the limits of integration by finding the values of w_1 and w_2 . These limits were carefully derived in [Ref. 2: pp. 15-31]. However, the following sections will display the key figures and equations in order to better familiarize future thesis students with the terms and physical concepts of Cerenkov radiation.

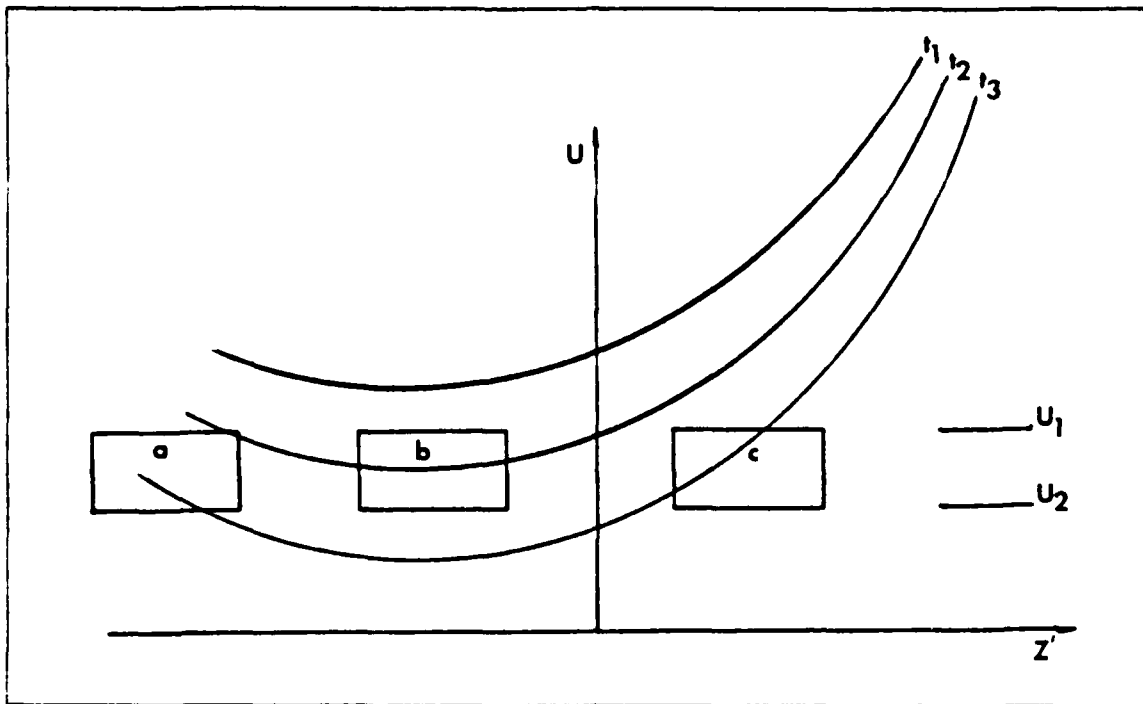


Figure 2.3 Function $u(z')$ and Three Finite Paths.

B. FINITE BEAM PATHS

1. Possible Observing Positions $P(z,s)$

When the path of the beam is infinite, the limits of integration are determined by the intersection of the $u(z')$ curve with the bounding values u_1 and u_2 . In the case of a path of finite length, the integration limits are determined by these intersections, and in addition, the intersection of the $u(z')$ curve with the limits of the path length.

Again, Figure 2.3 shows the three possible finite length beam paths, each with a different orientation with respect to the minimum in $u(z')$. Path "a" is to the left of the minimum, path "b" contains the minimum, and path "c" is to the right of the minimum. These three situations are labeled "path to the left", "path centered", and "path to the right" respectively. Furthermore, these three situations also correspond to three positions of interest relative to the Cerenkov angle θ_c , where $\theta_c = \arccos(1/\beta')$. This relation for θ_c is called the "Cerenkov relation". It is found by using Huygens construction found in [Ref. 2: p. 7], along with basic trigonometry. The actual relation given was $\cos \theta = 1/\beta n$, where n is the index of refraction and β is the dimensionless

constant v/c . The latter is a function of the energy level and is found by using the expression for the Lorentz contraction factor. Finally, the product $n\beta$ is defined as β' .

The three positions of interest are relative to the Cerenkov angle and subsequently the beam path. The path to the right means the observer is outside the Cerenkov cone. The path to the left means the observer is within the Cerenkov cone, and centered means the observer is on the cone. These three possible situations are shown in Figures 2.4 to 2.6, which were extracted from [Ref. 2: pp. 16,17]. With beam length L , and the position of the observer $P(z,s)$, Figures 2.4, 2.5, and 2.6 illustrate the path to the right, to the left, and centered respectively.

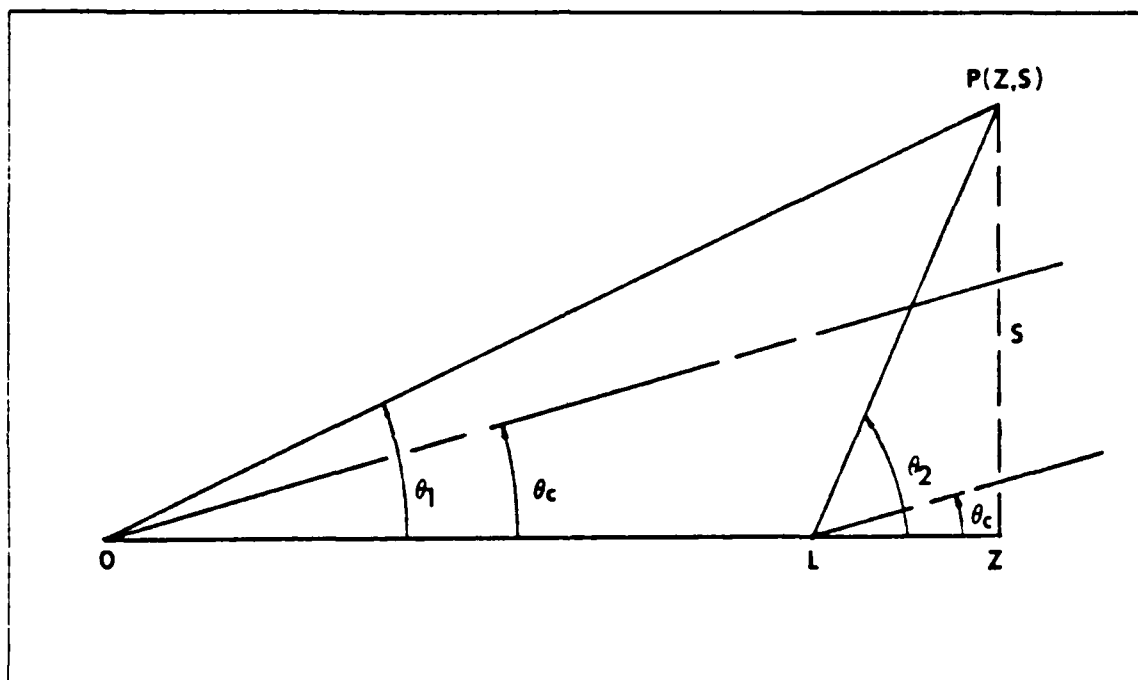


Figure 2.4 Path to the Right.

For the path to the right, θ_1 must be greater than θ_c ; for the path to the left, θ_2 must be less than θ_c ; for the path centered about the minimum, θ_1 must be less than θ_c and θ_2 must be greater than or equal to θ_c .

The integration limits are determined by the intersections of the $u(z)$ curve with the boundaries of the rectangle formed by the beam path and the length of the pulse rise. Changes in the limits occur when the $u(z)$ curve meets the corners, or when it becomes tangent to the upper and lower bounds. The latter happens in only the "centered" case. Labeling the corners of the rectangle as a, b, c, and d, the boundary

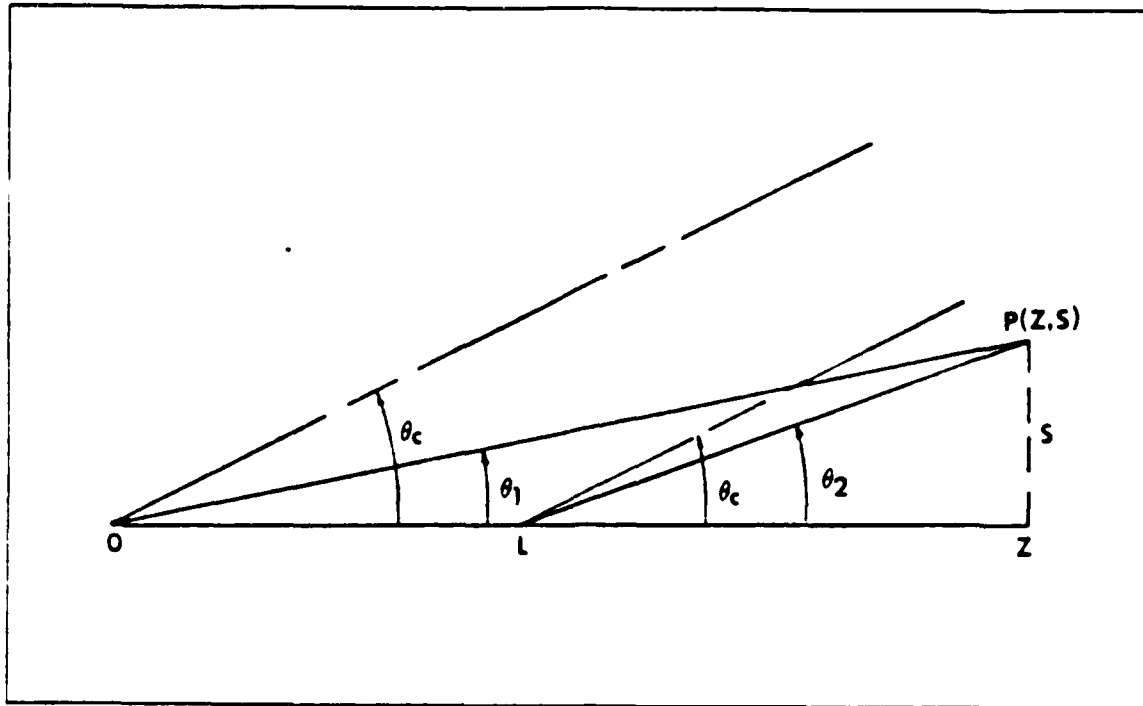


Figure 2.5 Path to the Left.

times are found by substituting the appropriate boundary coordinates into Equation 2.6. Different situations arise depending upon whether diagonally opposite or adjacent corners are simultaneously intersected by the $u(z')$ curve.

Figure 2.7 shows successive intersections of the descending $u(z')$ curve for the path to the right of the minimum. In this case, t_a is always the earliest time and t_d is the latest time. The order of the two times depends on the relative size of the beam path length and the length of the pulse rise. Figure 2.7 is drawn for $t_c > t_b$.

The boundary times t_a , t_b , t_c , and t_d are given in Equations 2.12 to 2.15 and are found in [Ref. 2: p. 15].

$$t_a = [\beta'(s^2 + z^2)^{1/2} - u_1] / v \quad (2.12)$$

$$t_b = [\beta'(s^2 + z^2)^{1/2} - u_2] / v \quad (2.13)$$

$$t_c = [L + \beta'(s^2 + (z - L)^2)^{1/2} - u_2] / v \quad (2.14)$$

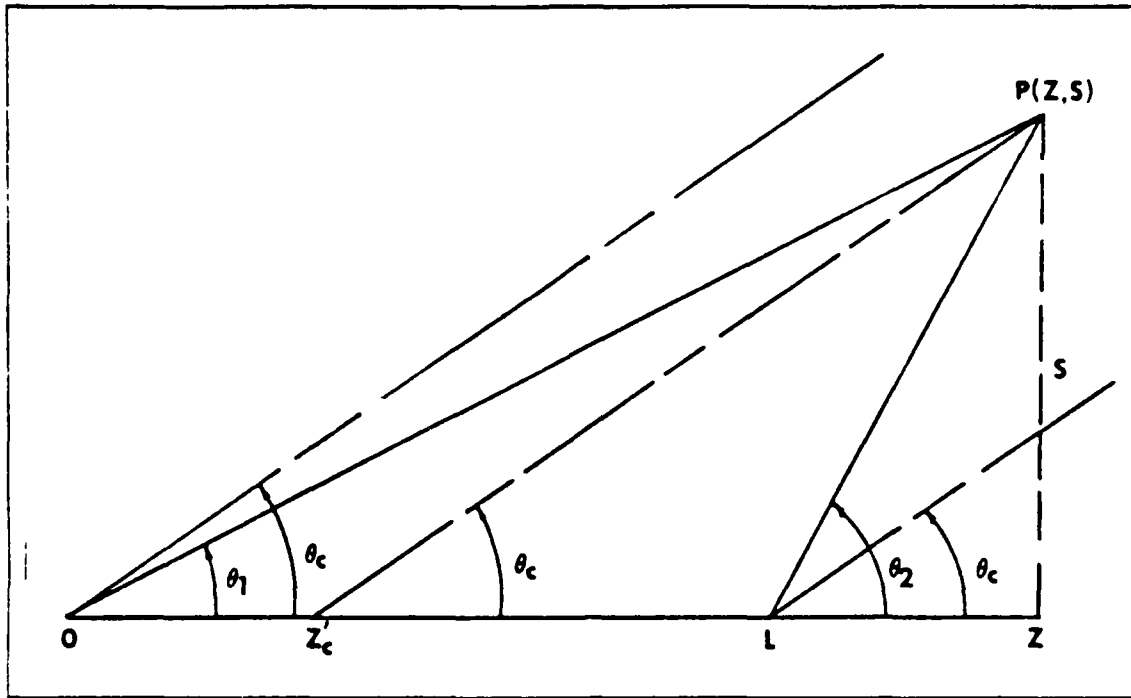


Figure 2.6 Path Centered About the Minimum.

$$t_d = [L + \beta'(s^2 + (z - L)^2)^{1/2} - u_2] / v \quad (2.15)$$

2. Limits of Integration

Using the critical times from the previous subsection, the limits of integration for Equation 2.11 can now be found. Since this thesis uses the results of [Ref. 2: pp. 15-31], the derivations are omitted. However, for the sake of clarity, Figures 2.8 thru 2.10 from [Ref. 2: pp. 19-21], are shown as a review to the way the magnetic fields are calculated in Appendix A.

As previously stated, Figure 2.7 illustrates the relationship between the function $u(z')$ and the finite path which falls to the right of the minimum. More specifically, Figures 2.8, 2.9, and 2.10 shows how the limits of integration are derived as some arbitrary time, t passes through the critical times t_a , t_b , t_c , and t_d . In [Ref. 2: pp. 19-20], the expressions for z'_i and z'_f were derived with the new variables $A_1 = u_1 + vt$ and $A_2 = u_2 + vt$. Equations 2.16 and 2.17 are the expressions for z'_i and z'_f respectively.

$$z'_i = \{(\beta'^2 z - A_2) + \beta'[(z - A_2)^2 - s^2(\beta'^2 - 1)]^{1/2}\} / (\beta'^2 - 1) \quad (2.16)$$

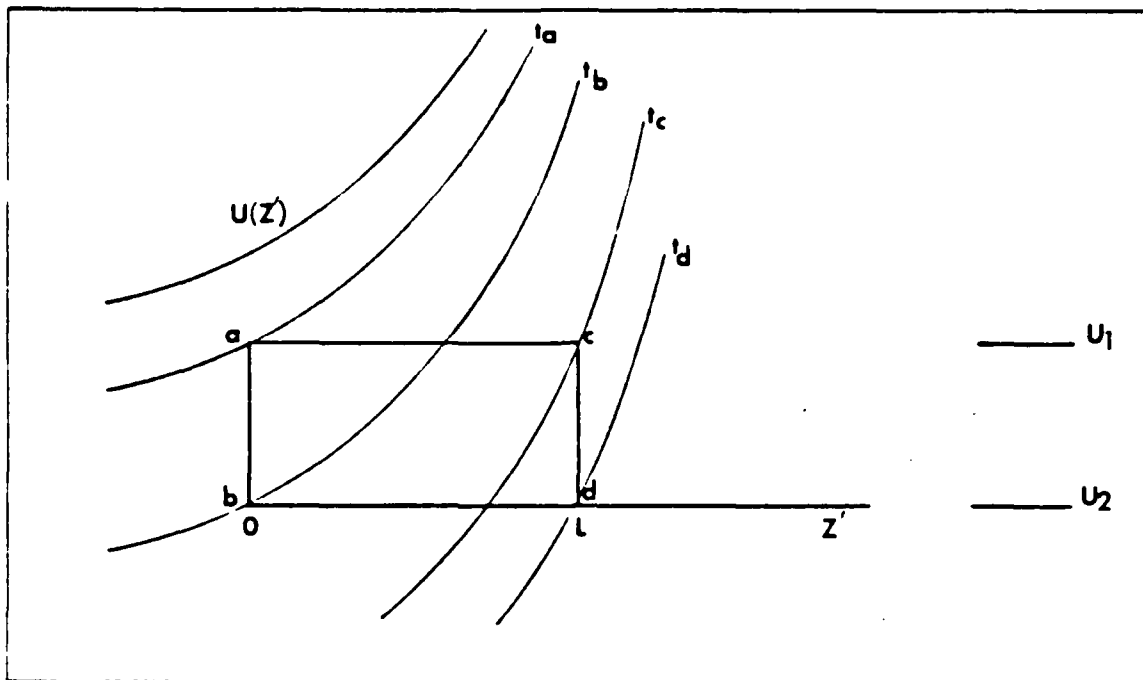


Figure 2.7 Path to the Right: $t_c > t_b$.

$$z'_r = \{(\beta'^2 z - A_1) + \beta'[(z - A_1)^2 - s^2(\beta'^2 - 1)]^{1/2}\} (\beta'^2 - 1) \quad (2.17)$$

In addition to $t_c > t_b$, there are two other cases to consider, namely $t_b > t_c$ and $t_b = t_c$. Figures 2.11 and 2.12 illustrate these cases.

The path to left case is similar to the path to the right case, but now the three cases are $t_a > t_d$, $t_a < t_d$, and $t_a = t_d$. These cases are shown in Figures 2.13, 2.14, and 2.15. Solving for the limits of integration is similar to the path to the right, but now the negative part is used due to the position relative to the minimum of $u(z')$. [Ref. 2: p. 25]. Equations 2.18 and 2.19 give the "path to the left" version of Equations 2.16 and 2.17.

$$z'_l = \{(\beta'^2 z - A_1) - \beta'[(z - A_1)^2 - s^2(\beta'^2 - 1)]^{1/2}\} (\beta'^2 - 1) \quad (2.18)$$

$$z'_l = \{(\beta'^2 z - A_2) - \beta'[(z - A_2)^2 - s^2(\beta'^2 - 1)]^{1/2}\} (\beta'^2 - 1) \quad (2.19)$$

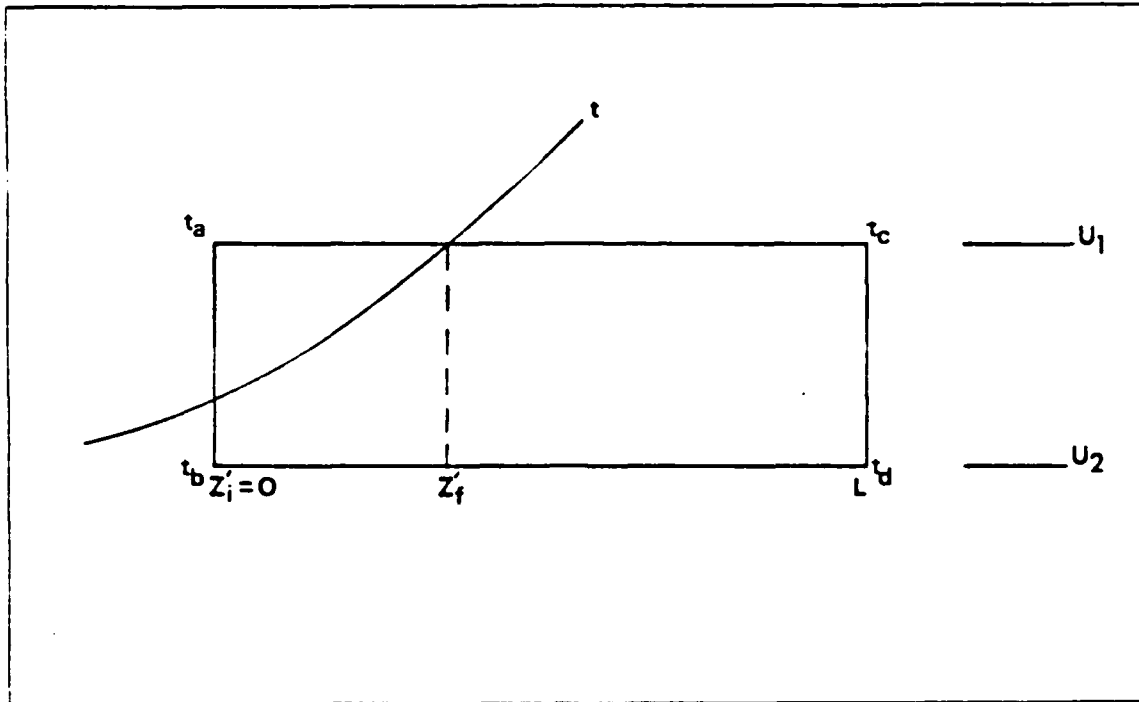


Figure 2.8 $t_c > t_b : t_a < t < t_b$.

When centered about the minimum, Figure 2.16 introduces the new variables t_1 , t_2 , z'_c , and t_3 . Equations 2.20, 2.21, and 2.22 are the expressions for these variables and are found in [Ref. 2: pp. 28,74]. In Equation 2.22, f equals $\tan(\theta_c)$ and the variable t_3 is the larger of t_b or t_d .

$$t_1 = \{z'_c + \beta[s^2 + (z - z'_c)^2]^{1/2} - u_1\} / v \quad (2.20)$$

$$t_2 = \{z'_c + \beta[s^2 + (z - z'_c)^2]^{1/2} - u_2\} / v \quad (2.21)$$

$$z'_c = z - (s^2 / f) \quad (2.22)$$

In the centered case, the critical times to integrate between are t_1 , t_2 , and t_3 . The arbitrary time t , is integrated between t_1 and t_2 and then t_2 and t_3 . Figures 2.17 and 2.18 illustrate this integration process. The new limits from Figure 2.17 are given in Equations 2.23 and 2.24.

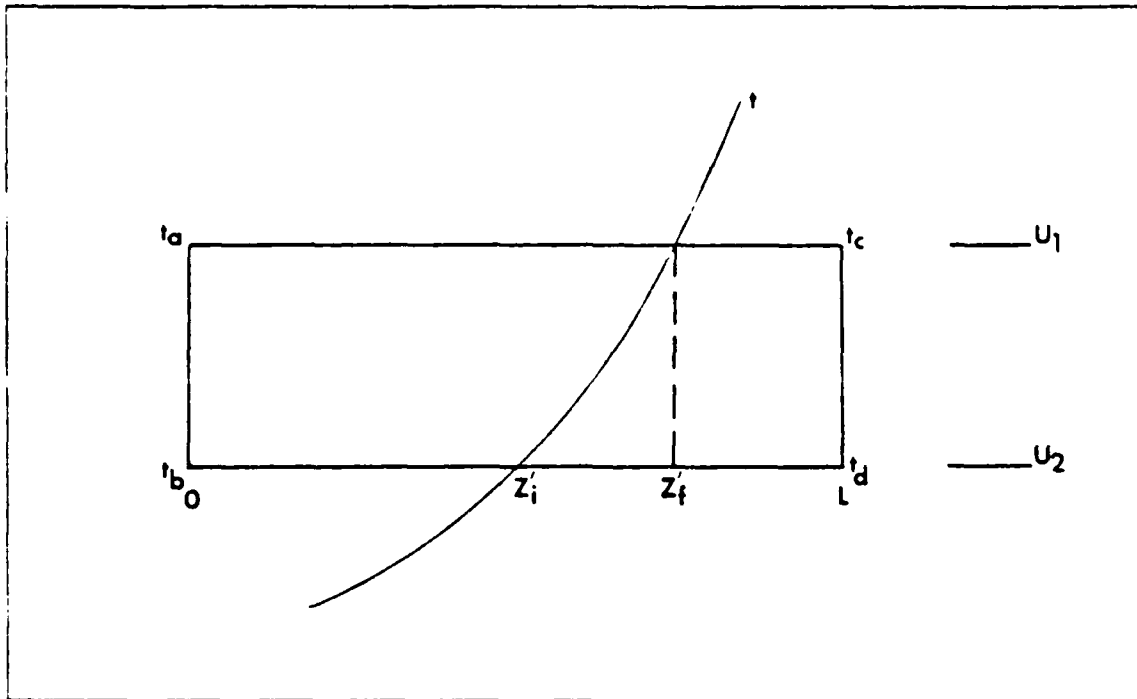


Figure 2.9 $t_c > t_b : t_b < t < t_c$.

$$z'_+ = \{(\beta'^2 z - A_1) + \beta'[(z - A_1)^2 - s^2(\beta'^2 - 1)]^{1/2}\} / (\beta'^2 - 1) \quad (2.23)$$

$$z'_- = \{(\beta'^2 z - A_1) - \beta'[(z - A_1)^2 - s^2(\beta'^2 - 1)]^{1/2}\} / (\beta'^2 - 1) \quad (2.24)$$

From Figure 2.18, the new variables that must be considered here are $z'_-(u_1)$, $z'_+(u_1)$, $z'_-(u_2)$, and $z'_+(u_2)$. As stated in [Ref. 2: p. 31], $z'_-(u_1)$ is found using Equation 2.24 for the first integral and z'_f will always be $z'_-(u_2)$, where $z'_-(u_2)$ is given by Equation 2.25.

$$z'_-(u_2) = \{(\beta'^2 z - A_2) - \beta'[(z - A_2)^2 - s^2(\beta'^2 - 1)]^{1/2}\} / (\beta'^2 - 1) \quad (2.25)$$

When $z'_-(u_1)$ is greater than zero, z'_f will equal $z'_-(u_1)$, otherwise z'_f will equal zero.

Similarly, the limits for the second integral, $z'_+(u_1)$ and $z'_+(u_2)$ will be the same as the above equations in which the second term is positive. In this case, z'_f will always be equal to $z'_+(u_2)$, whereas z'_f will equal $z'_+(u_1)$ if the latter is less than L, otherwise z'_f will equal L.

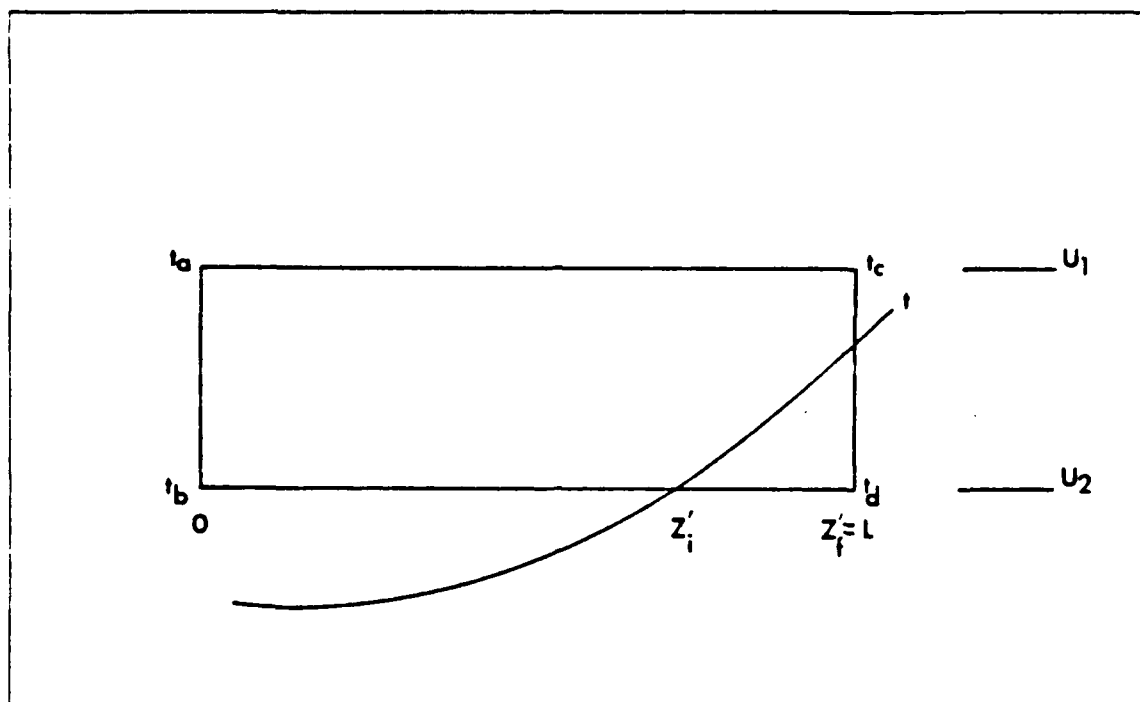


Figure 2.10 $t_c > t_b : t_c < t < t_d$.

3. Normalized Coordinates

As a prelude to the summary of results, it was decided that working in normalized time would make the graphs produced by Appendix A easier to study. A good base time for normalization is the time it takes for an electron bunch to travel the distance L . To this end, dividing the boundary times (Equations 2.12 to 2.15) by $\tau = L/v$ gives the new normalized boundary times. As a reminder, L is the beam length and v is the particle velocity which is equal to βc_0 . The tables at the end of the chapter give the times in normalized times and are indicated by T_i (where $i = \{a,b,c,d,1,2,3\}$).

For ease of reference, the above limits are summarized for use in Appendix A. Tables 1, 2, and 3 from [Ref. 2: pp. 24,25,31], give the expressions for z' (in $w = z - z'$) for the paths to the right, left, and centered respectively. The expressions for a and b found in Table 1, are given in Equations 2.16 and 2.17. In Table 2, the expressions for aa and bb are given in Equations 2.18 and 2.19.

The magnetic fields can now be calculated for any location $P(z,s)$. The next chapter uses Appendix A to generate magnetic field (Cerenkov pulse) graphs for a couple of illustrative examples. Each case will use a 50 MeV energy level, but will vary

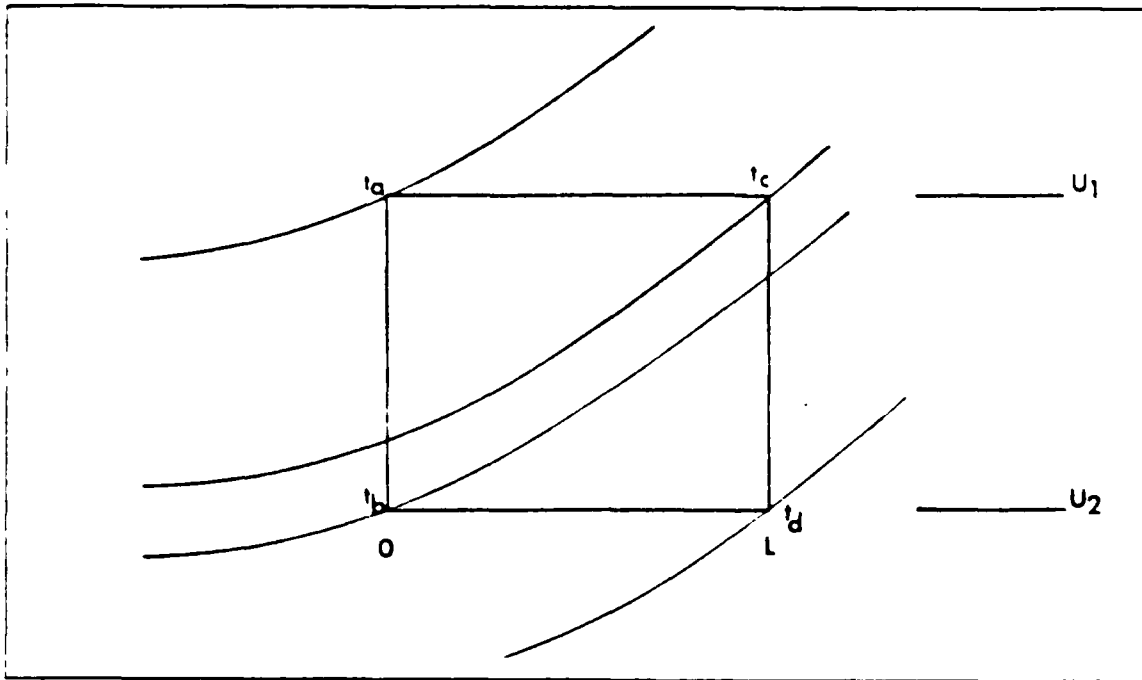


Figure 2.11 Path to the Right: $t_c < t_b$.

the $\Delta u L$ values in order to study any differences. Also, the development of the S-Z plane is easier to explain since establishing the origin of the boundary times in Equations 2.12 through 2.15.

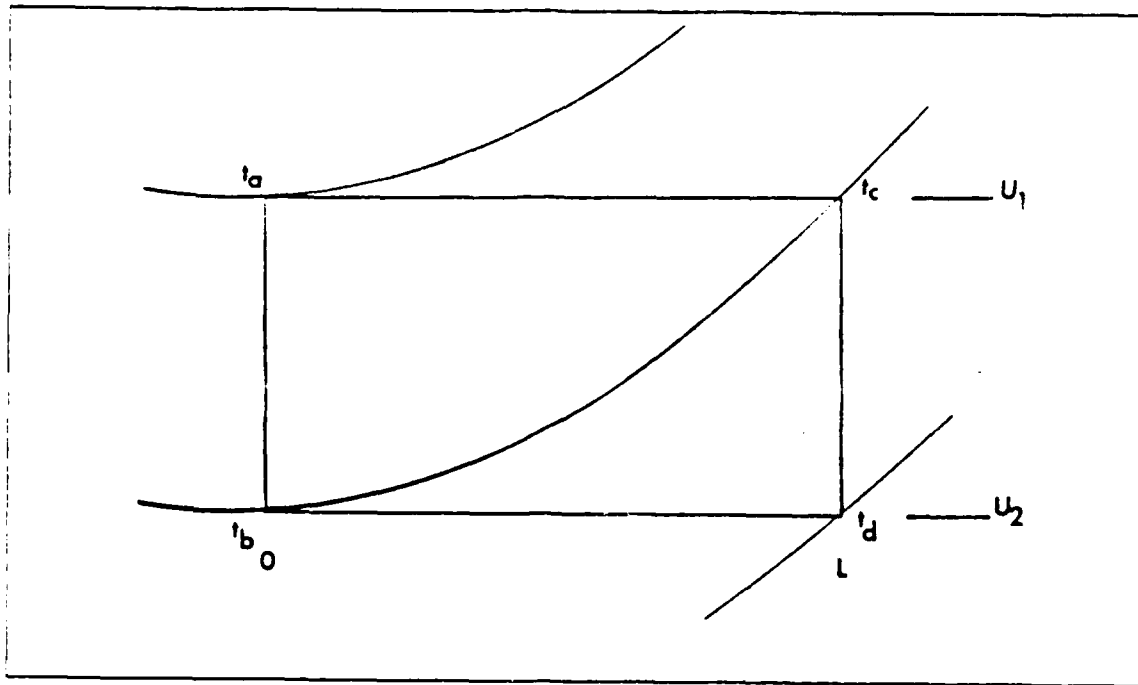


Figure 2.12 Path to the Right: $t_b = t_c$.

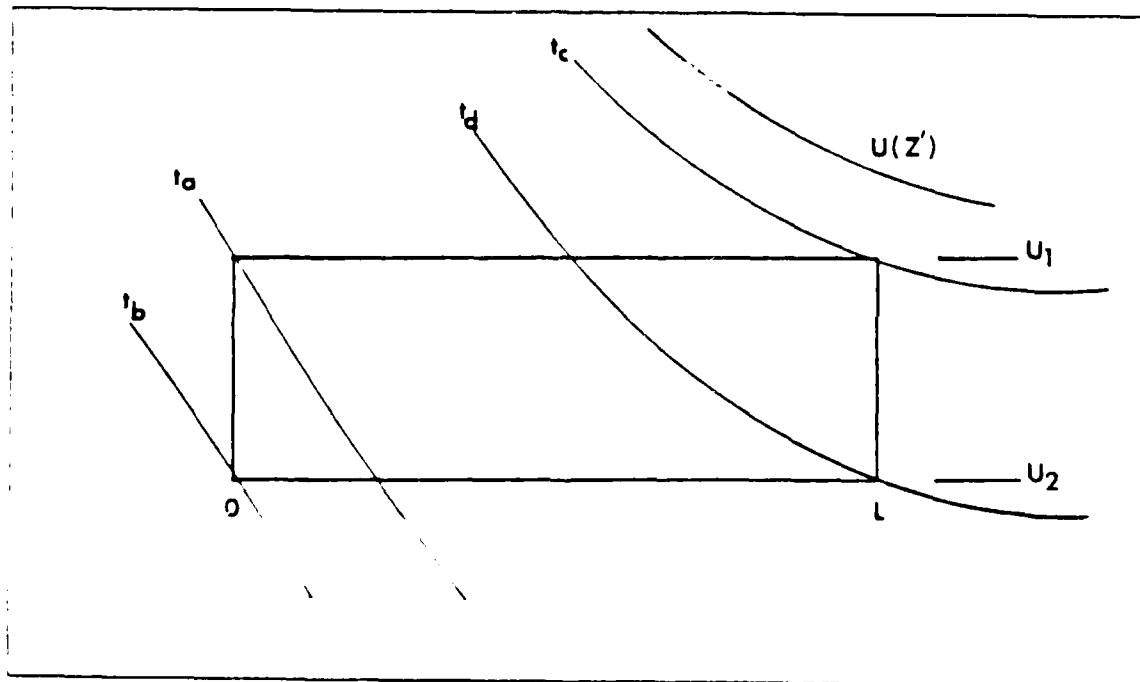


Figure 2.13 Path to the Left: $t_a > t_d$.

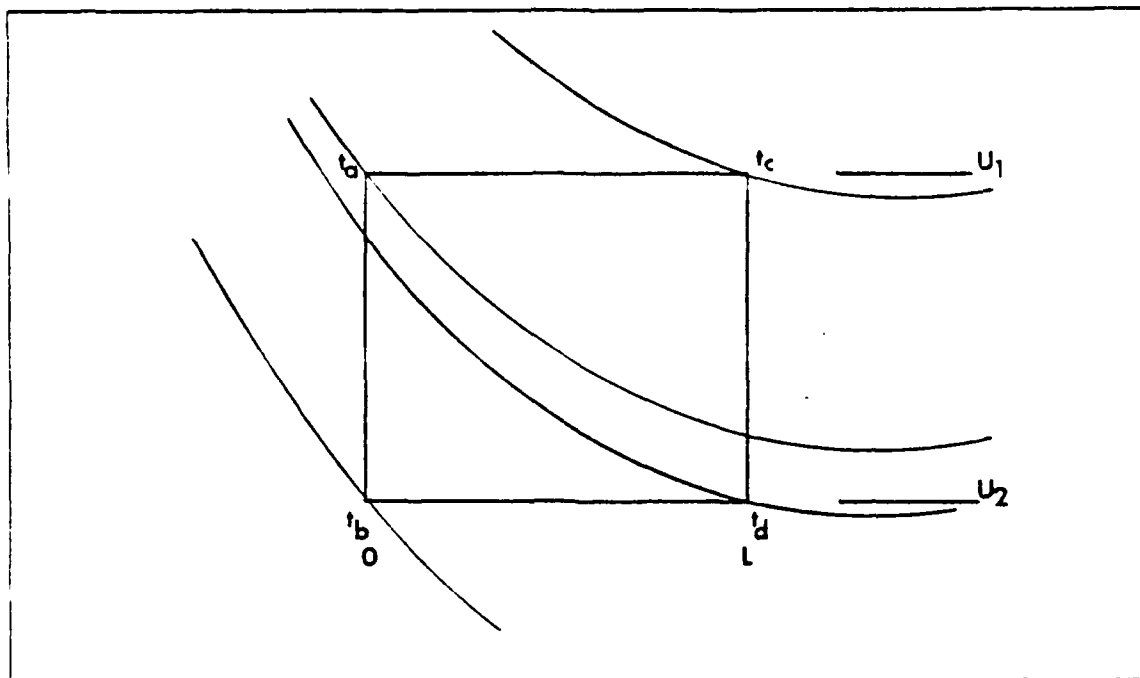


Figure 2.14 Path to the Left: $t_a < t_d$.

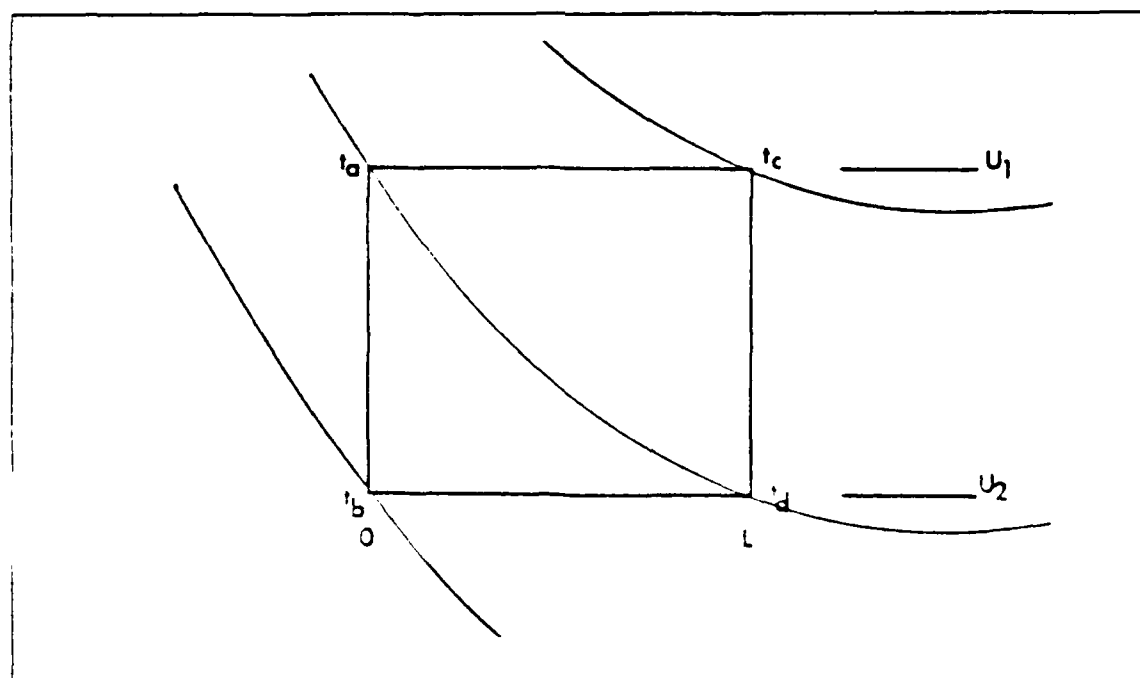


Figure 2.15 Path to the Left: $t_a = t_d$.

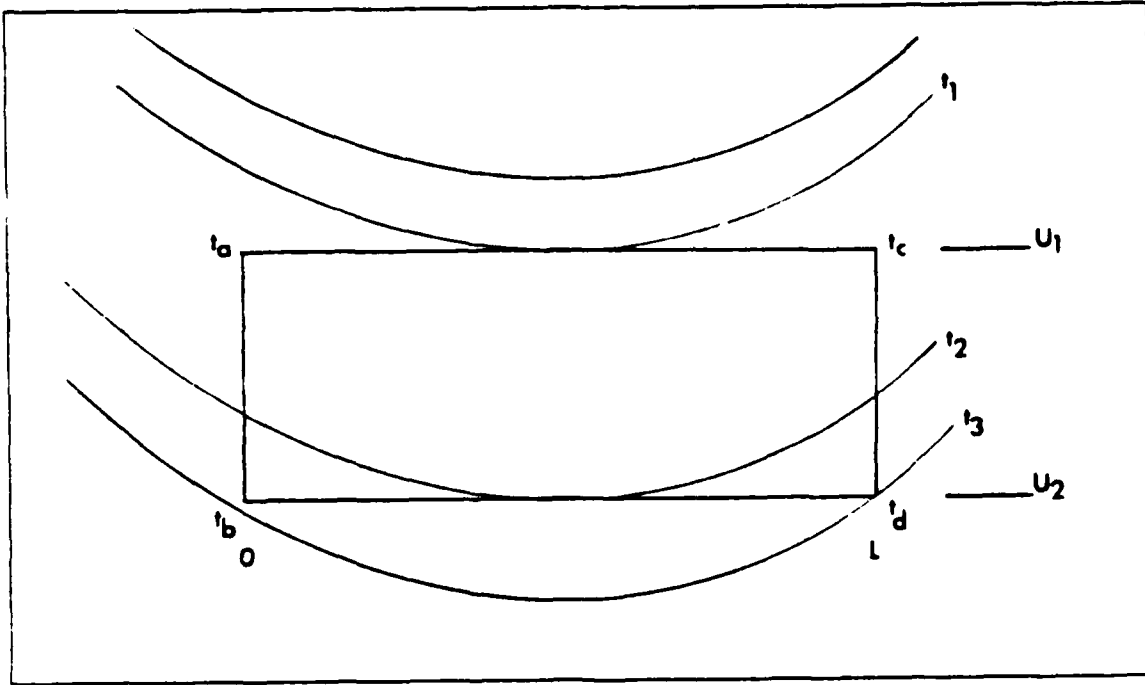


Figure 2.16 Centered About the Minimum.

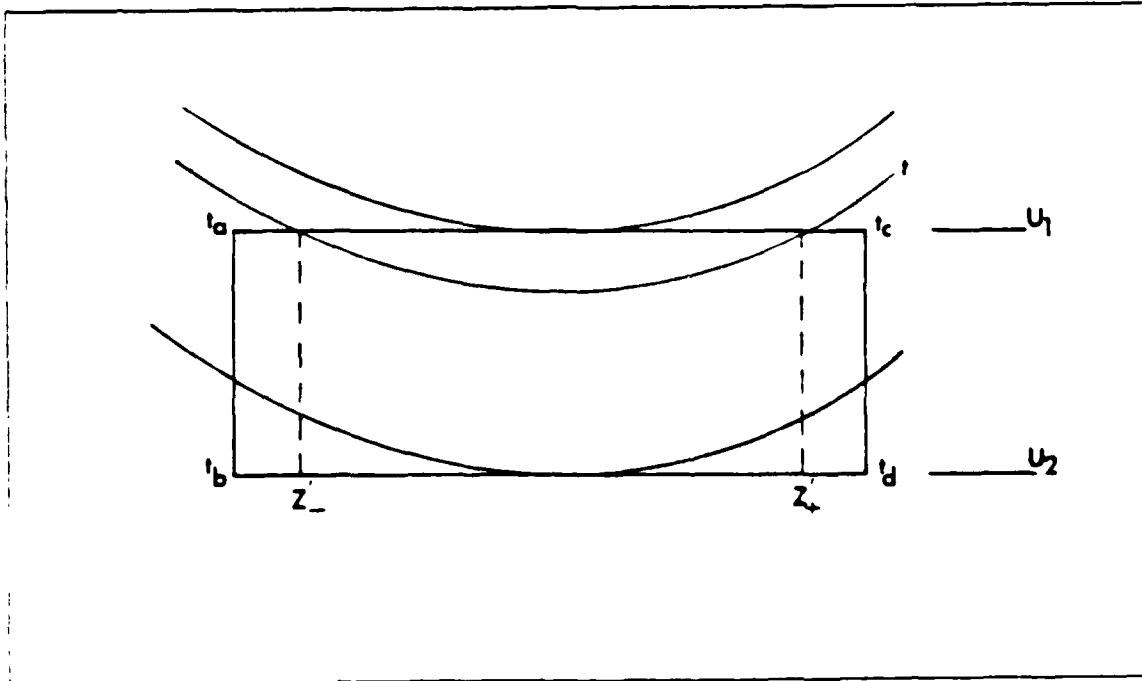


Figure 2.17 $t_1 < t < t_2$.

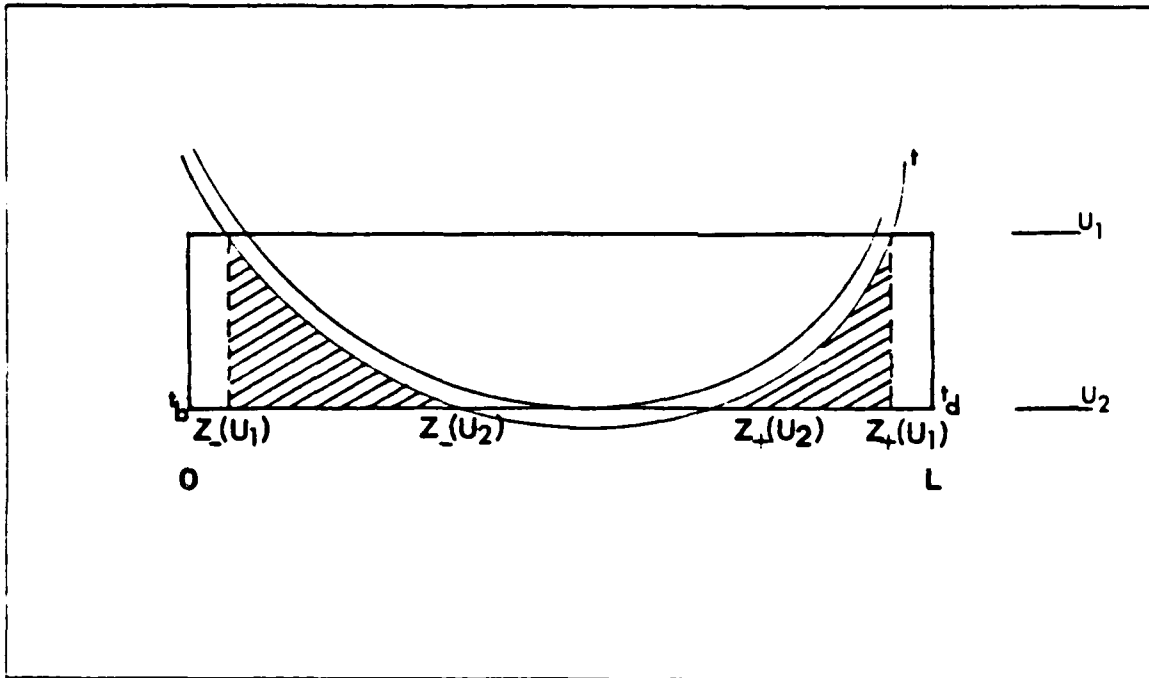


Figure 2.18 $t_2 < t < t_3$.

TABLE I
LIMITS OF INTEGRATION: PATH TO THE RIGHT

$T_c > T_b:$	$T_a < T < T_b$	$T_b < T < T_c$	$T_c < T < T_d$
z_i	0	b	b
z_f	a	a	L
$T_c < T_b:$	$T_a < T < T_c$	$T_c < T < T_b$	$T_b < T < T_d$
z_i	0	0	b
z_f	a	L	L
$T_c = T_b:$	$T_a < T < T_b$	$T_b < T < T_d$	
z_i	0	b	
z_f	a	L	

TABLE 2
LIMITS OF INTEGRATION: PATH TO THE LEFT

$T_a < T_d:$	$T_c < T < T_a$	$T_a < T < T_d$	$T_d < T < T_b$
z'_i	aa	0	0
z'_f	L	L	bb
$T_a > T_d:$	$T_c < T < T_d$	$T_d < T < T_a$	$T_a < T < T_b$
z'_i	aa	aa	0
z'_f	L	bb	bb
$T_a = T_b:$	$T_c < T < T_a$	$T_d < T < T_b$	
z'_i	aa	0	
z'_f	L	bb	

TABLE 3
LIMITS OF INTEGRATION: CENTERED

$T_1 < T < T_2$	$z'_- \leq 0$	$z'_- > 0$	$z'_+ \geq L$	$z'_+ < L$
z'_i	0	z'_-		
z'_f			L	z'_+
$T_2 < T < T_3$				
First Integral				
z'_i	0	$z'_-(u_1)$		
$z'_f = z'_-(u_2)$				
Second Integral				
$z'_i = z'_-(u_2)$				
z'_f			L	$z'_+(u_1)$

III. ANALYSIS OF THE S-Z PLANE

A. S/L VERSES Z/L

After establishing the pertinent variables, relative observing positions, and the different situations for each observing position in the previous chapter, the S/L vs. Z/L graph can now be constructed and studied. This particular graph gives some insight to the integration procedures used in the previous chapter since the limits of integration change at certain times. The S/L vs. Z/L graph plots out the conditions where the previously derived boundary times are equal and also presents the plane of radiation and the beam. Figure 3.1 (page 36) illustrates this graph and was produced using the following values: $\beta' = 1.1$, $n = 1.100057203$, $L = 150.0$ meters, and $\Delta u/L = 0.05$. These particular values spread the plotted lines out and allows us to study their true shapes. The functions that plot these lines are obtained by setting $t_b = t_c$ (solid line), $t_a = t_d$ (dashed line), $t_c = t_a$ or $t_b = t_d$ (chain-dashed line). The FORTRAN program in Appendix B creates the data that plots out each function in Figure 3.1. The conditions that must exist in order to plot the above functions are expressed in Equations 3.1 to 3.3 for $t_b = t_c$, $t_a = t_d$, and $t_a = t_c$ respectively.

$$\Delta u = L + \beta'[(s^2 + (z - L)^2)^{1/2} - (s^2 + z^2)^{1/2}] \quad (t_b = t_c) \quad (3.1)$$

$$\Delta u = \beta'[(s^2 + z^2)^{1/2} - (s^2 + (z - L)^2)^{1/2}] - L \quad (t_a = t_d) \quad (3.2)$$

$$L = \beta'[(s^2 + z^2)^{1/2} - (s^2 + (z - L)^2)^{1/2}] \quad (t_a = t_c) \quad (3.3)$$

Equation 3.3 can also be derived by setting $t_b = t_d$ and is not dependent on Δu . Figure 3.2 is the expanded version of Figure 3.1 and is shown in order illustrate where remote observing positions fail.

To see where the Cerenkov region (marked center) falls on the S-Z plane, the value of θ_c is measured from the horizontal at the beam discharge point ($S/L = 0$, $Z/L = 0$), and the end of the beam ($S/L = 0$, $Z/L = 1$). By projecting a line from each point at the angle θ_c to the end of the S-Z plane gives the Cerenkov region. In Figures

3.1 and 3.2 this region falls between the two dotted parallel lines. The three possible observer regions are shown in Figure 3.1. From the beam discharge point to the first encountered Cerenkov boundary, are all points to the right of the path. In the Cerenkov region, all points are centered about the minimum. From the Cerenkov region in the increasing Z/L direction are all points which fall to the left of the path.

B. HYPERBOLAS IN THE S-Z PLANE

Inspection of the curves in Figures 3.1 and 3.2 leads one to inquire if they have a simple mathematical expression. As mentioned in the previous section, particular boundary times were set equal in order to obtain these three functions of interest. The initial mathematical expression that appears after equating these times is given by Equation 3.4, where $y = S/L$ and $x = Z/L$.

$$(x^2 + y^2)^{1/2} - ((x - 1)^2 + y^2)^{1/2} = Q \quad (3.4)$$

The value of Q is unique to each function and is always a positive constant. Equations 3.5, 3.6, and 3.7 are the three expressions for Q that originate when setting $t_b = t_c$ (right), $t_a = t_d$ (left), and $t_a = t_c$ (center) respectively.

$$Q_r = [1 - \Delta u/L]/\beta' \quad (3.5)$$

$$Q_l = [1 + \Delta u/L]/\beta' \quad (3.6)$$

$$Q_c = 1/\beta' \quad (3.7)$$

Equation 3.4 is the difference between two distances equated to a constant. This constitutes the standard form of a hyperbola. In order to write a program for plotting hyperbolas, an explicit expression for y as a function of x is needed. After some cumbersome algebra, Equation 3.4 becomes Equation 3.8.

$$y = [((x^2 - (x - 1)^2 - Q^2)^2/4Q^2) - (x - 1)^2]^{1/2} \quad (3.8)$$

The next step is to take Equation 3.8 and work it into the classical form of a hyperbola where there is an axis translation. This allows one to find the coordinates (x_0, y_0) of the axis translation. Equation 3.9 gives the classical form where the hyperbola is symmetric about x_0 and y_0 .

$$(x - x_0)^2/a^2 - (y - y_0)^2/b^2 = 1 \quad (3.9)$$

The best approach to achieving the classical form is to work with Equation 3.8. By carrying out the square in the $(x - 1)^2$ term and performing other algebraic operations, a general form for conical sections is recognized. Equation 3.10 takes on the form $Ax^2 + Bx + Cy^2 + Dy + E = 0$.

$$y^2 - (1/Q^2 - 1)x^2 + [2 - (1 + Q^2)/Q^2]x - (1 - 2Q^2 + Q^4)/4Q^2 = 0 \quad (3.10)$$

A hyperbola exists if AC is negative. An ellipse or parabola exists if AC is positive or zero respectively. From Equation 3.4, the only possible shapes that form on the S-Z plane are hyperbolas. To determine the conditions for the existence of a hyperbola, a closer look at the coefficient of the x^2 term is required.

Since the only true shapes on the S-Z plane are hyperbolas, then the coefficient of x^2 must be positive. In other words the inequality 3.11 must be satisfied.

$$1/Q > 1 \quad (3.11)$$

Using the expressions for Q in Equations 3.5, 3.6, and 3.7 with the particular values of Δu , L, and β' , the inequality is easier to satisfied when considering Equations 3.5 and 3.7. However, when using Equation 3.6, difficulties are more likely to arise in obtaining the expected hyperbolas. Substituting in Q1 for Q in the inequality 3.11, allows one to see how the values of β' , Δu , and L govern the inequality. The inequality 3.12 is the result of this substitution.

$$\beta' > 1 + \Delta u/L \quad (3.12)$$

If the inequality 3.12 is satisfied, the time equalities which give rise to Equations 3.1 to 3.3 are satisfied. The most common values encountered with the variables β' and Δu L cause the inequality 3.12 to be unsatisfied.

In summary, hyperbolic shapes exist in the S-Z plane when the above inequalities are satisfied. Without explicitly defining the values of a^2 and b^2 , it can easily be shown from Equation 3.10 that the hyperbolas take on the form

$$(x - 0.5)^2/a^2 - y^2/b^2 = 1. \quad (3.13)$$

The values of a and b depend on the function that is being plotted and are subsequently functions of the corresponding value of Q .

C. CERENKOV PULSE SHAPES

From Appendix A, Cerenkov pulses are generated from knowing many variables, particularly the location of the observer with respect to the beam discharge point. From here, the relationship between the Cerenkov pulse shape and position relative to time boundaries in the S-Z plane can be studied graphically. The best way to study this relationship is to methodically choose points on the S-Z plane that cross the critical time and position boundaries. Other points are also chosen in order to aid in developing general trends in the way the pulse shape changes as the observing points move across the S-Z plane. The plus signs in Figures 3.1 and 3.2 indicate the points where the Cerenkov pulses are calculated. Each observing position is numbered in order to simplify the discussion in the conclusions. As indicated in the right margin, $\beta' = 1.1$, $\Delta u/L = DU/L = 0.05$, and $L = 150.0$ meters. Choosing a constant S/L value of 0.26 and different Z/L values near a critical boundary, gives a good representation of how the pulse shape varies. Figures 3.3, 3.4, and 3.5 fall behind the beam discharge point. The magnitudes have been scaled up by a factor of ten in order to better examine the shape of the pulse. Figures 3.6 to 3.13 continue to move in the plus Z/L direction while crossing critical boundaries. Since the magnitude of the Cerenkov pulses are large enough, their values are not scaled up. By visual inspection, one can observe that the pulse peaks increase as you approach the Cerenkov region. After the maximum peak occurs, the magnitude of the peaks decrease with increasing Z/L . The observed breaks in the pulse shapes occur at the defined normalized boundary times T_a , T_b , T_c , and T_d .

The remote observing points are shown in Figures 3.14 to 3.20. These points are indicated on Figure 3.2 and are selected to fall around critical boundaries. Figures 3.14 and 3.15 are located to the right of the path. The pulse shapes peak at T_b then

gradually decreases in magnitude to T_c before decreasing to zero at T_d . Figures 3.18 and 3.19 are points which fall in the Cerenkov region. The pulses begin at time T_1 and end at time T_3 with a peak at T_2 . The peaks of each of the pulses appear flat, and show no gradual decline as did the pulses to the right of the path. Figure 3.20 is a pulse to the left of the path with shape characteristics that are similar to Figures 3.18 and 3.19.

To continue this study of the relationship between the S-Z plane and the Cerenkov pulse shapes, the parameter $\Delta u/L$ (DU/L) is changed from 0.05 to 0.15. Figures 3.21 and 3.22 are shown as were Figures 3.1 and 3.2 with the regions marked and the points (plus signs) for evaluation indicated. However, the dashed line (where $t_a = t_d$) is not present. This is due to the fact that the inequality 3.12 is not satisfied as a result of the new $\Delta u/L$ ratio. Thus, only two hyperbolic shapes exist in Figures 3.21 and 3.22.

Figures 3.23 to 3.34 are the same in shape as Figures 3.3 and 3.13. The magnitudes are larger even though the points from which these pulses were generated are a longer distance away from the discharge point. Figures 3.35 through 3.41 are the pulses at the points indicated on Figure 3.22. The shapes are again somewhat expected for each case. The points located to the right of the path peak and break at the critical times, as does the points located to the left and on the center. However, the pulses located in the Cerenkov region and to the left of the path have flattop peaks. As an obvious observation, the remote points in each $\Delta u/L$ case have later times at which the pulse is starting to be observed. This is due to the longer distances that the emissions have to travel in order to get to the observing positions.

The next approach which aids in gaining better insight in the study of the pulse shapes, is to examine points that are an equal distance from the origin of the beam. Figures 3.42 and 3.43 originate from generating the S-Z plane using the $\Delta u/L$ ratio of 0.05 as in Figures 3.1 and 3.2. The reason for using this case as an example is because all three hyperbolic shapes exist. Figures 3.42 and 3.43 represent the close and far observing positions respectively. The expressions close and far observing positions are defined in terms of their relative magnitudes. Close simply describes an observing position that is nearer to the beam. The points where the pulses are calculated are again indicated by a plus sign. The quarter circle (solid line) has a radius of curvature pointed toward the beam discharge point. Figures 3.44 to 3.48 are the pulse shapes from Figure 3.42. Figures 3.44 and 3.45 fall to the right of the path. Figures 3.46 and

3.47 lie in the Cerenkov region (centered), and Figure 3.48 falls to the left of the path. Figures 3.49 to 3.57 correspond to the points on Figure 3.43. The arrival time of the emitted signal is the start of each pulse and is the same when comparing two points in the same region. The earliest arrival times occur to the left of the path, when considering the equal distance criterion, while the latest arrival times occur to the right of the path. As a quick observation, the magnitudes of the pulses get larger and the pulse widths narrower as the Cerenkov region is approached. More detailed conclusions and observations will follow in the next chapter.

TIME LINES

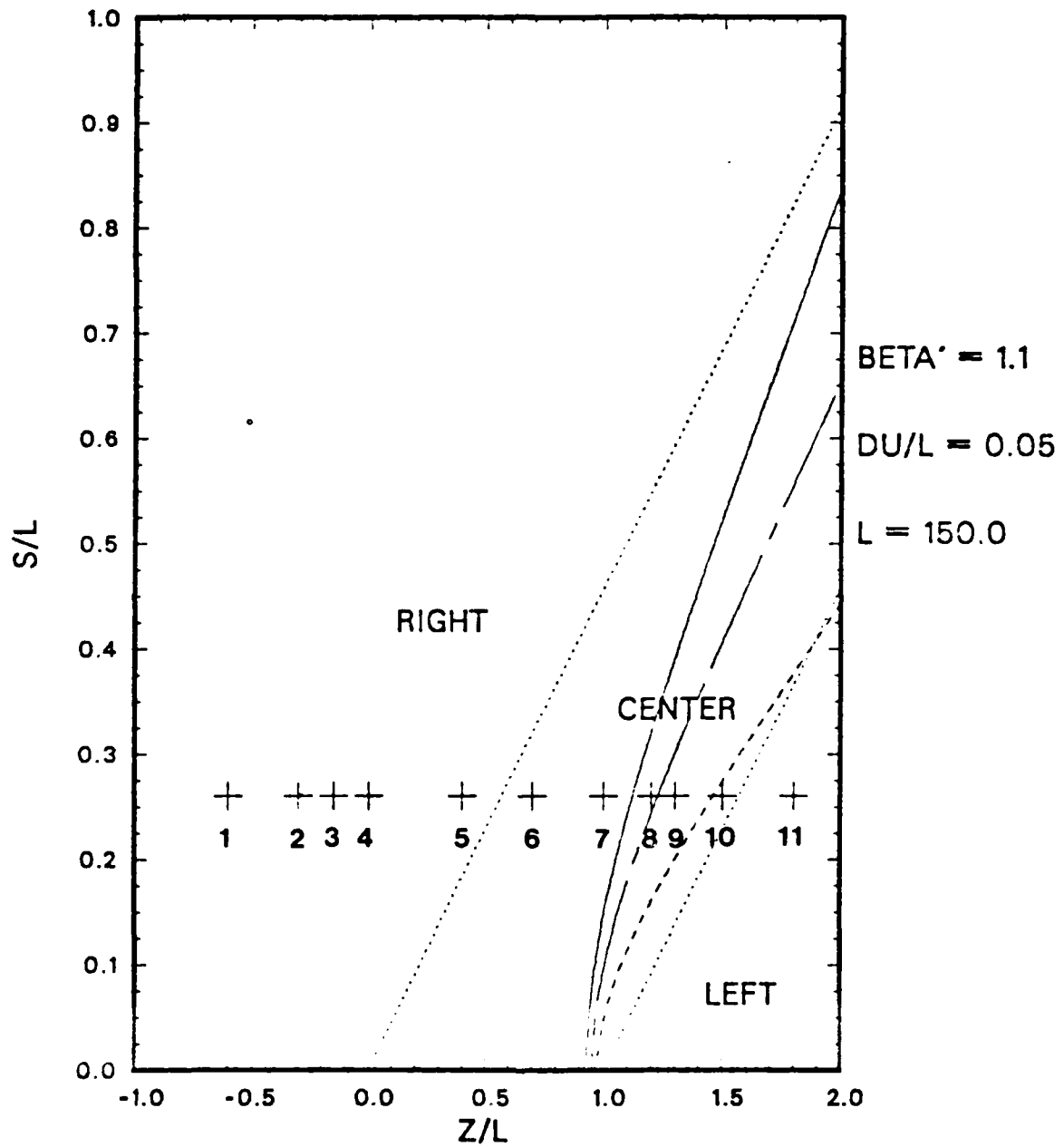


Figure 3.1 The S-Z Plane.

TIME LINES

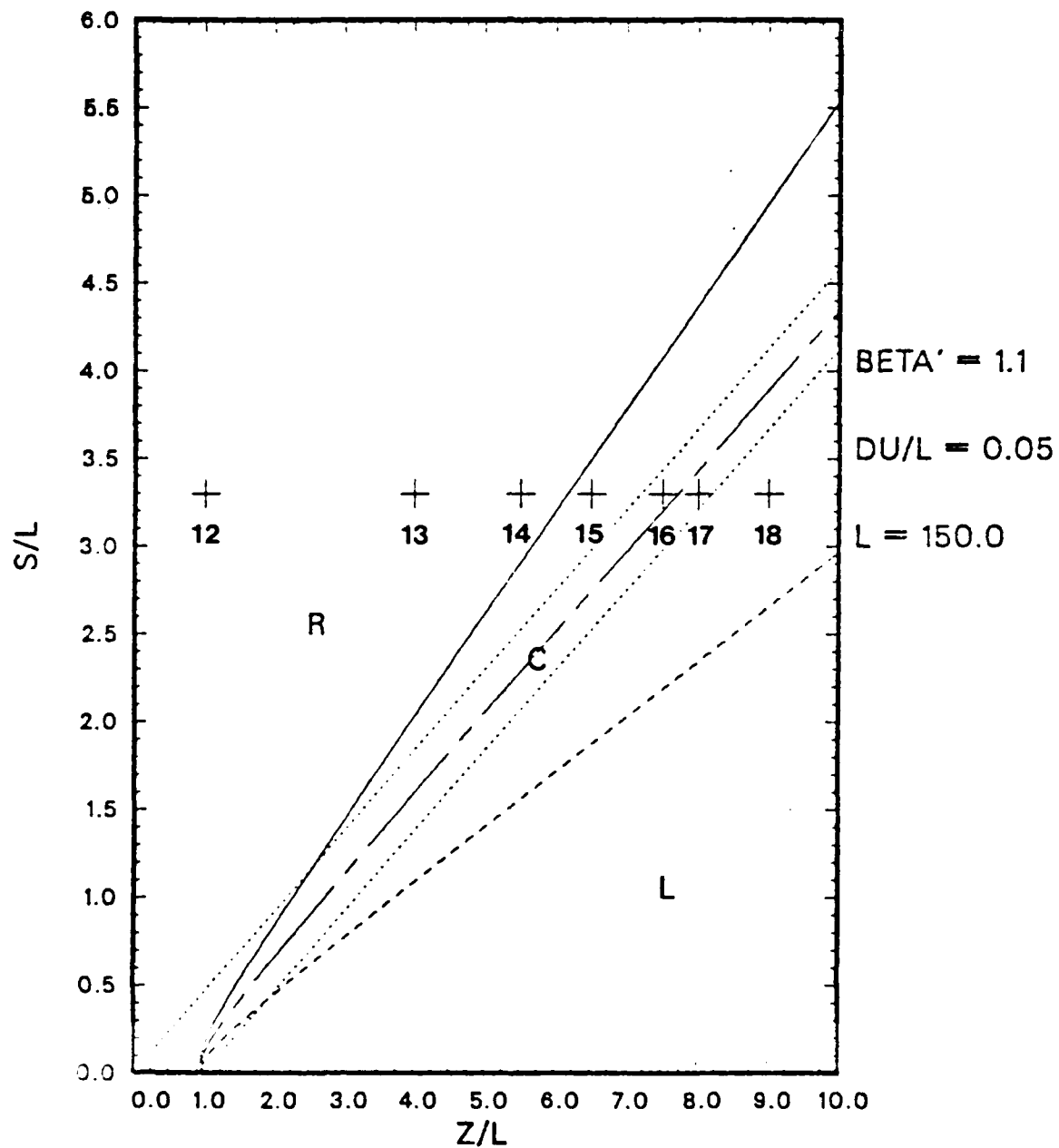


Figure 3.2 The S-Z Plane.

CERENKOV PULSE

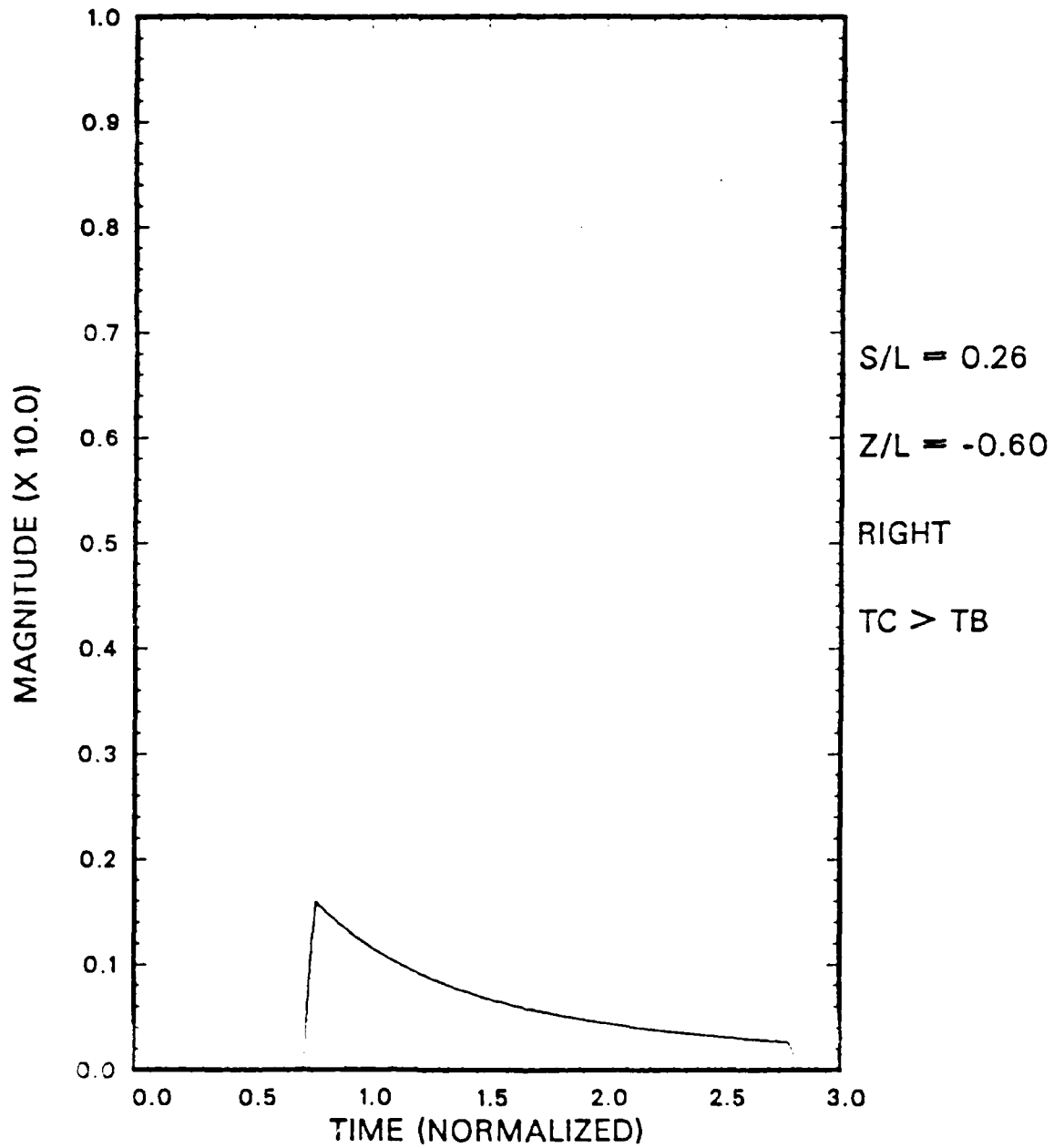


Figure 3.3 From Figure 3.1: Pulse 1.

CERENKOV PULSE

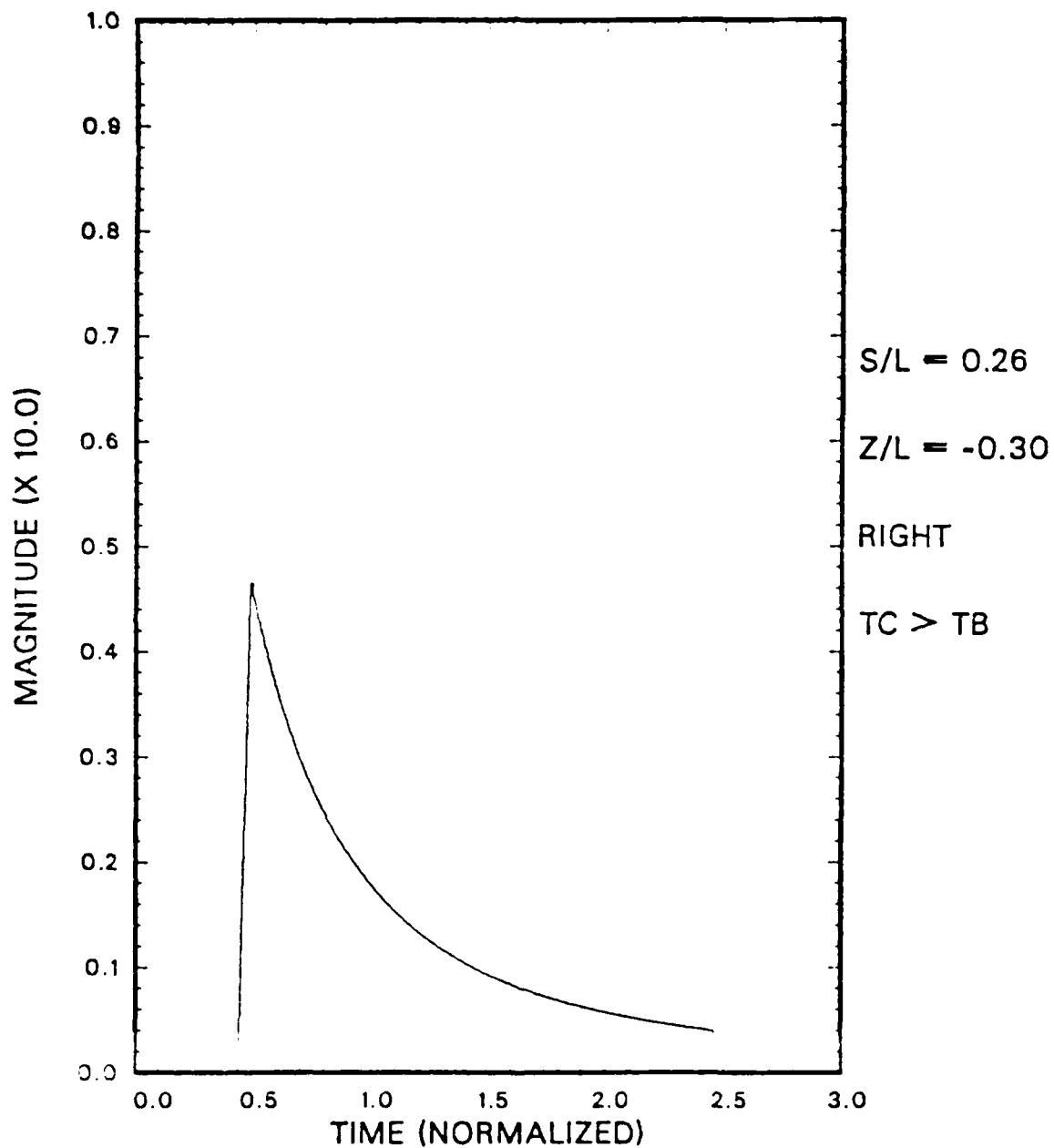


Figure 3.4 From Figure 3.1: Pulse 2.

CERENKOV PULSE

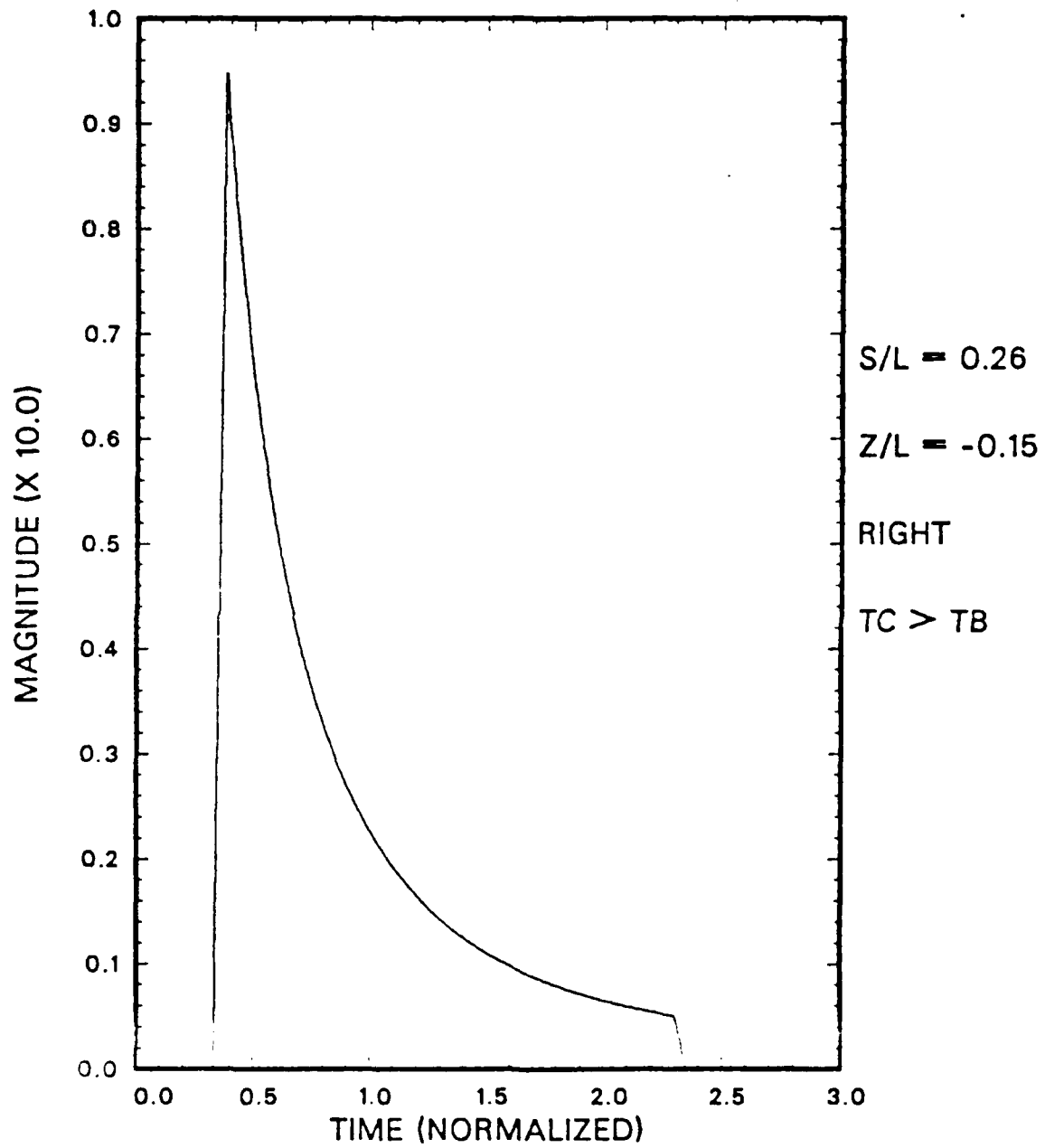


Figure 3.5 From Figure 3.1: Pulse 3.

CERENKOV PULSE

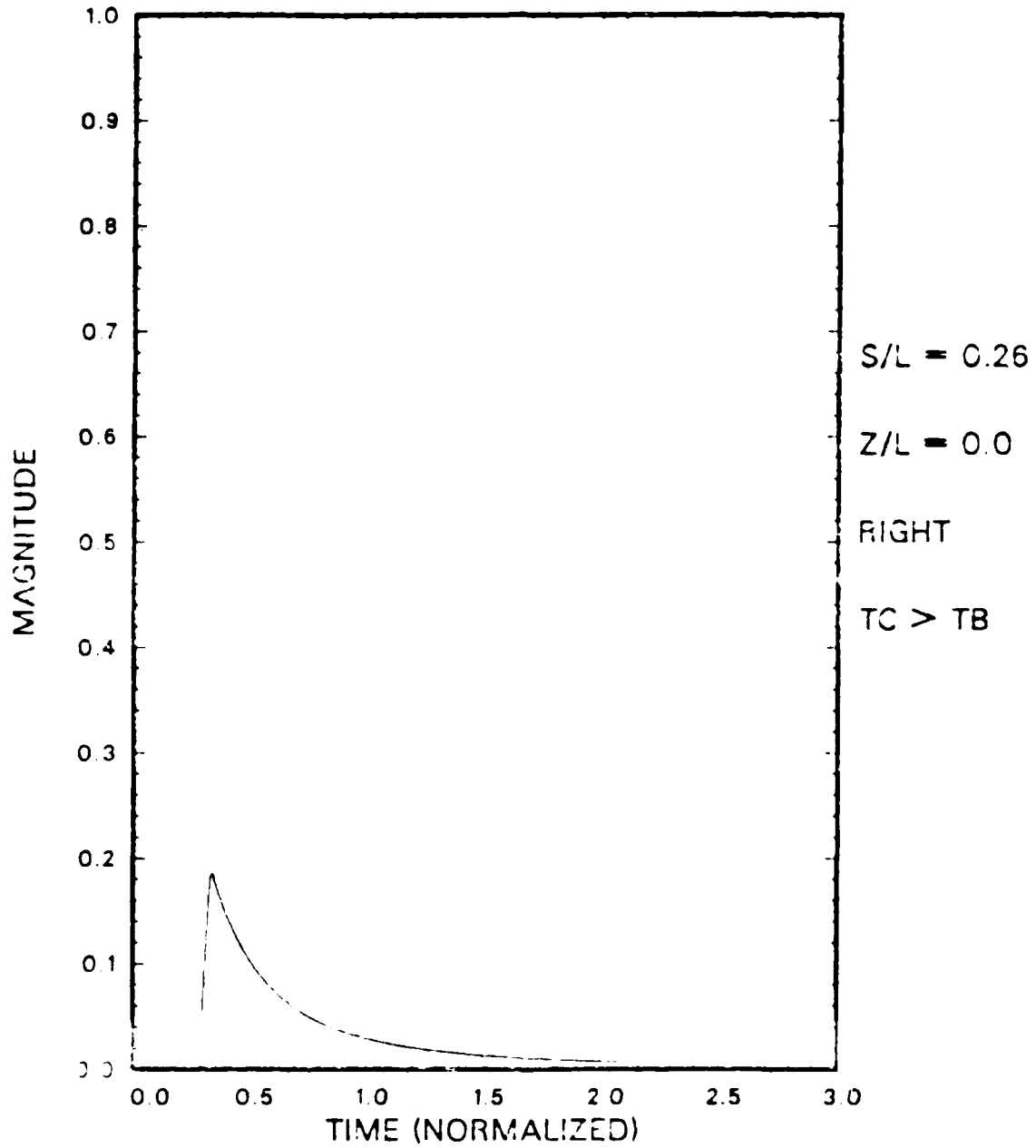


Figure 3.6 From Figure 3.1: Pulse 4.

CERENKOV PULSE

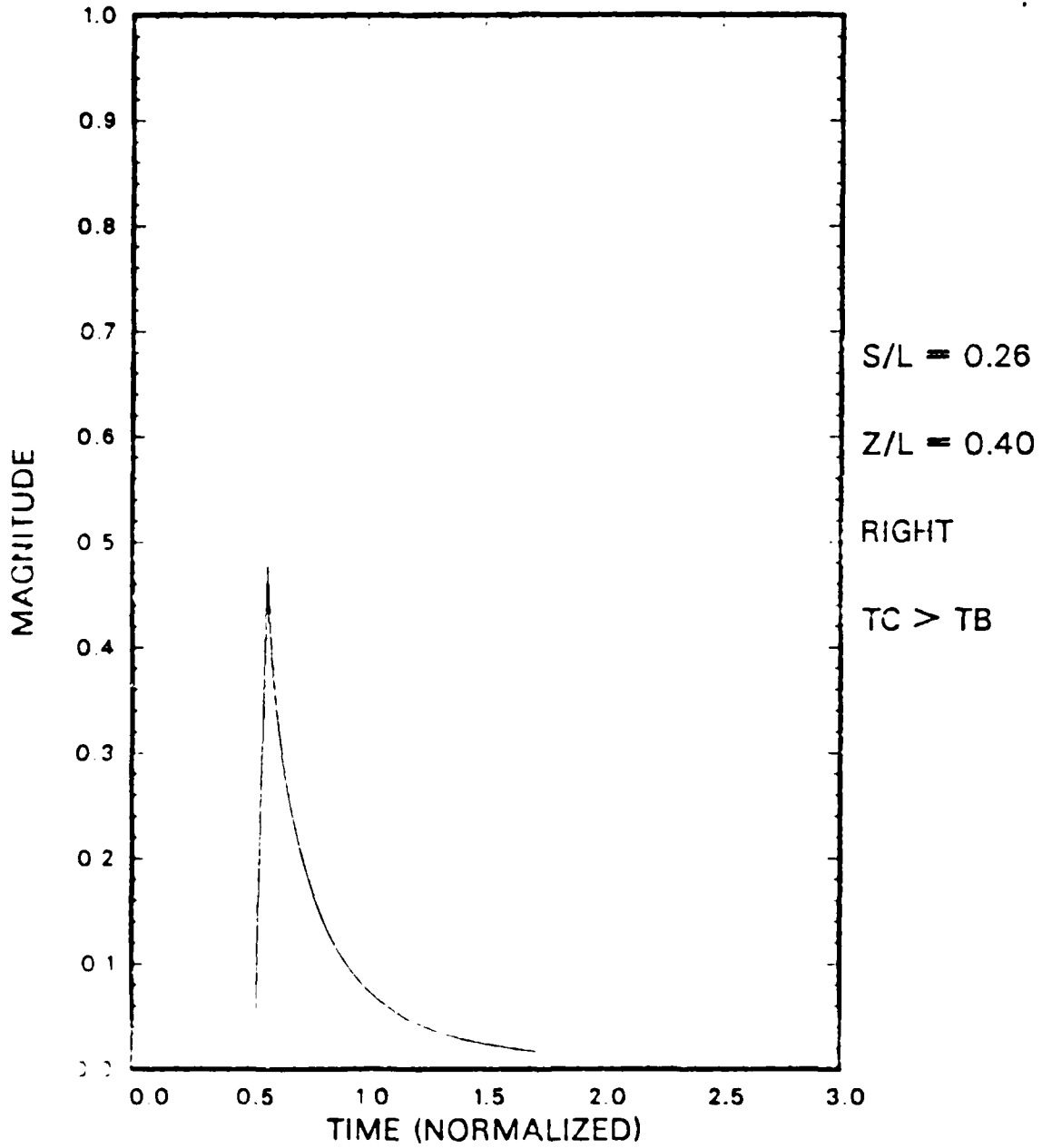


Figure 3.7 From Figure 3.1: Pulse 5.

CERENKOV PULSE

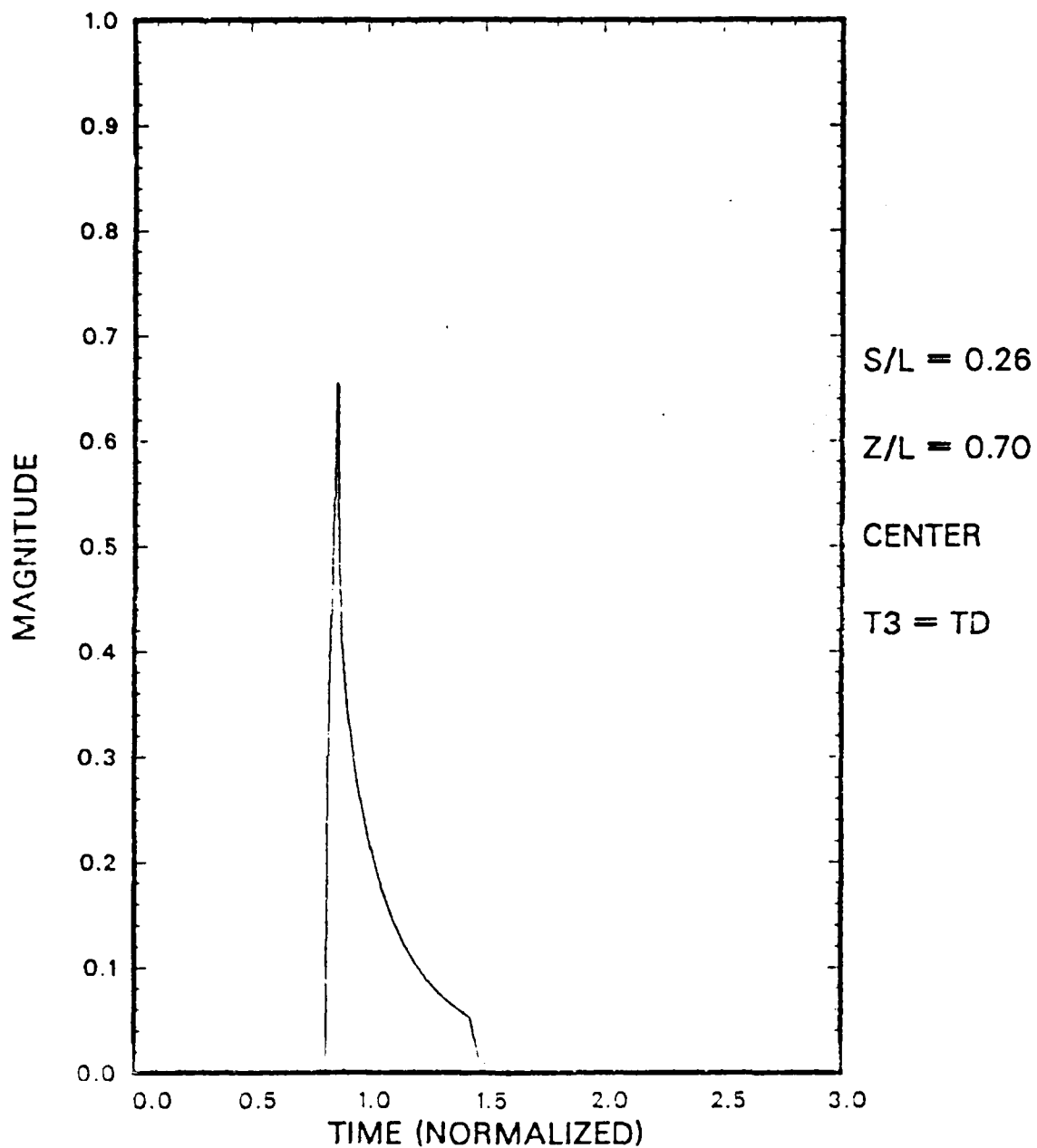


Figure 3.8 From Figure 3.1: Pulse 6.

CERENKOV PULSE

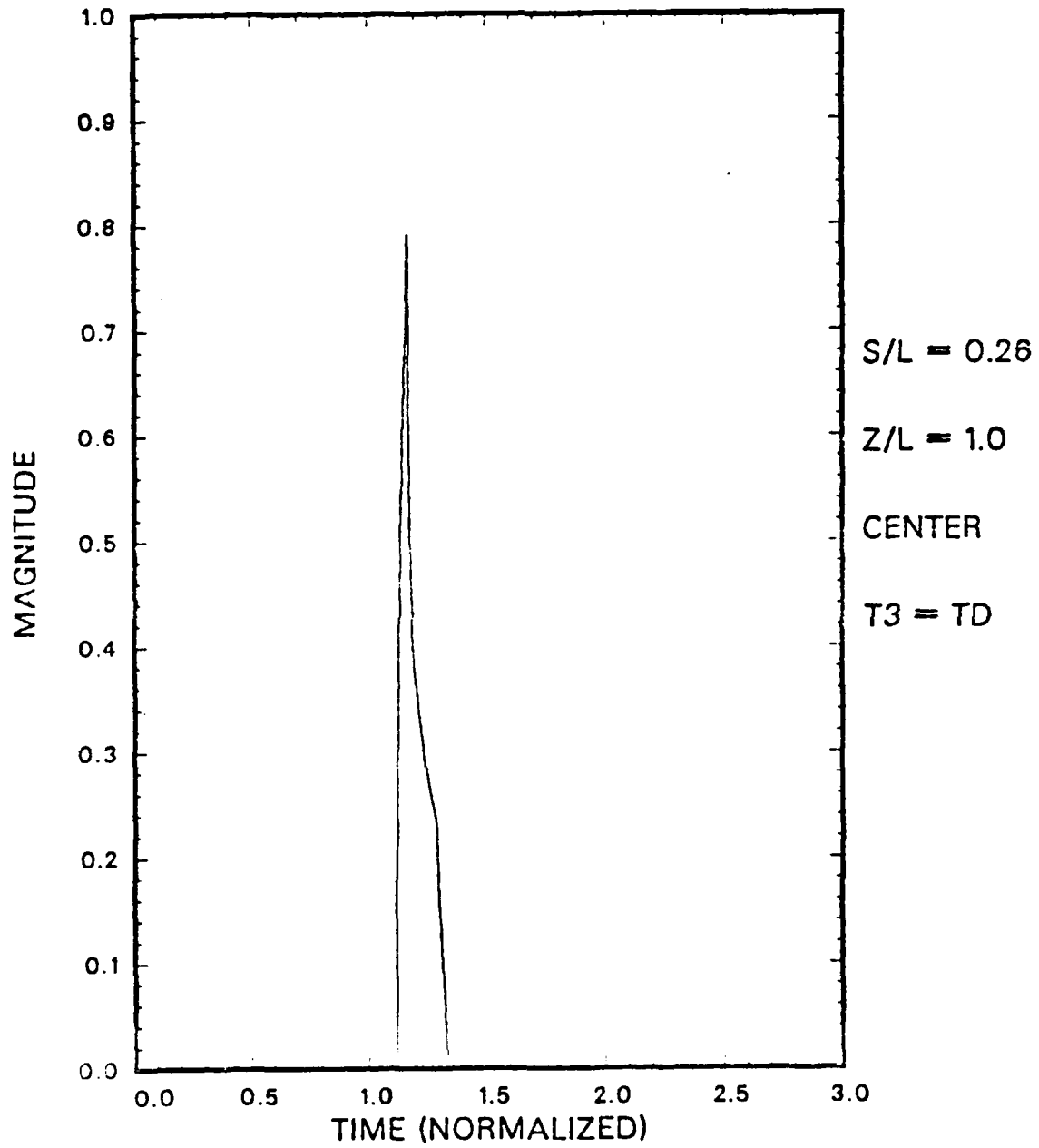


Figure 3.9 From Figure 3.1: Pulse 7.

CERENKOV PULSE

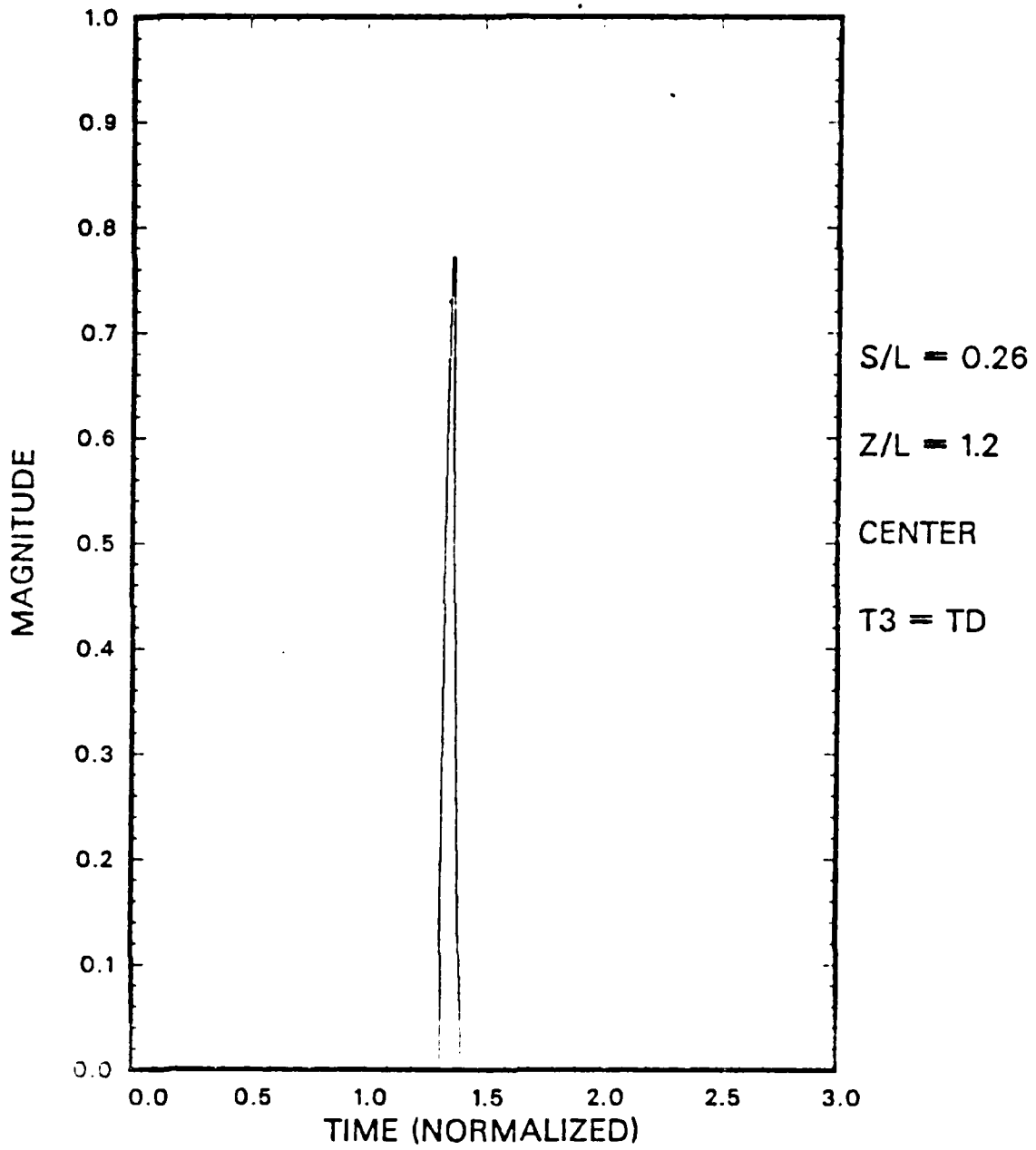


Figure 3.10 From Figure 3.1: Pulse 8.

CERENKOV PULSE

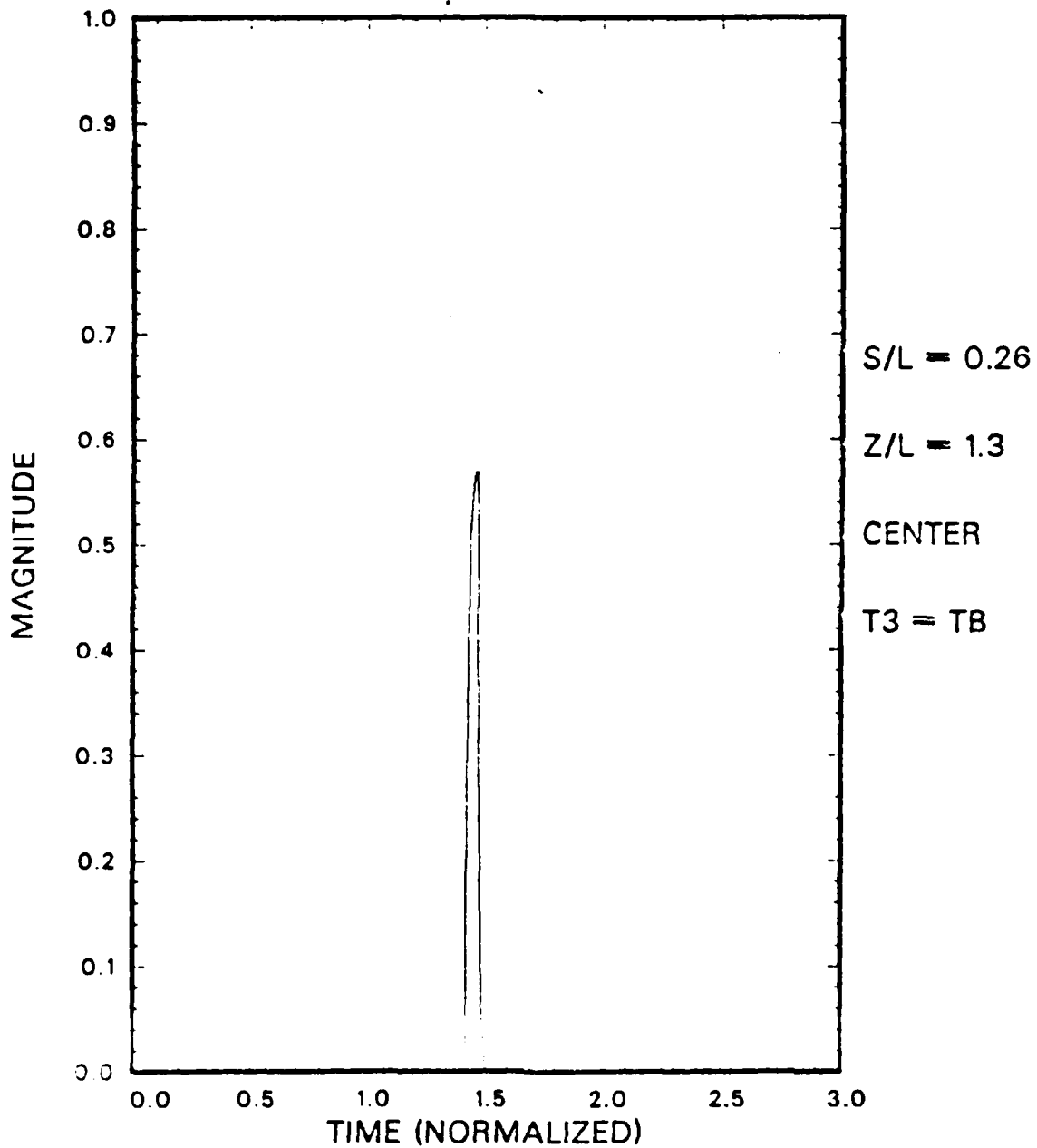


Figure 3.11 From Figure 3.1: Pulse 9.

CERENKOV PULSE

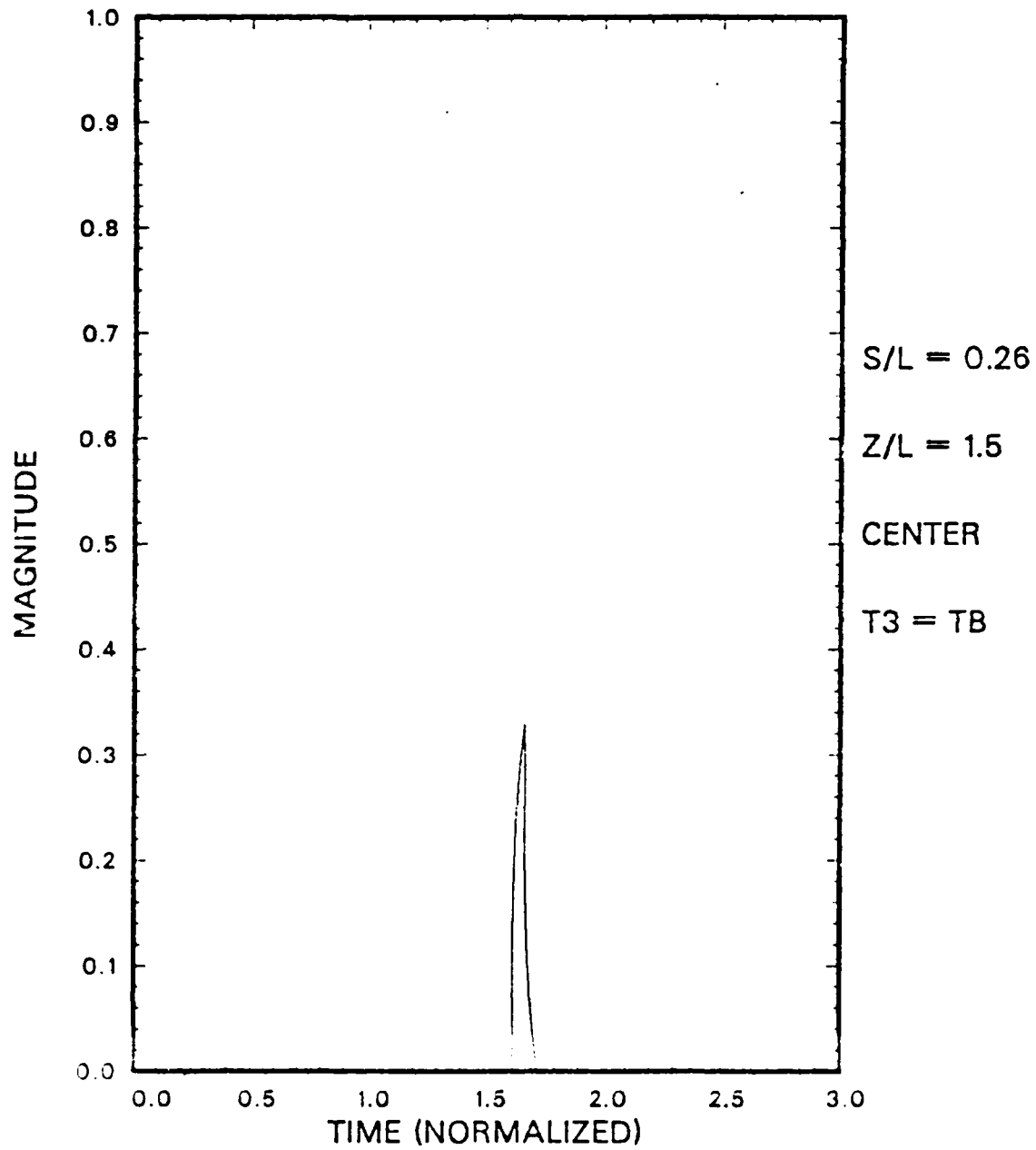


Figure 3.12 From Figure 3.1: Pulse 10.

CERENKOV PULSE

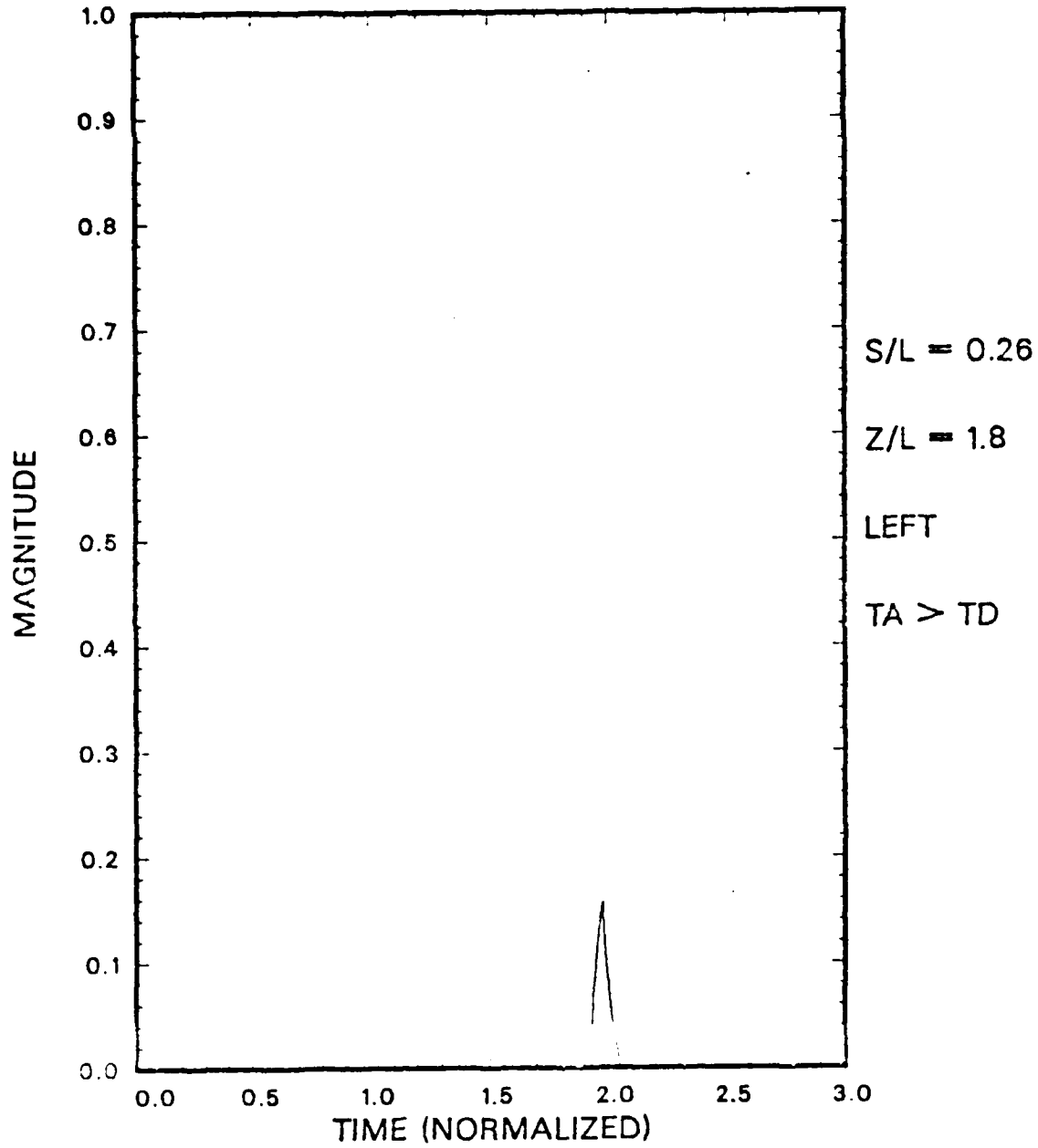


Figure 3.13 From Figure 3.1: Pulse 11.

CERENKOV PULSE

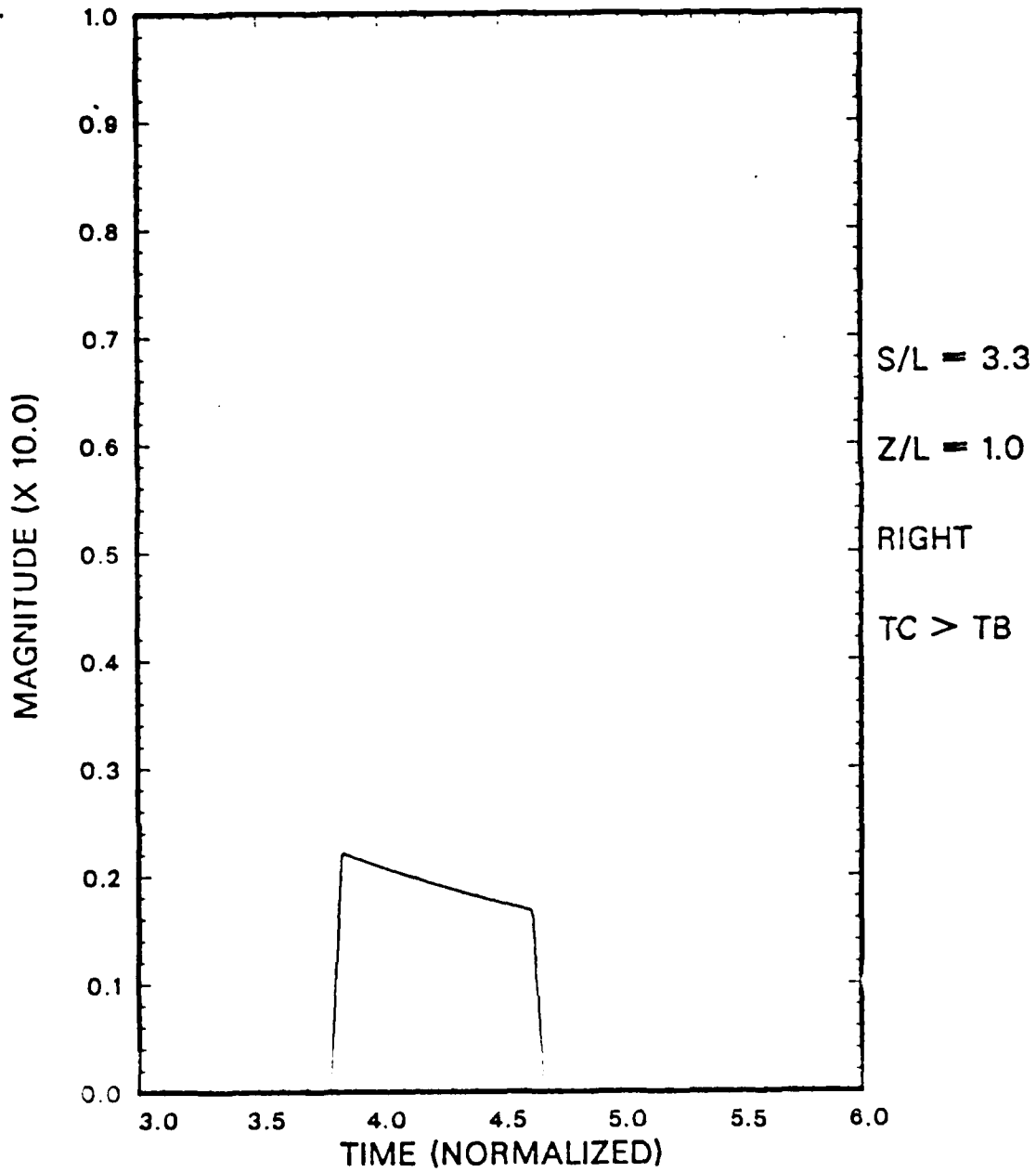


Figure 3.14 From Figure 3.2: Pulse 12.

CERENKOV PULSE

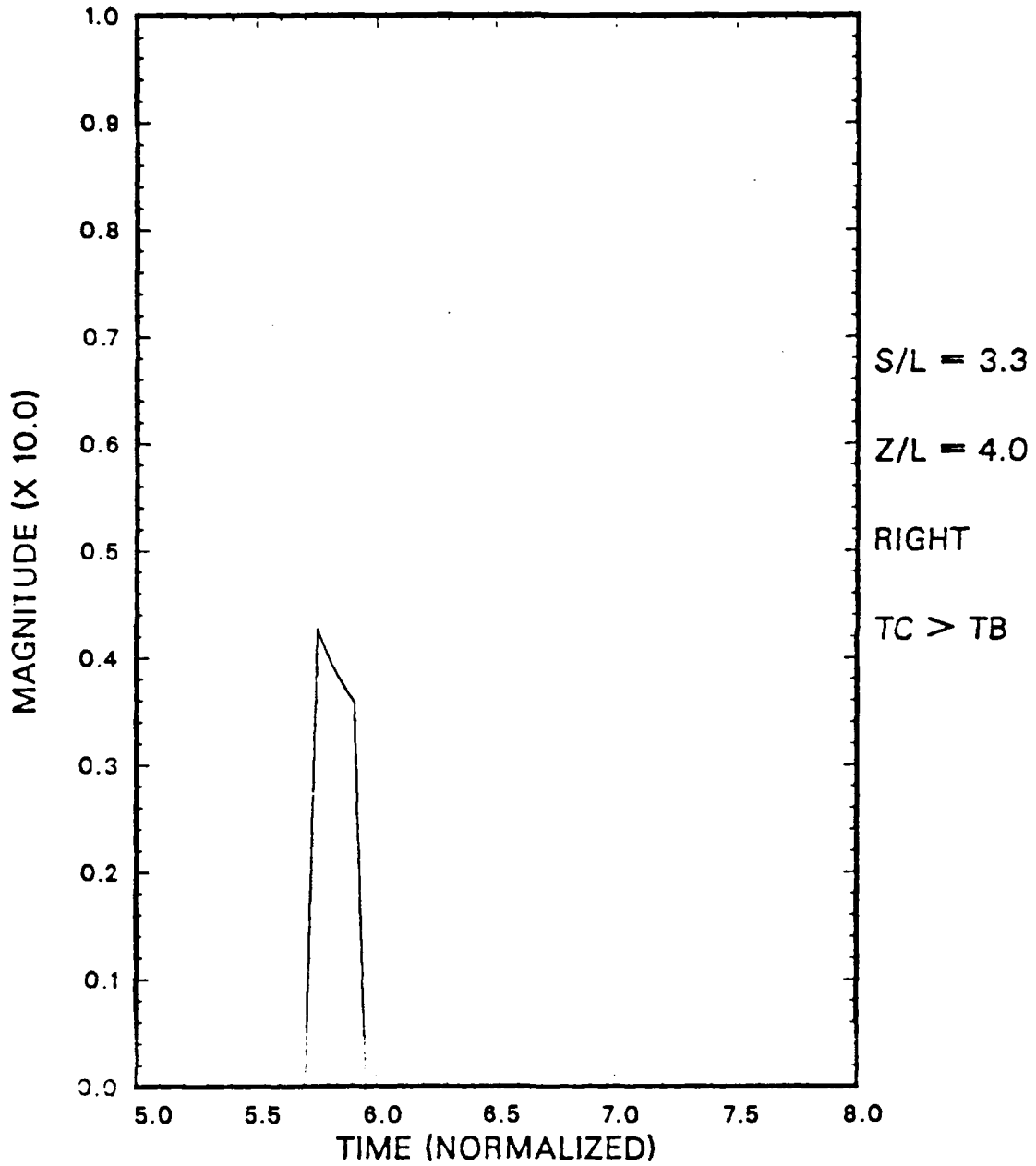


Figure 3.15 From Figure 3.2: Pulse 13.

CERENKOV PULSE

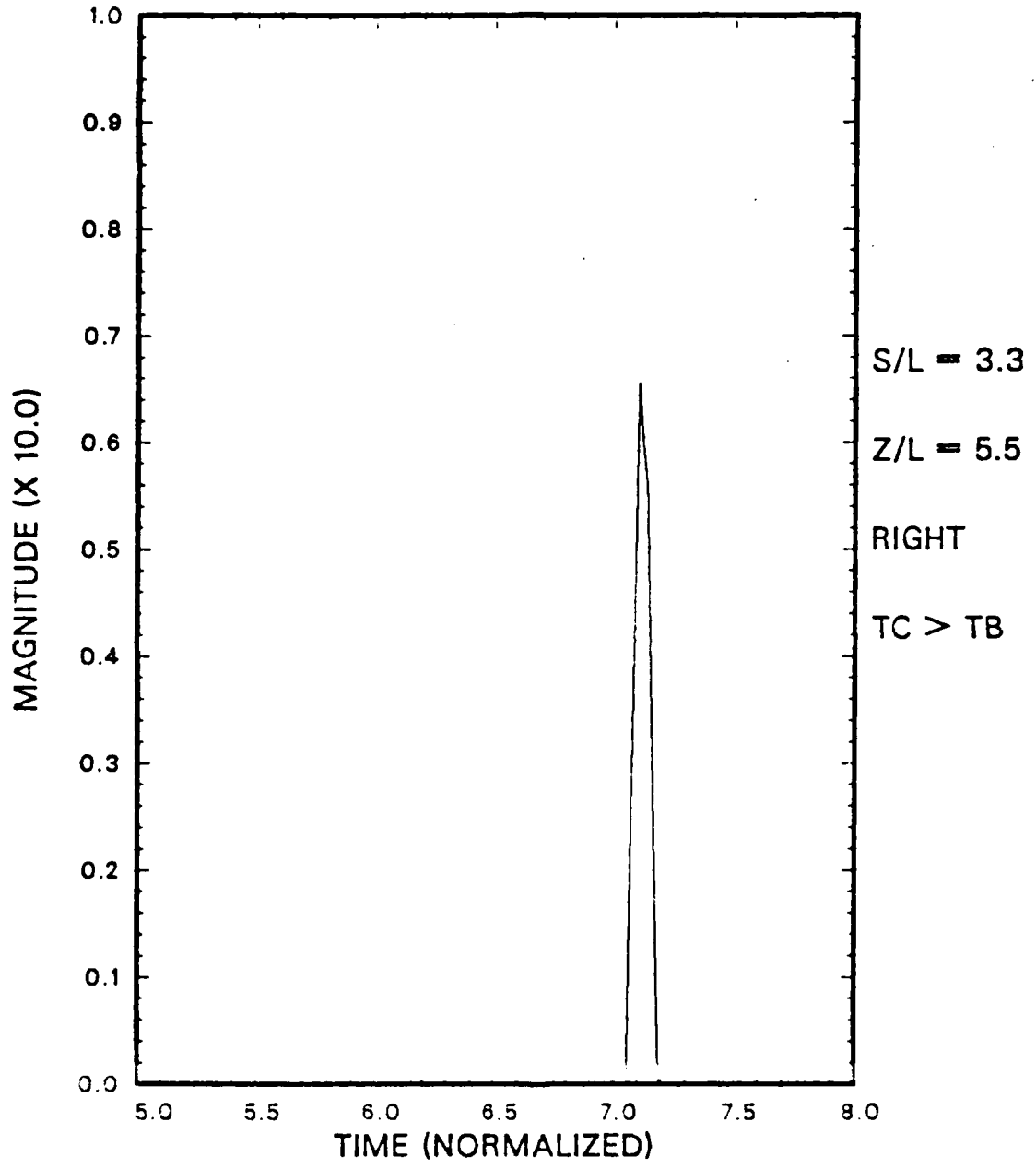


Figure 3.16 From Figure 3.2: Pulse 14.

CERENKOV PULSE

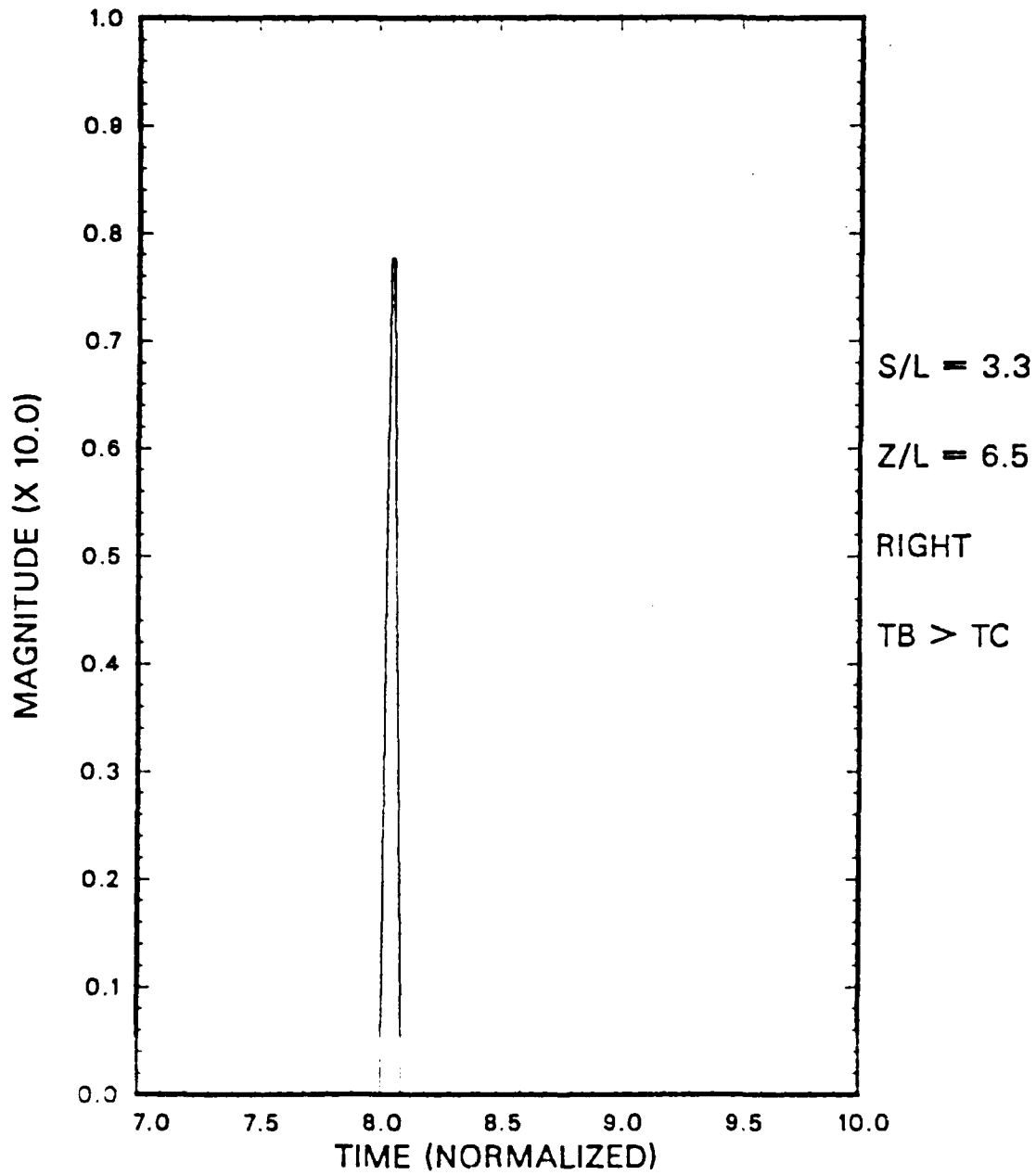


Figure 3.17 From Figure 3.2: Pulse 15.

CERENKOV PULSE

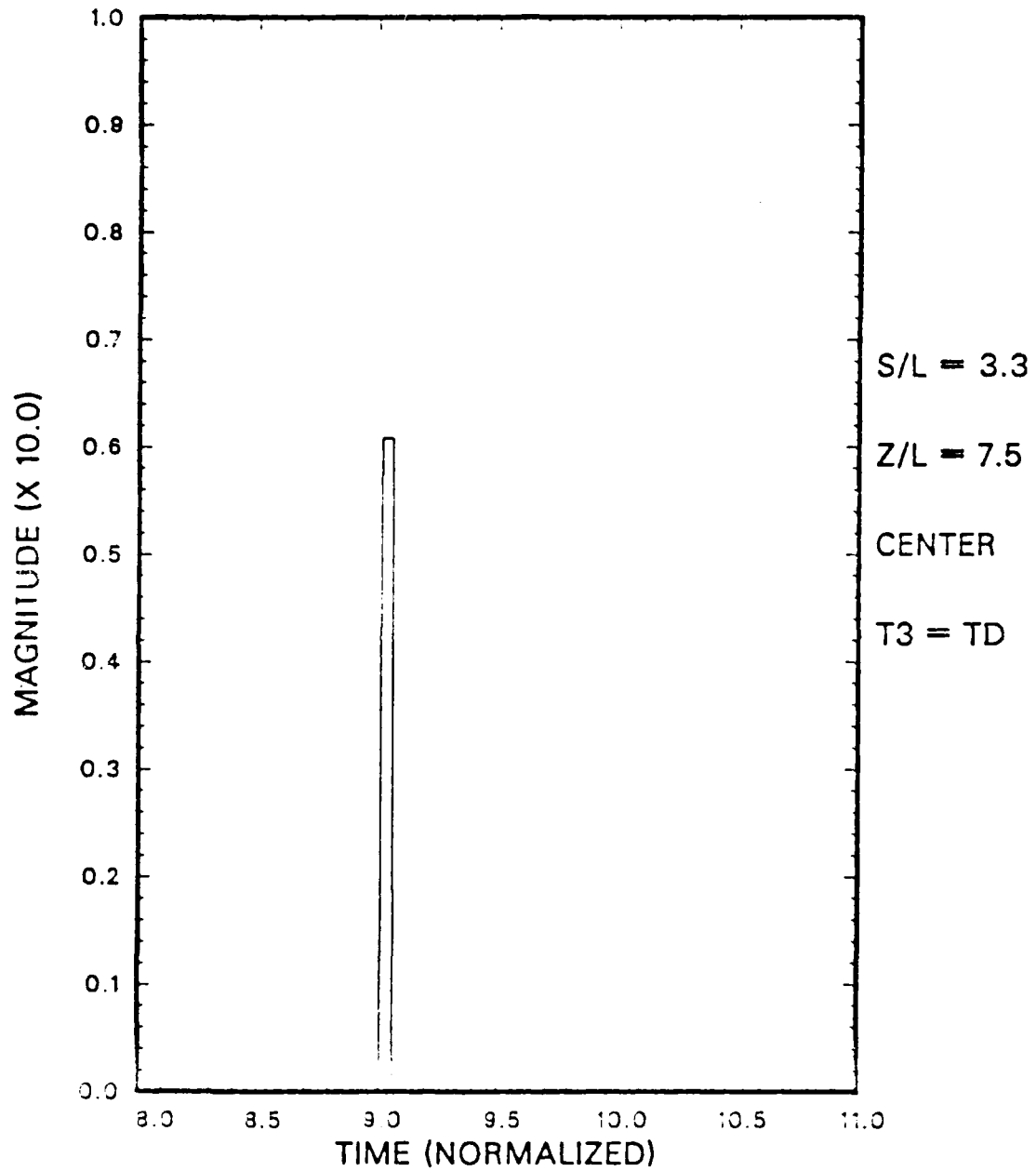


Figure 3.18 From Figure 3.2: Pulse 16.

CERENKOV PULSE

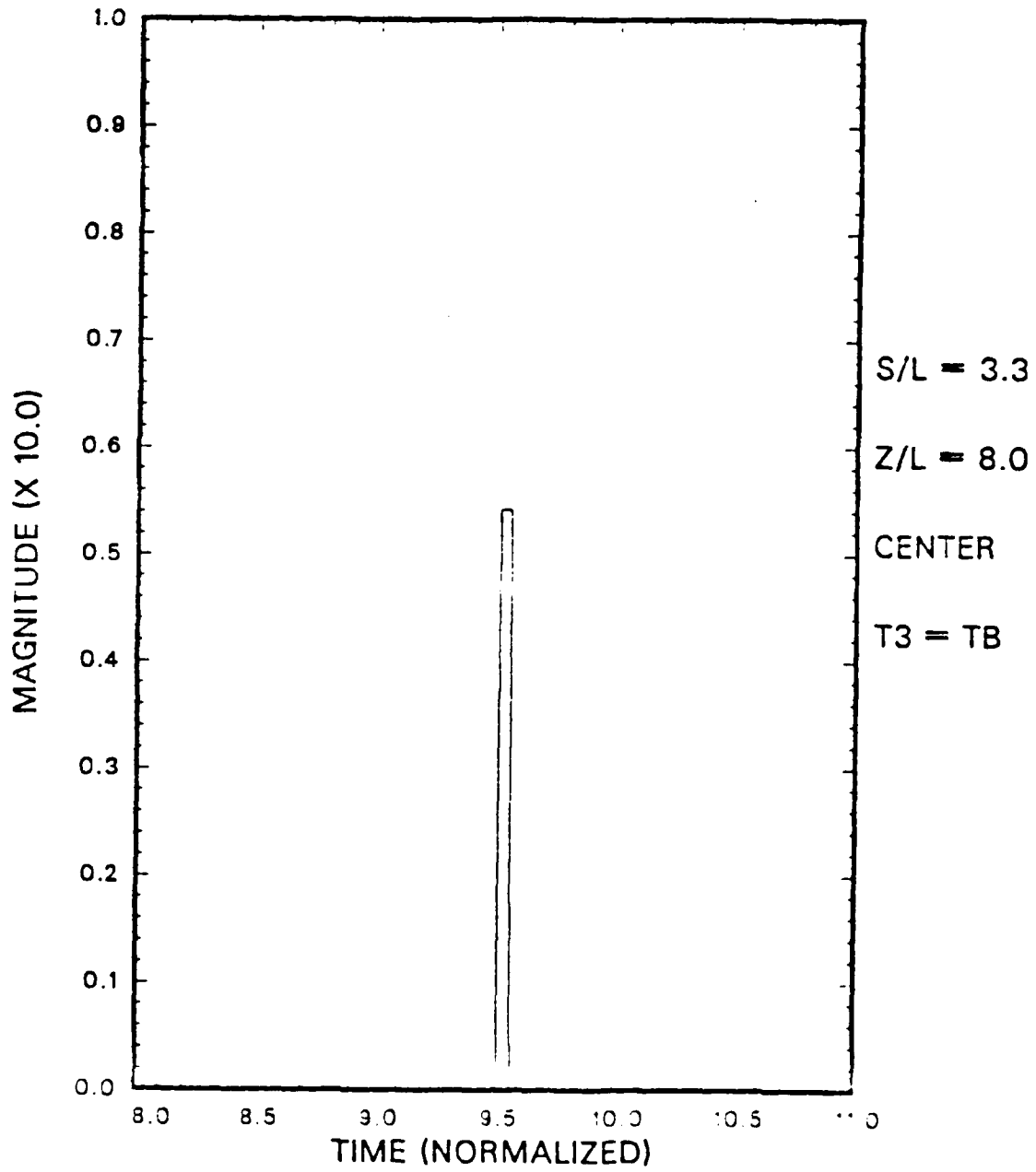


Figure 3.19 From Figure 3.2: Pulse 17.

CERENKOV PULSE

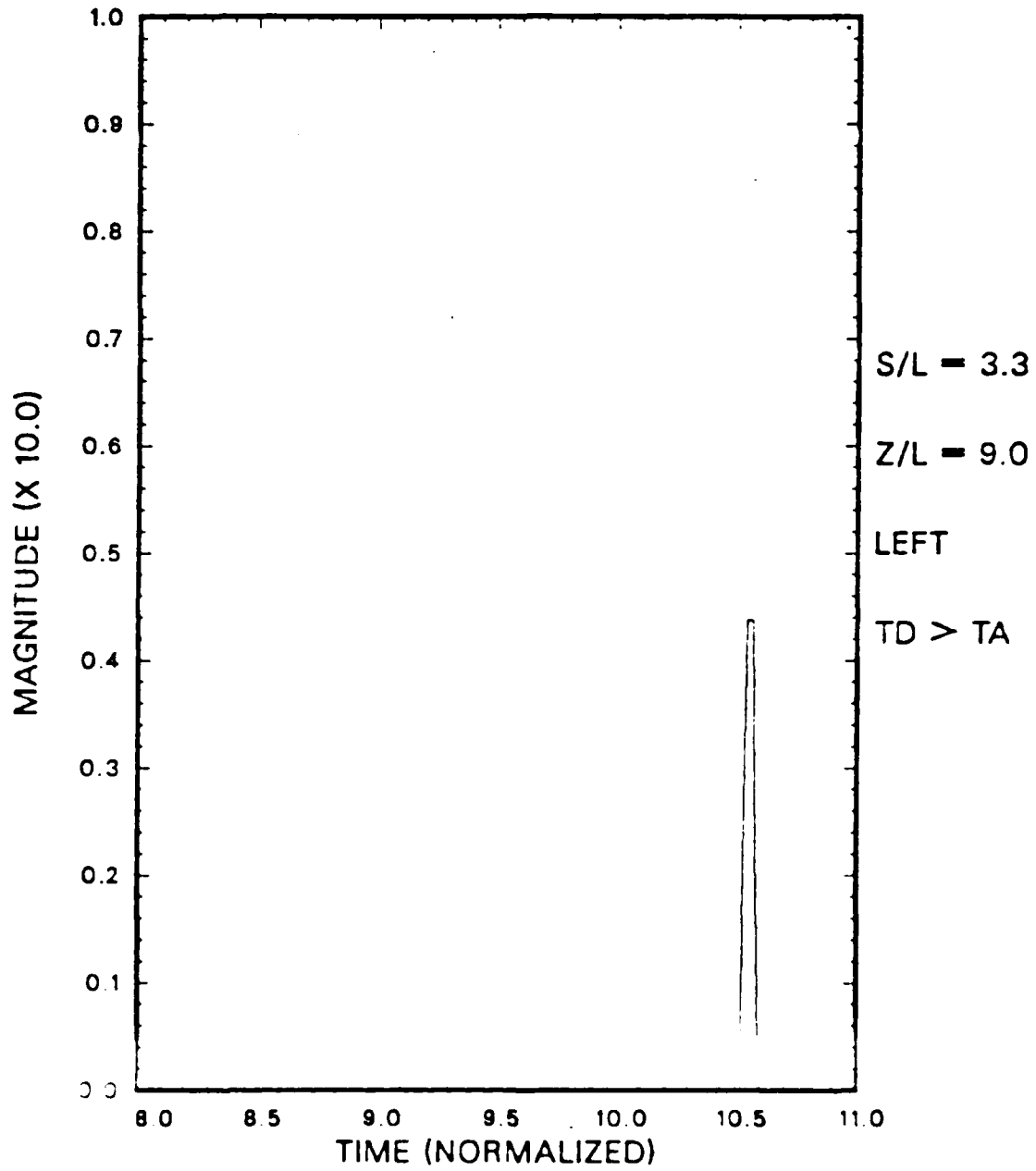


Figure 3.20 From Figure 3.2: Pulse 18.

TIME LINES

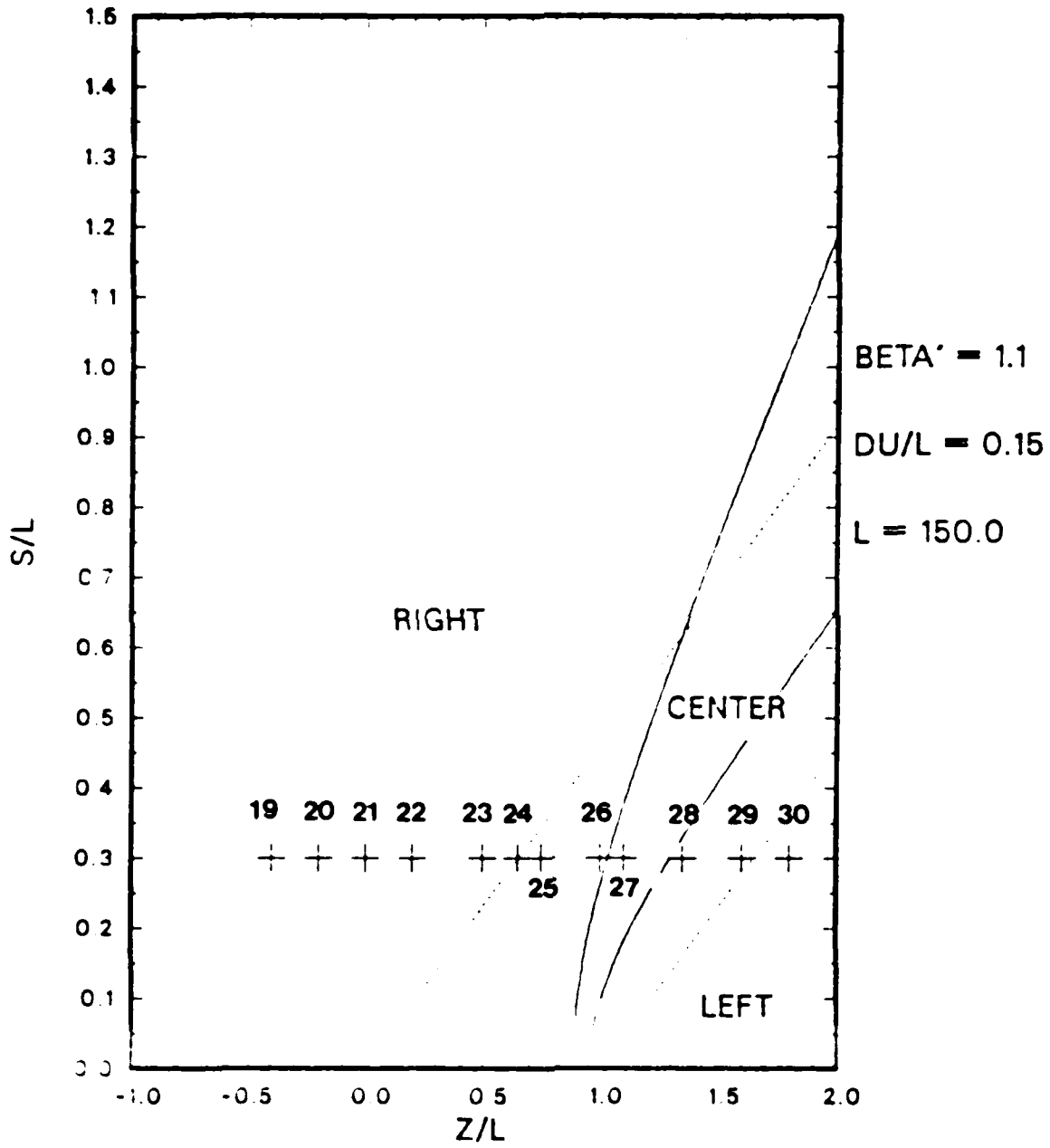


Figure 3 21 The S-Z Plane.

TIME LINES

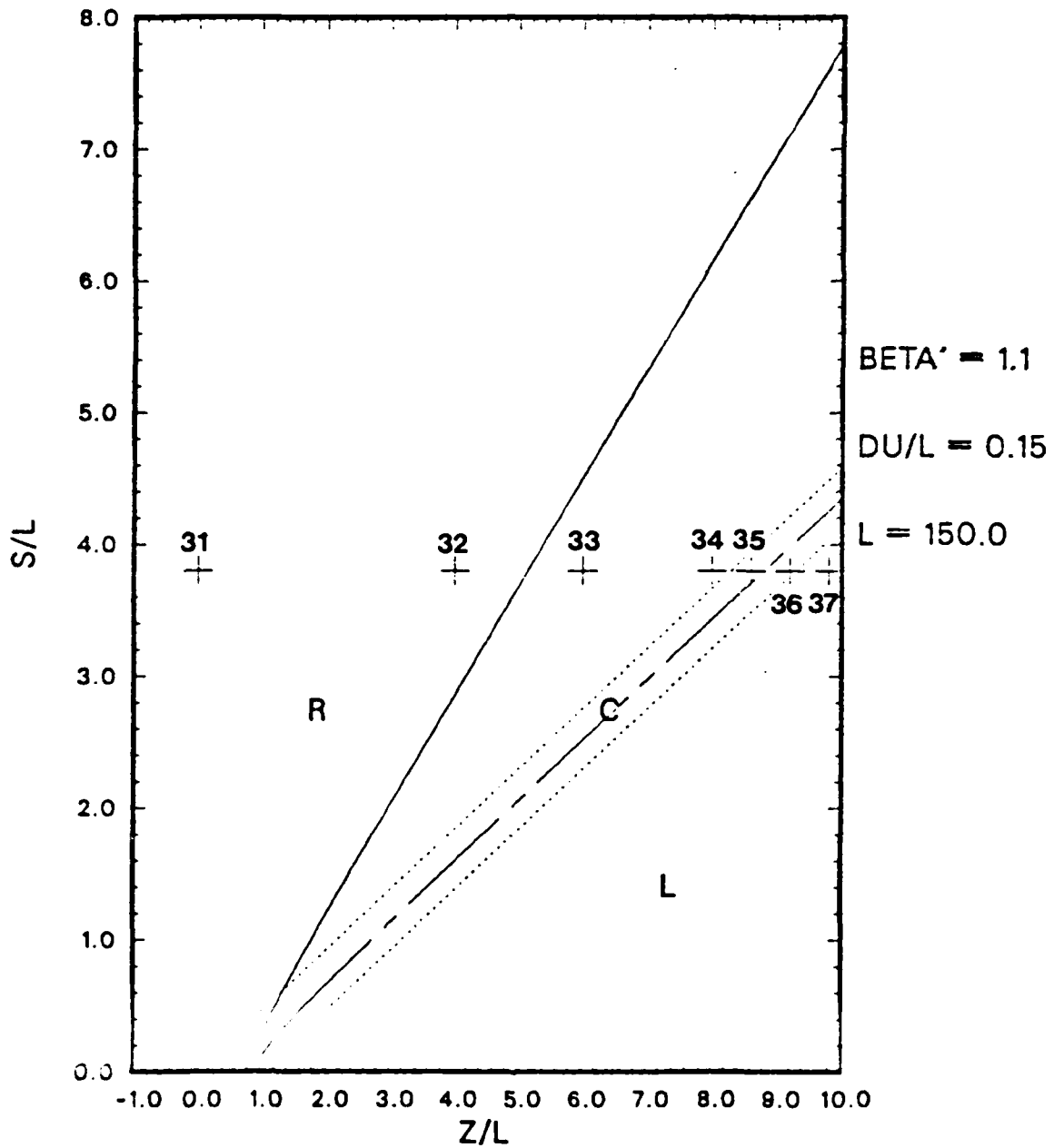


Figure 3.22 The S-Z Plane.

CERENKOV PULSE

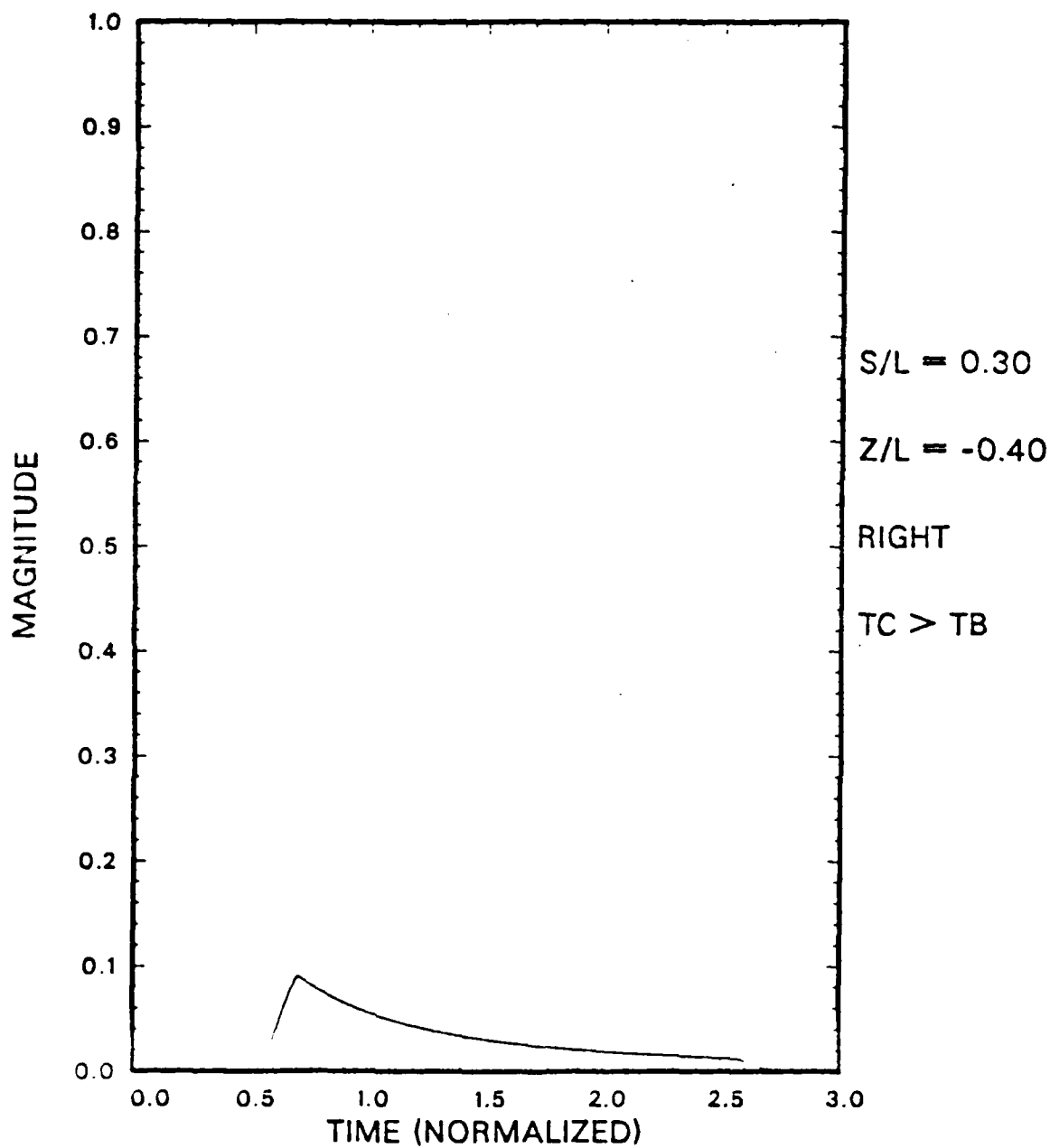


Figure 3.23 From Figure 3.21: Pulse 19.

CERENKOV PULSE

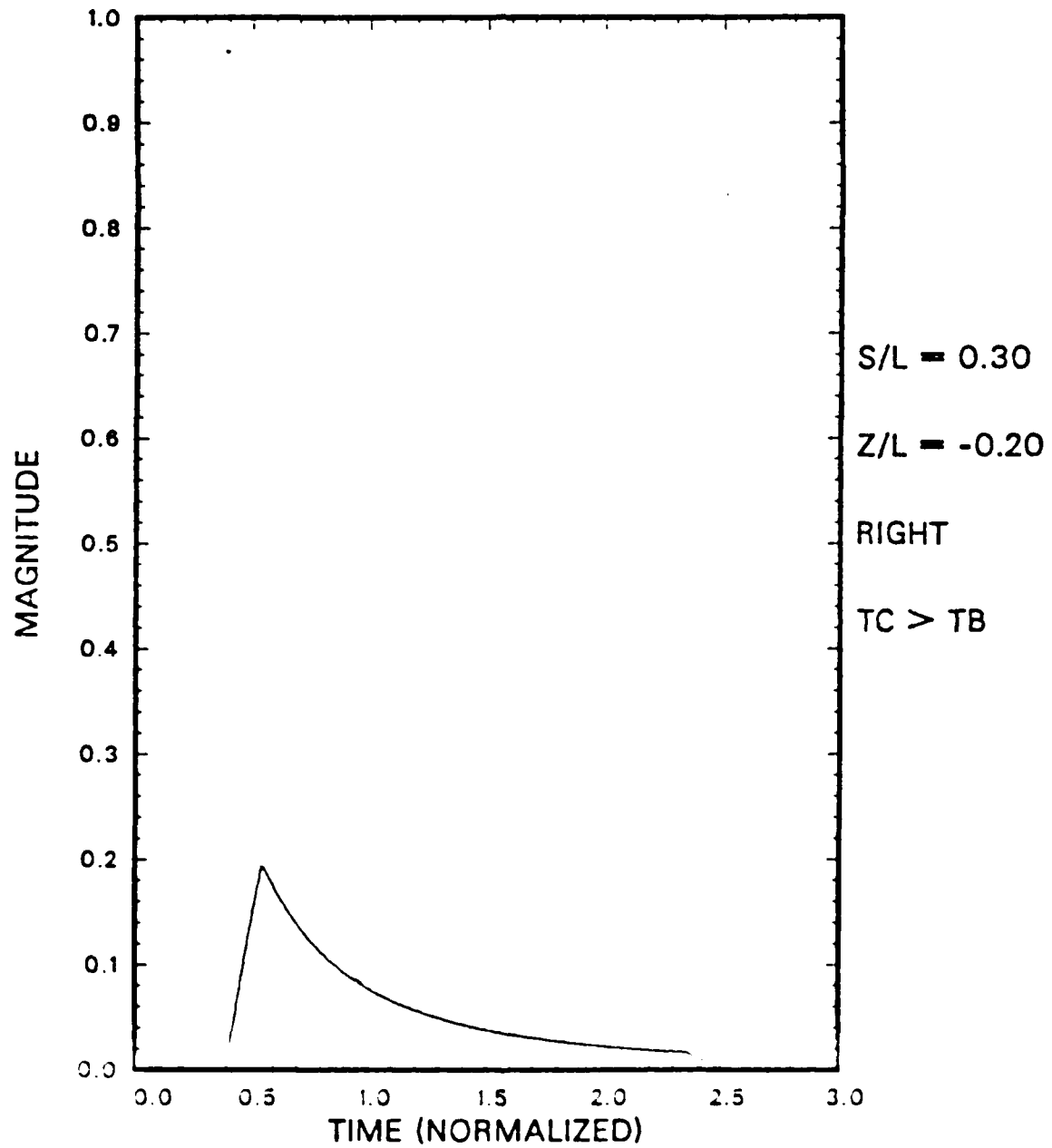


Figure 3.24 From Figure 3.21: Pulse 20.

CERENKOV PULSE

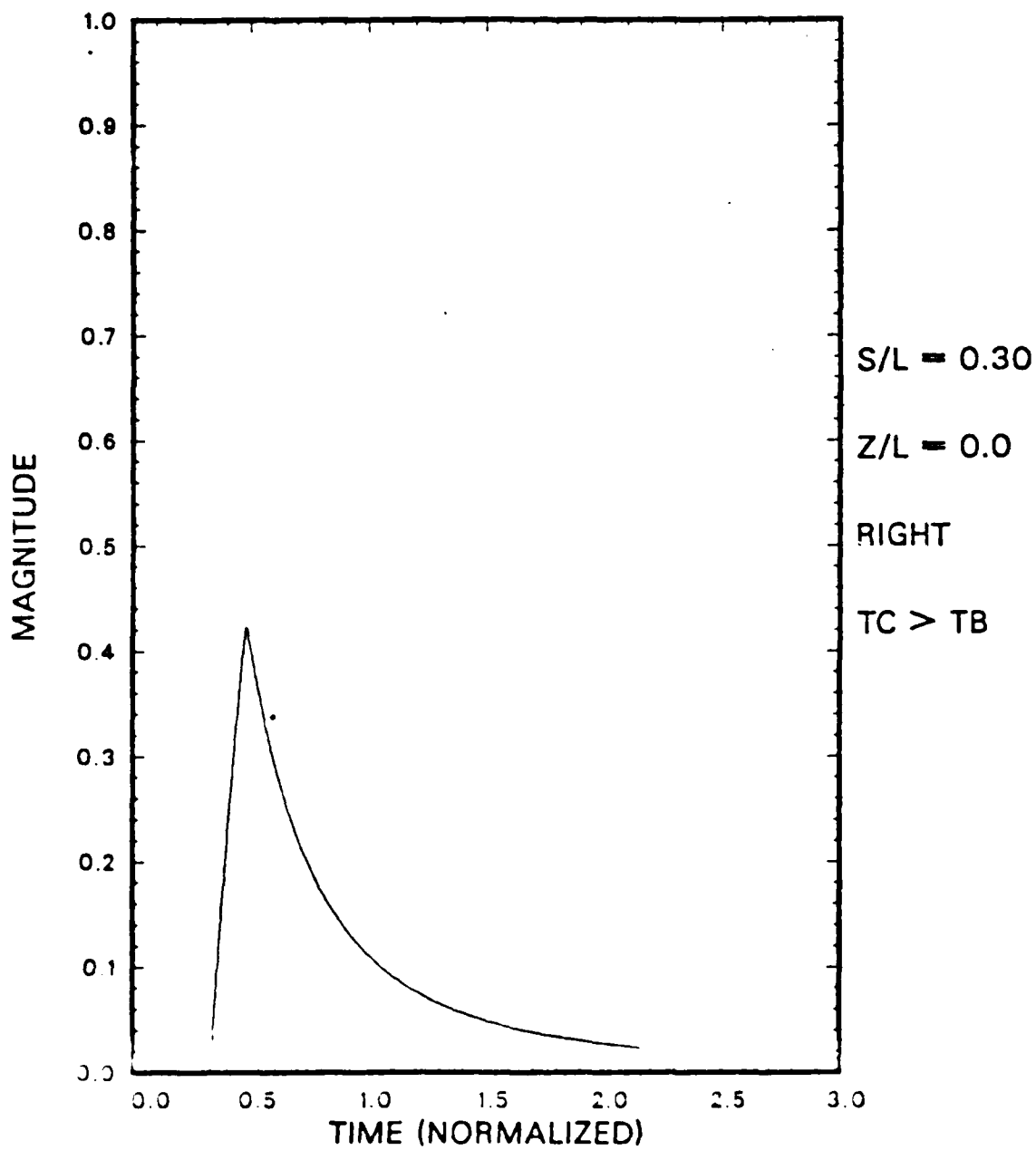


Figure 3.25 From Figure 3.21: Pulse 21.

CERENKOV PULSE

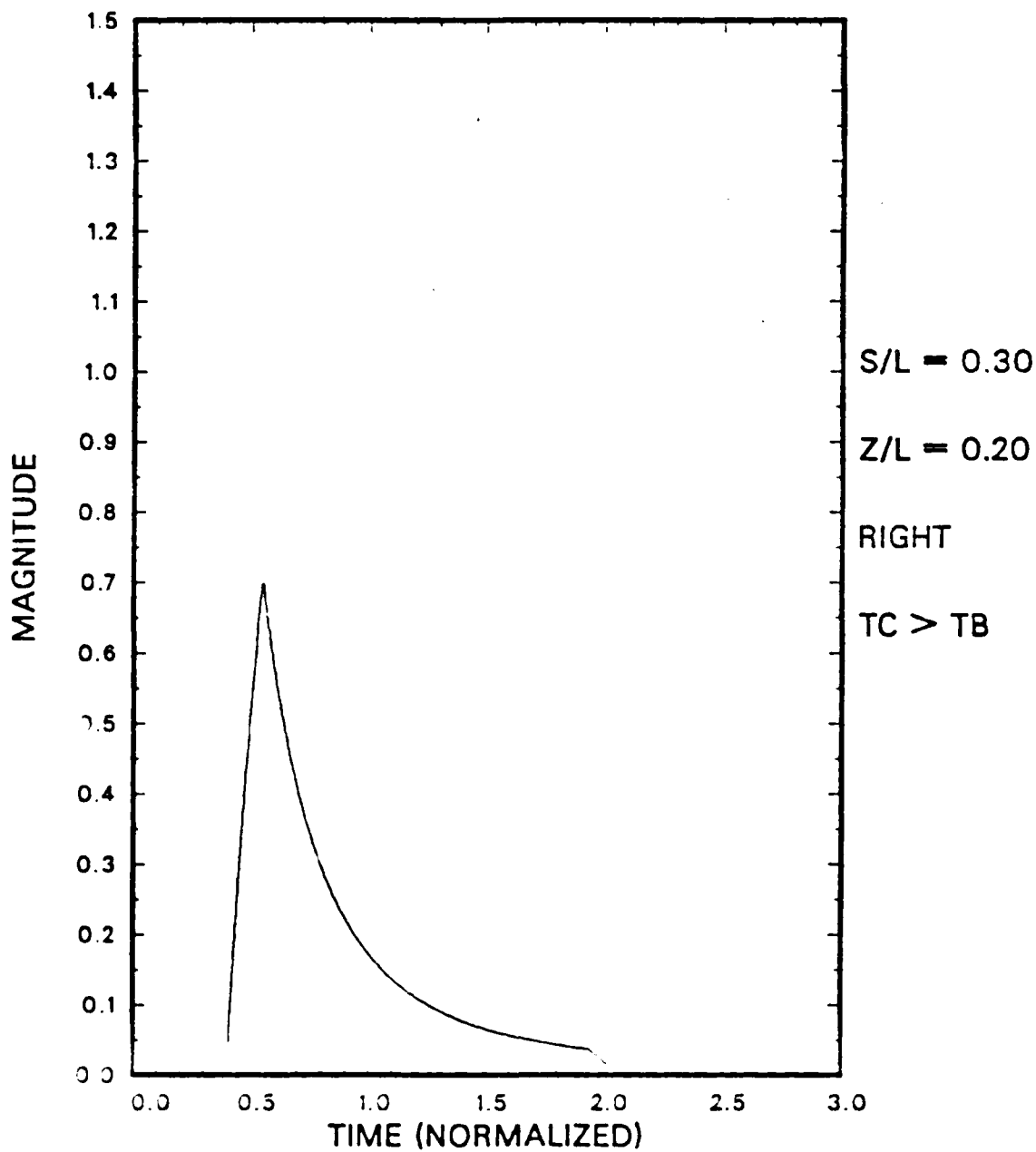


Figure 3.26 From Figure 3.21: Pulse 22.

CERENKOV PULSE

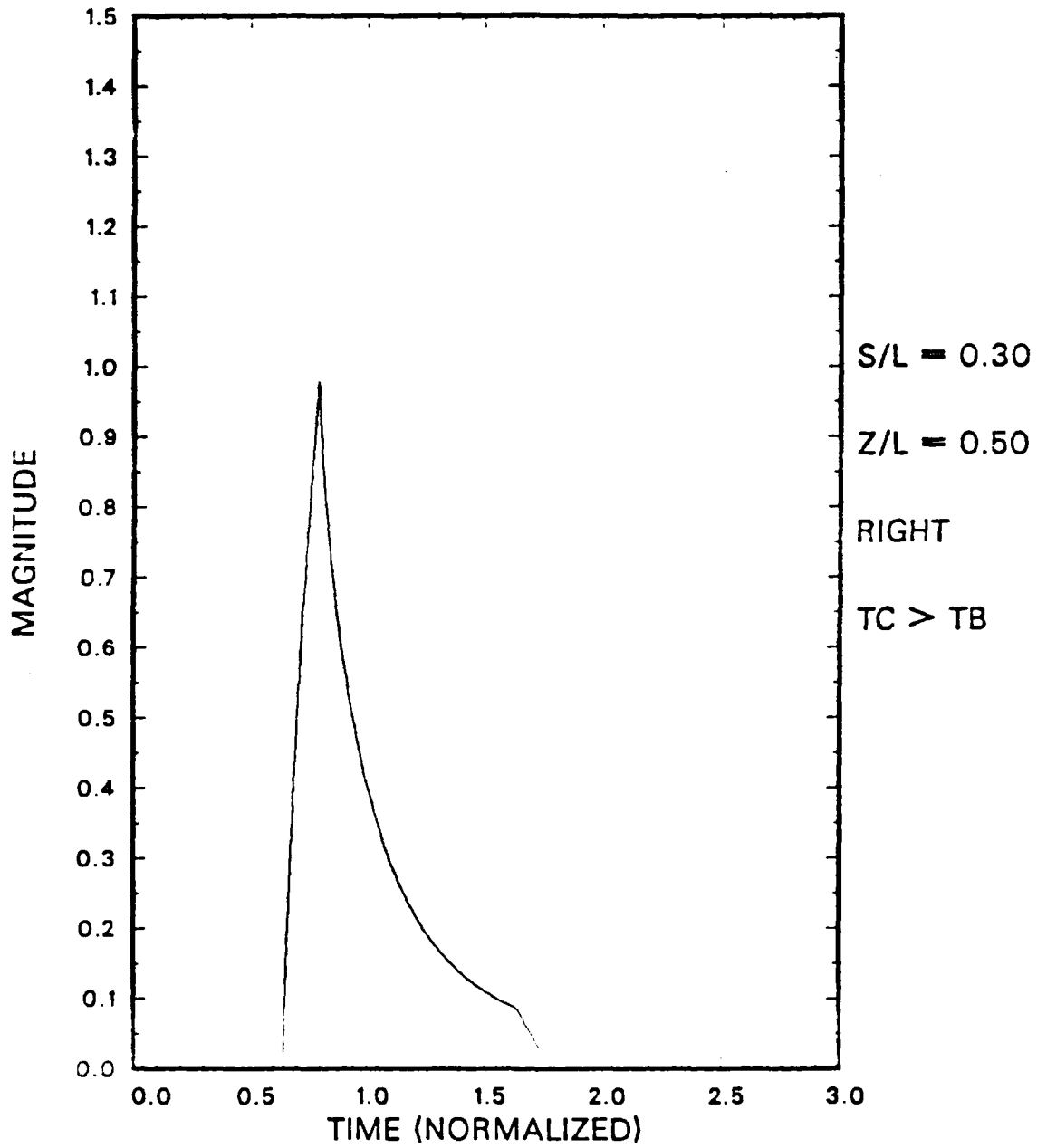


Figure 3.27 From Figure 3.21: Pulse 23.

CERENKOV PULSE

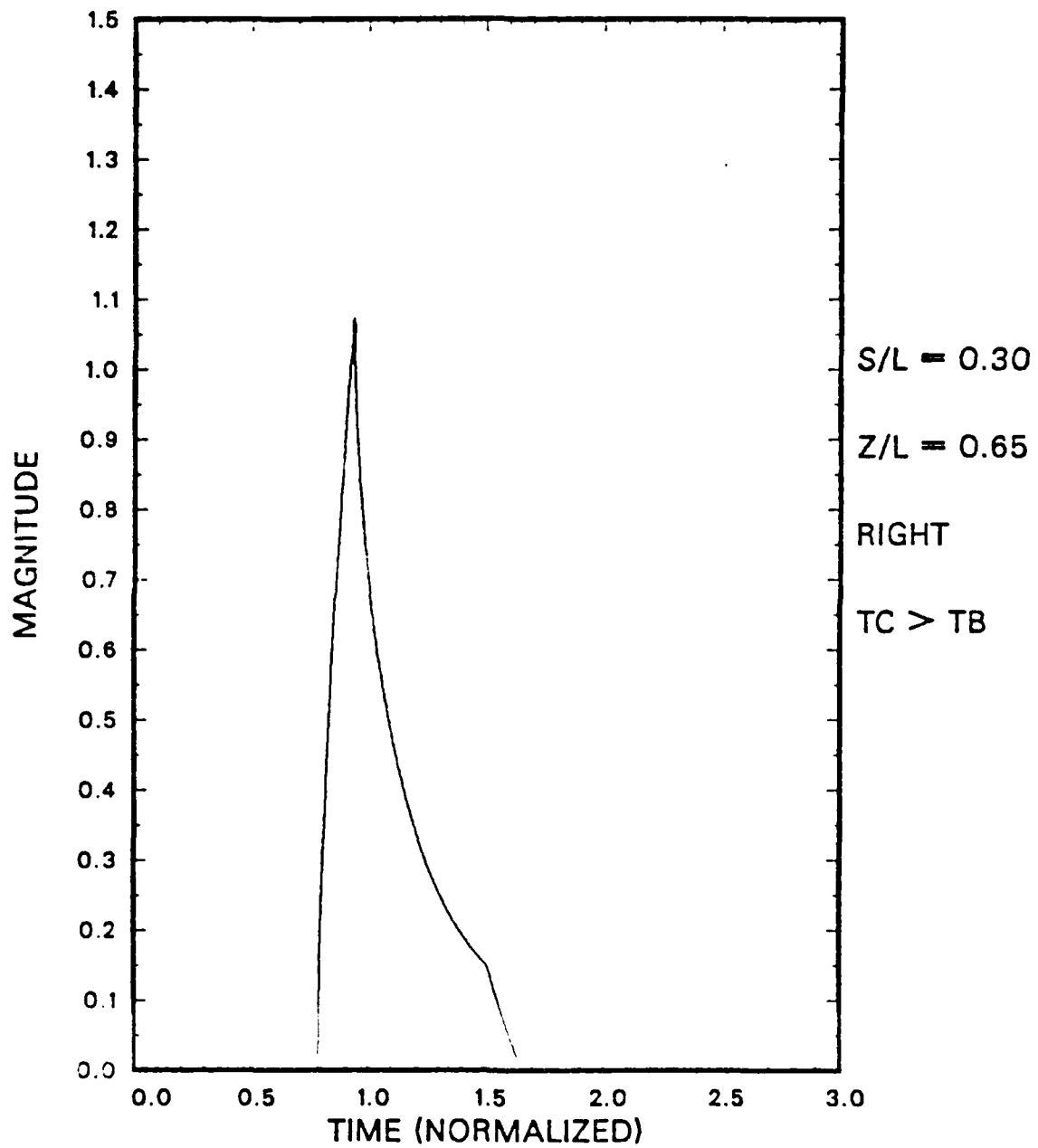


Figure 3.28 From Figure 3.21: Pulse 24.

CERENKOV PULSE

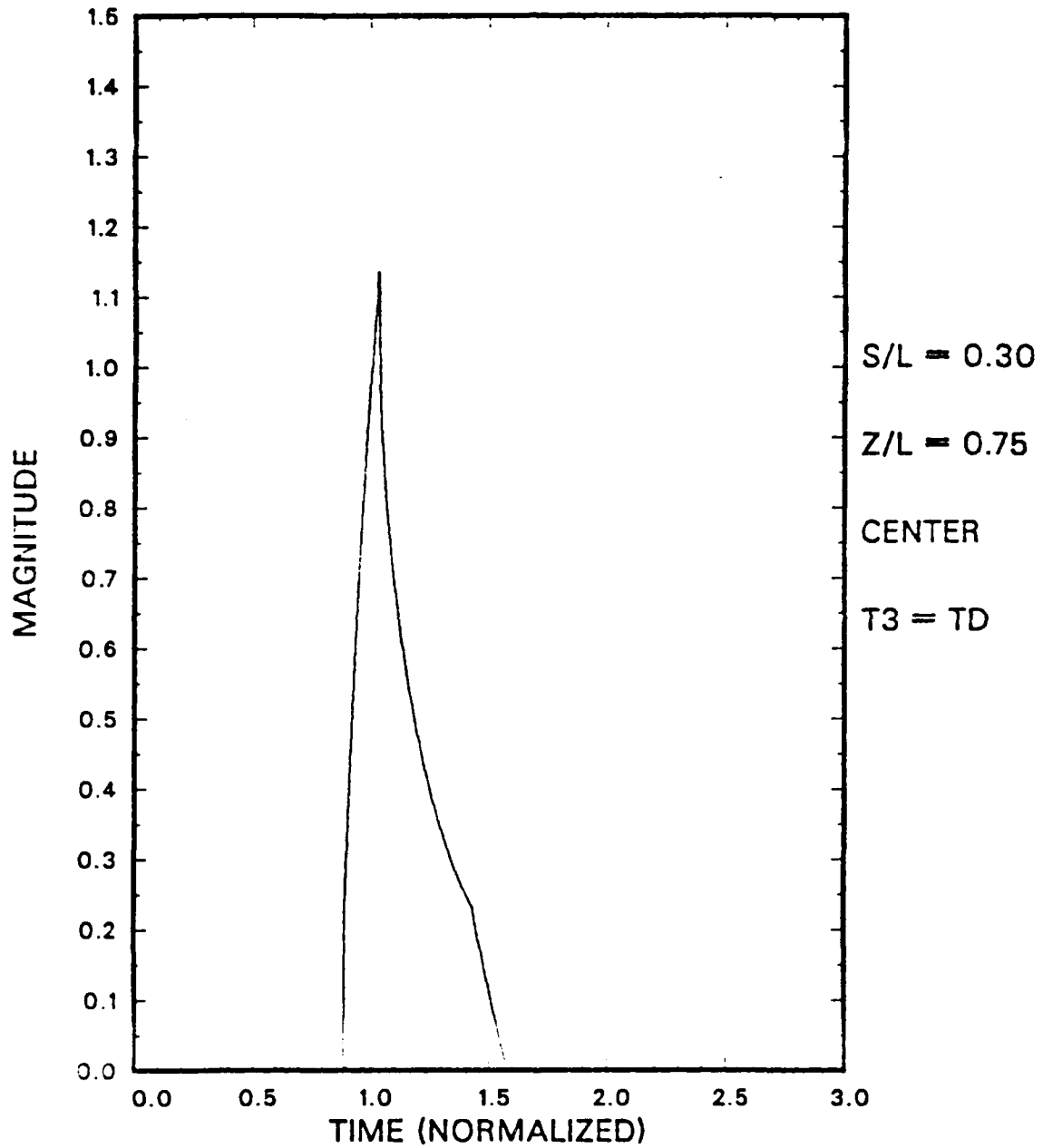


Figure 3.29 From Figure 3.21: Pulse 25.

CERENKOV PULSE

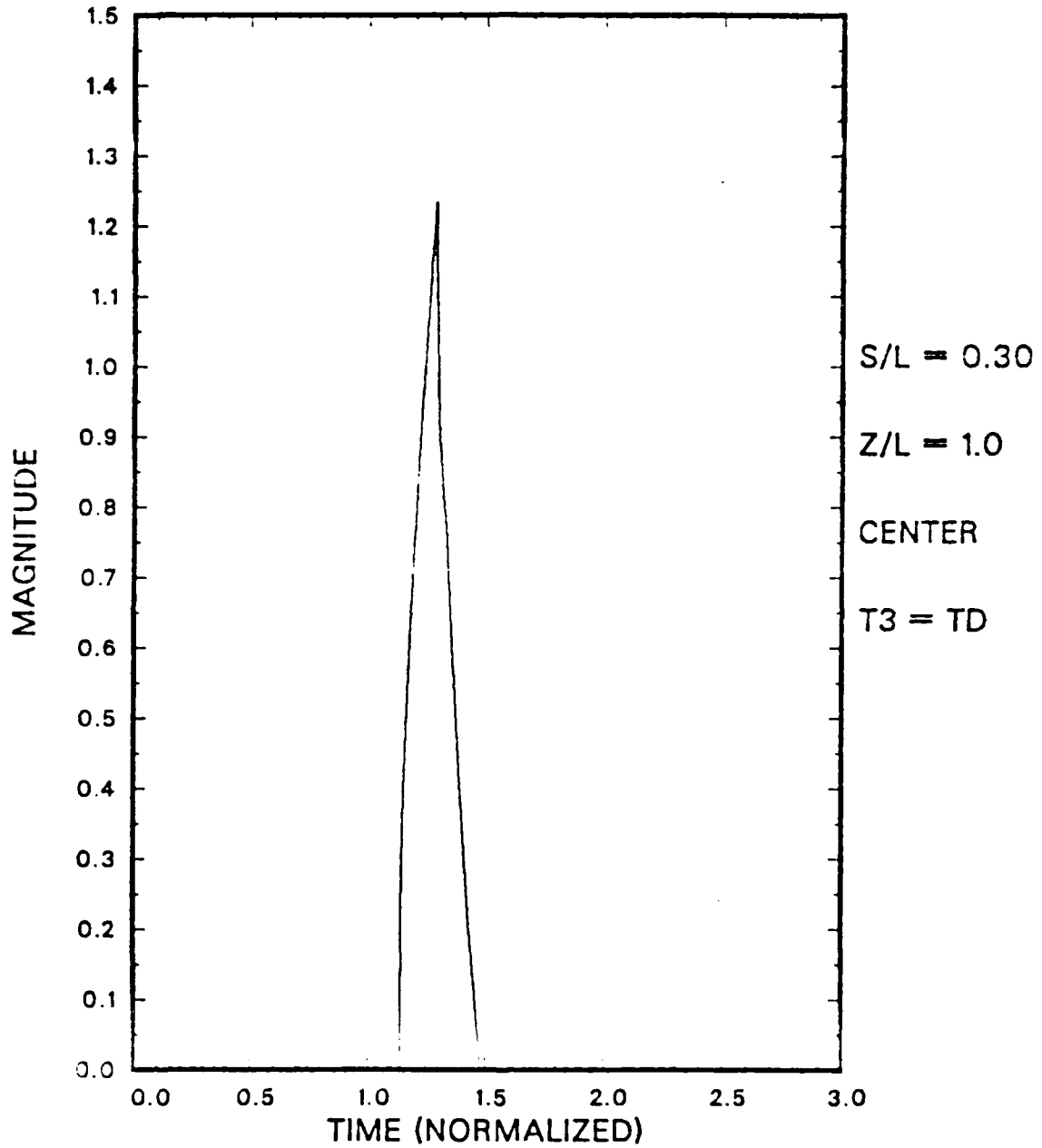


Figure 3.30 From Figure 3.21: Pulse 26.

CERENKOV PULSE

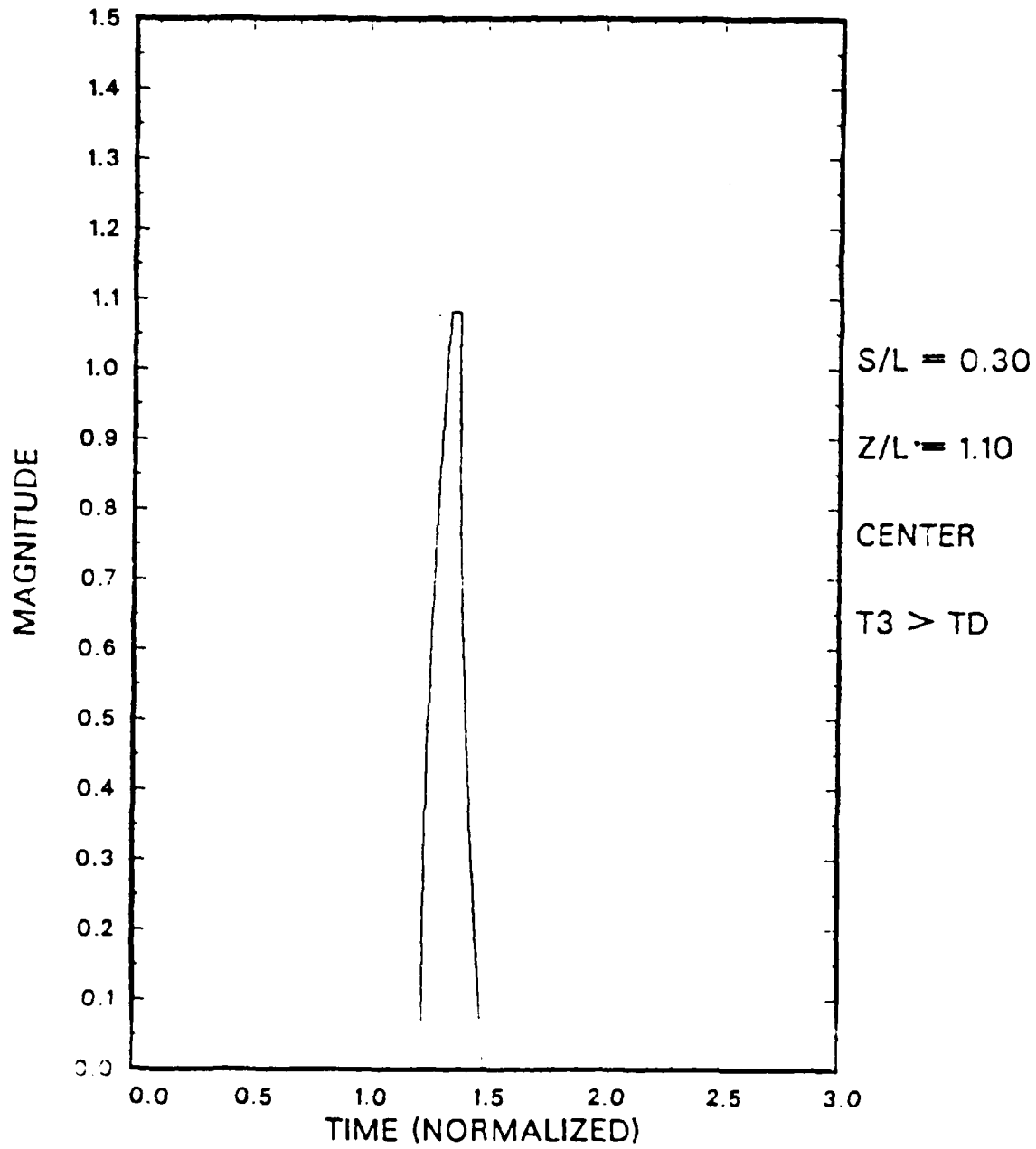


Figure 3.31 From Figure 3.21: Pulse 27.

CERENKOV PULSE

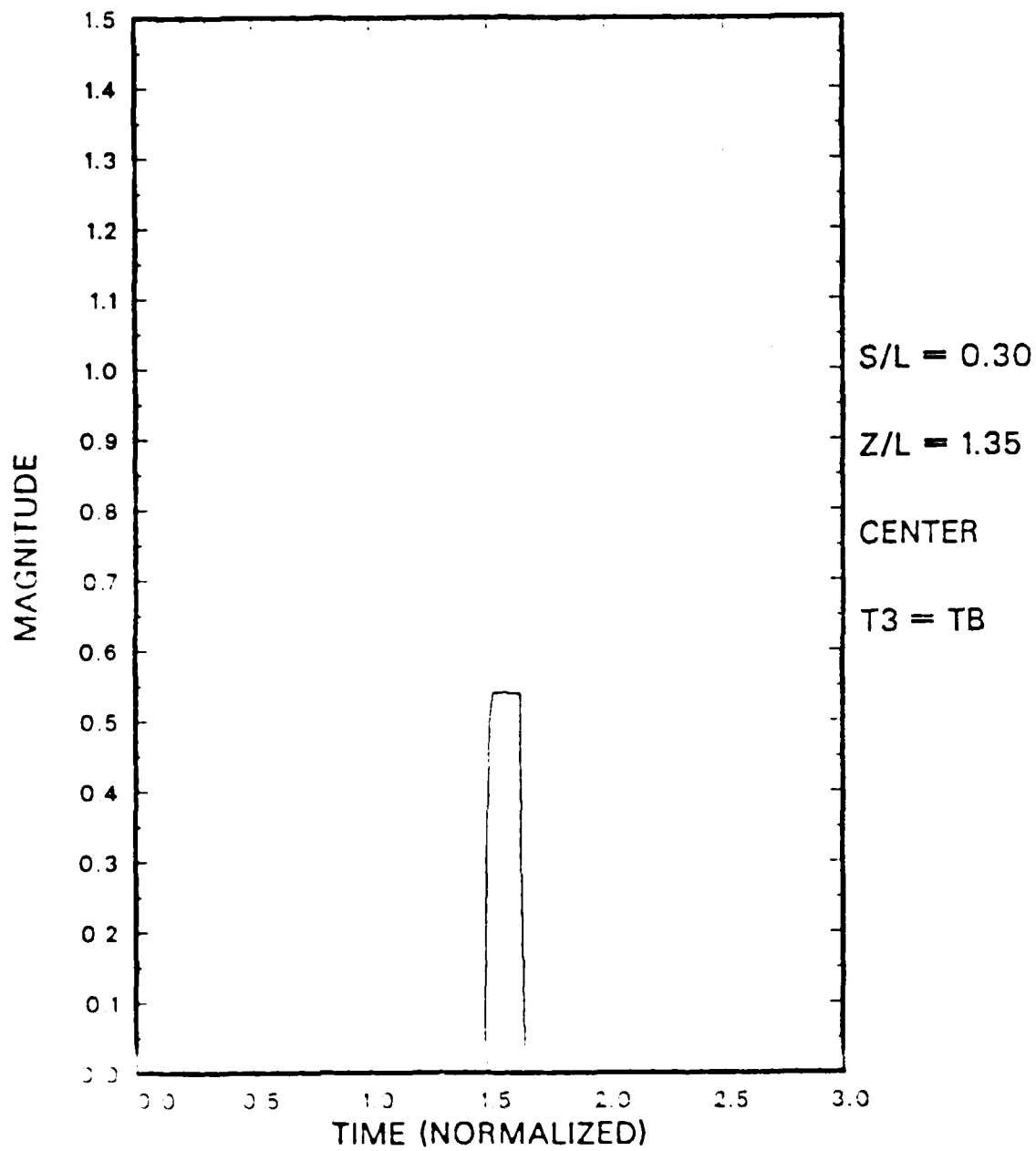


Figure 3.32 From Figure 3.21: Pulse 28.

CERENKOV PULSE

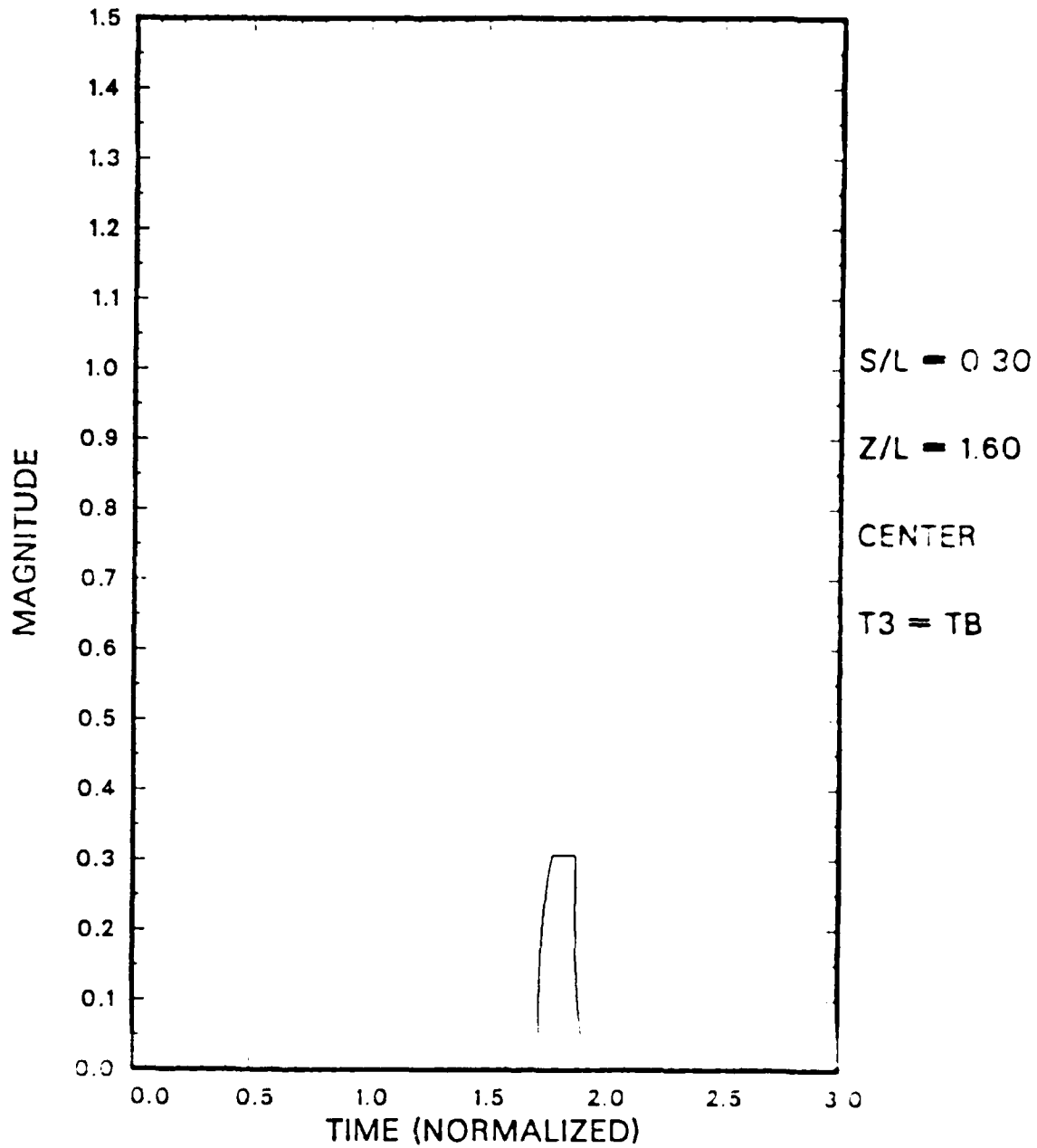
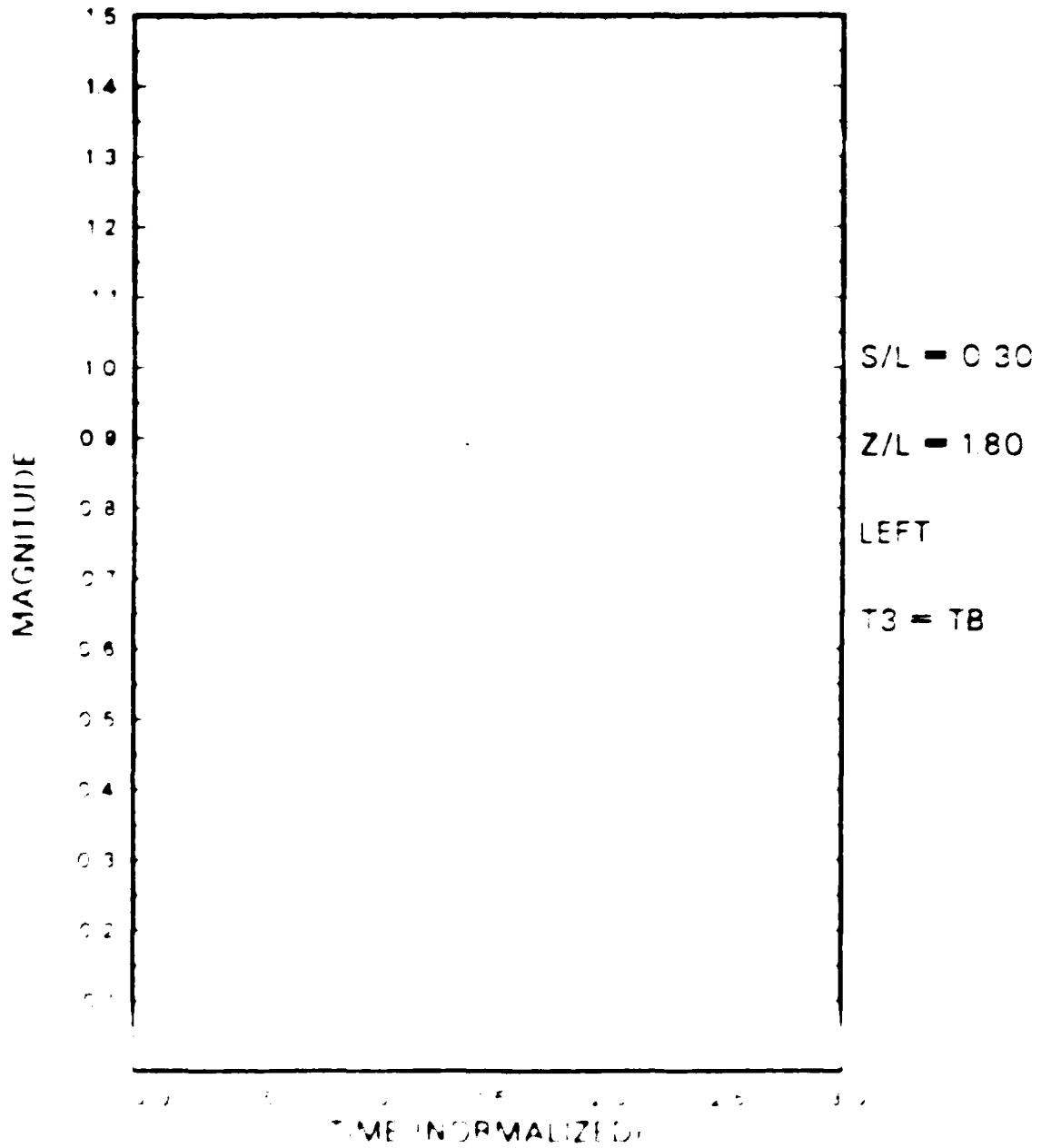


Figure 3.33 From Figure 3.21: Pulse 29.

CERENKOV PULSE



CERENKOV PULSE

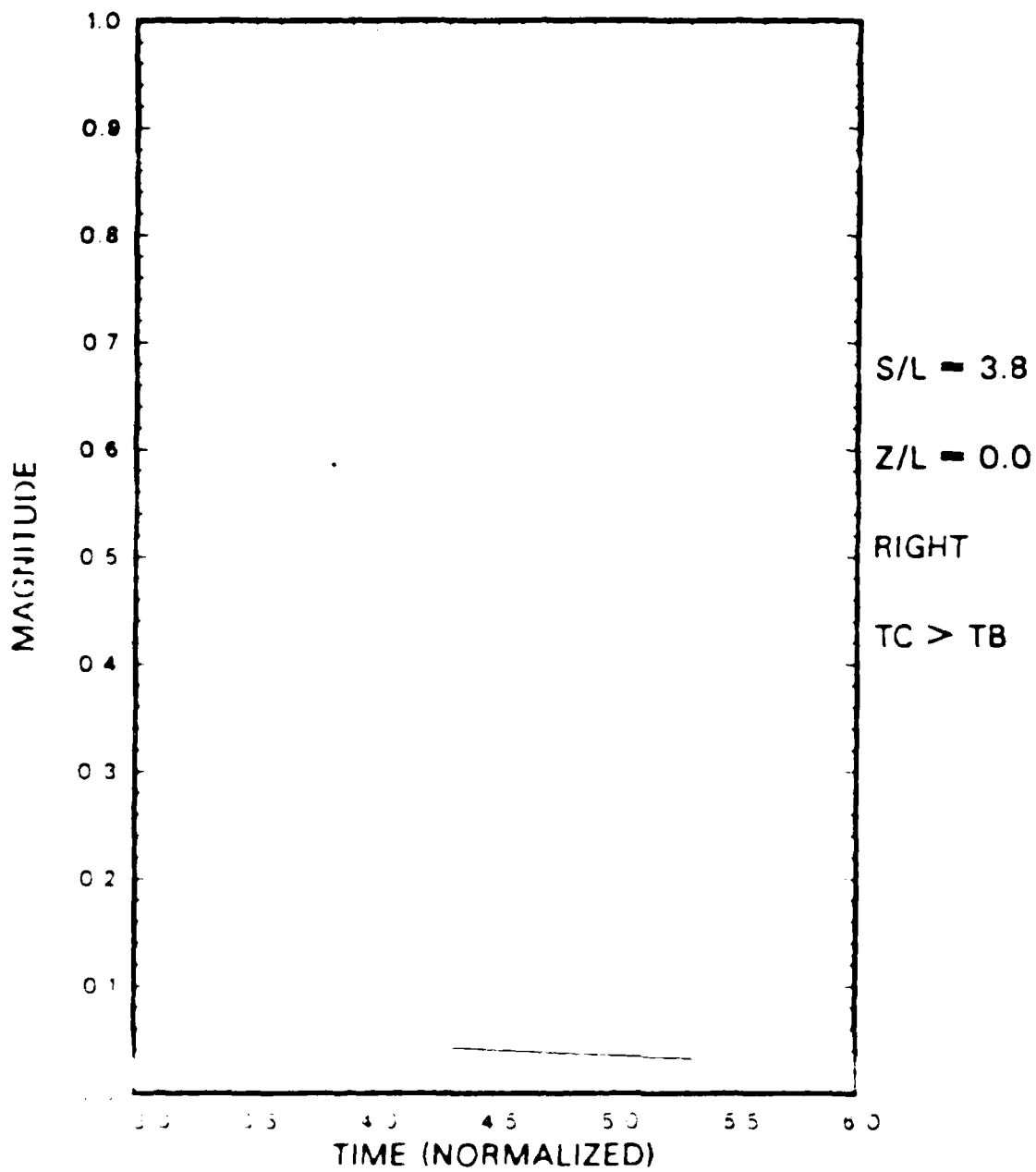


Figure 3.35 - From Figure 3.22 - Pulse 31

CERENKOV PULSE

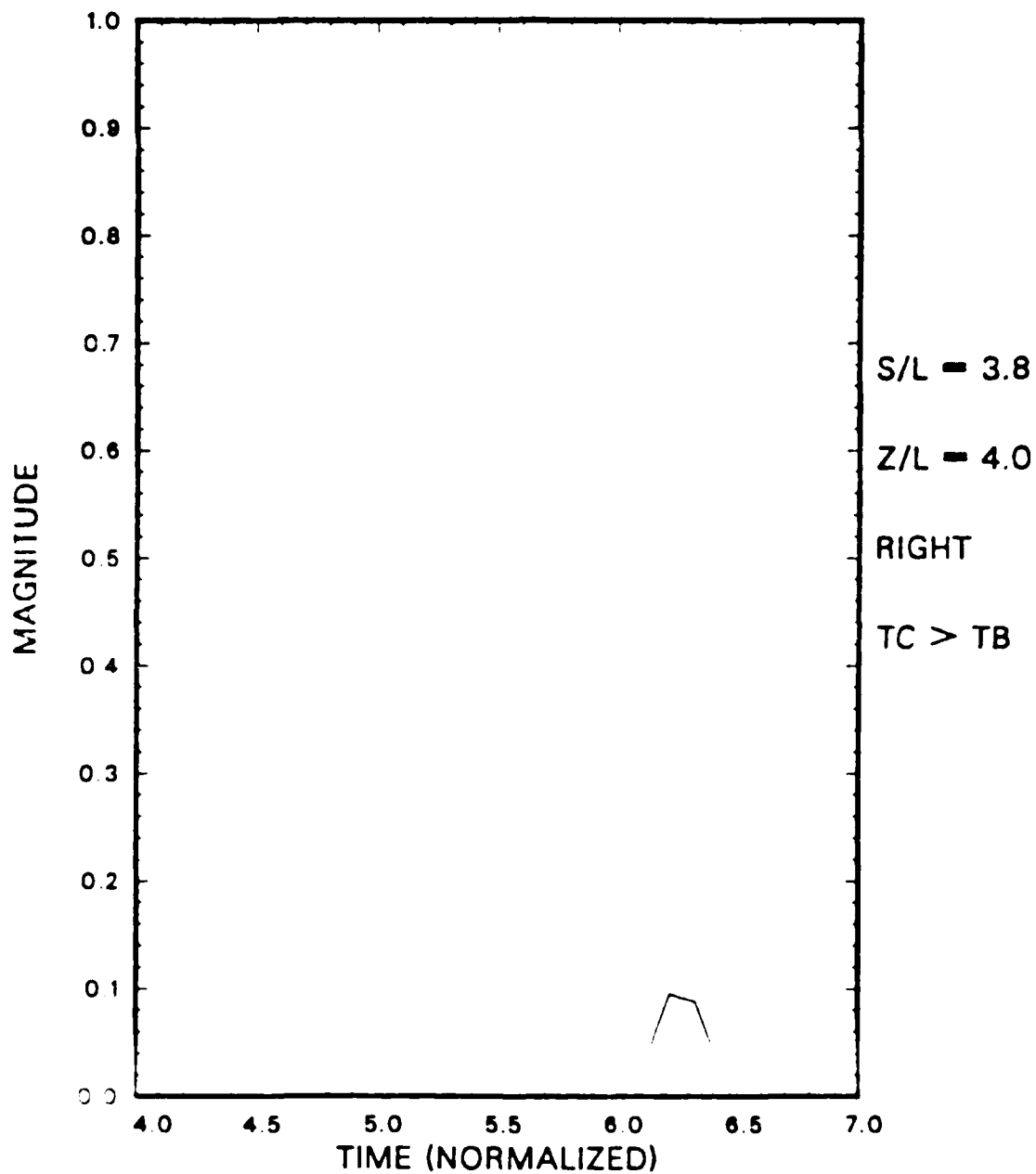


Figure 3.36 From Figure 3.22: Pulse 32.

CERENKOV PULSE

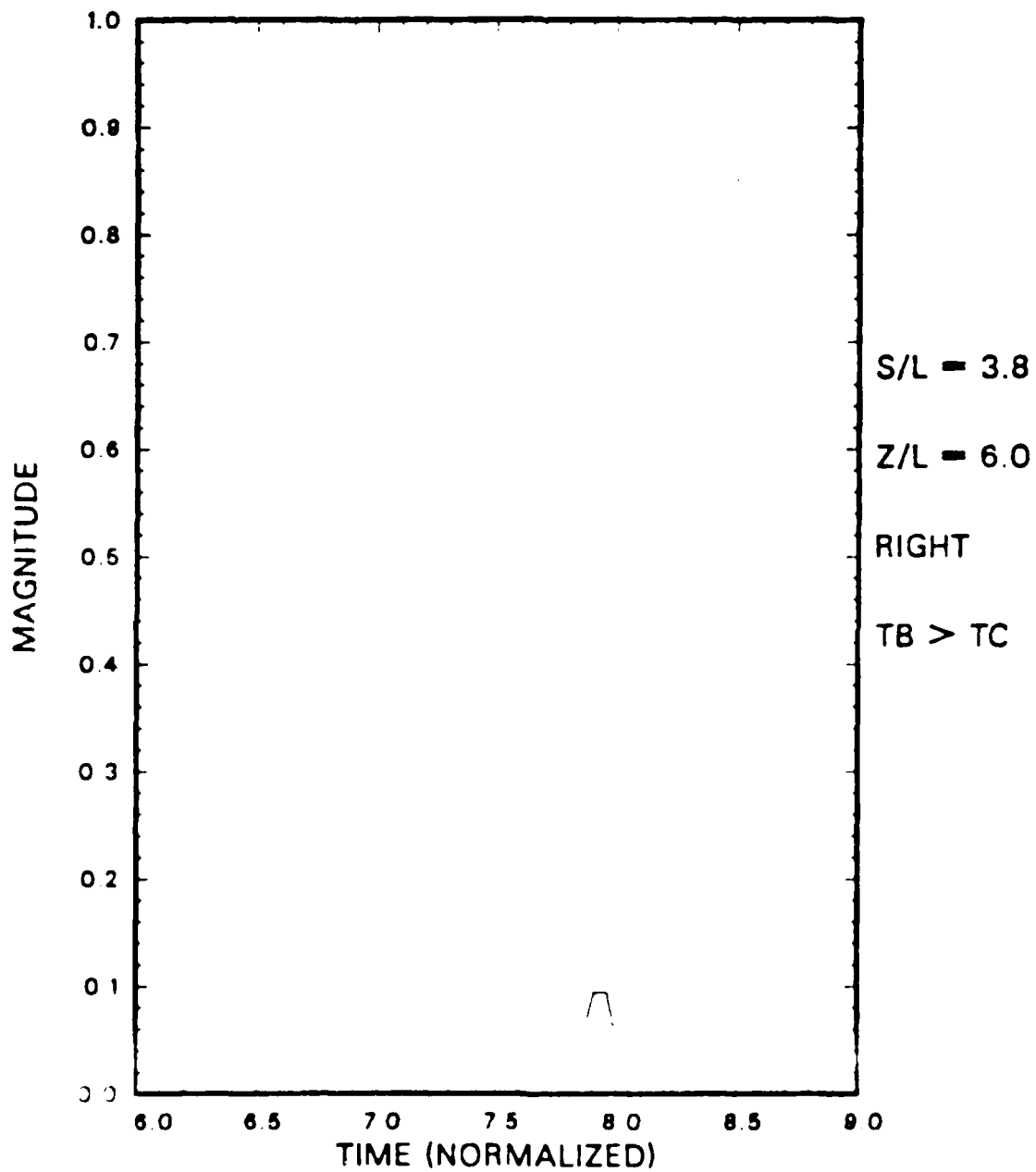


Figure 3.37 From Figure 3.22 Pulse 33.

CERENKOV PULSE

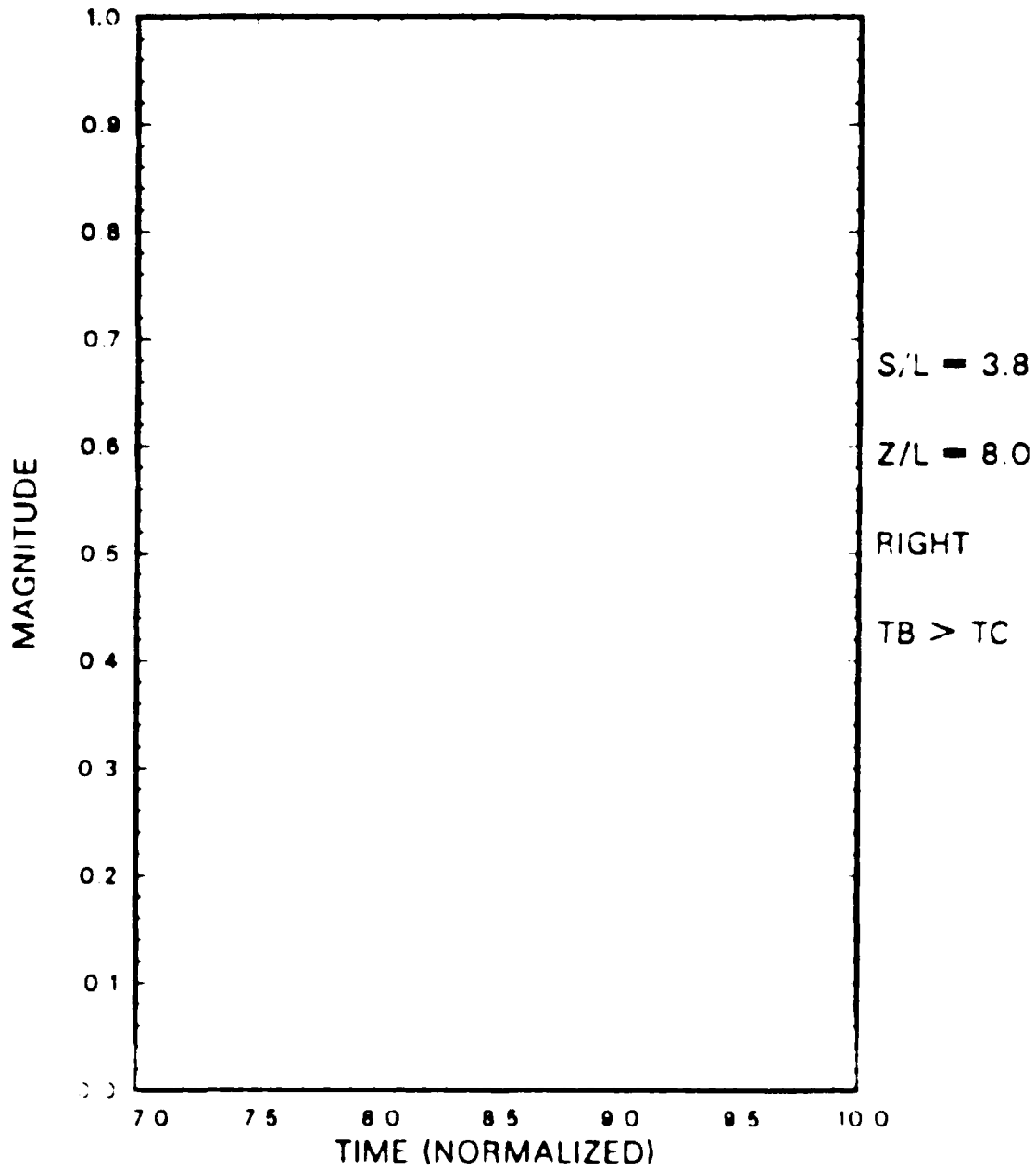


Figure 3.35 From Figure 3.22 Pulse 34

CERENKOV PULSE

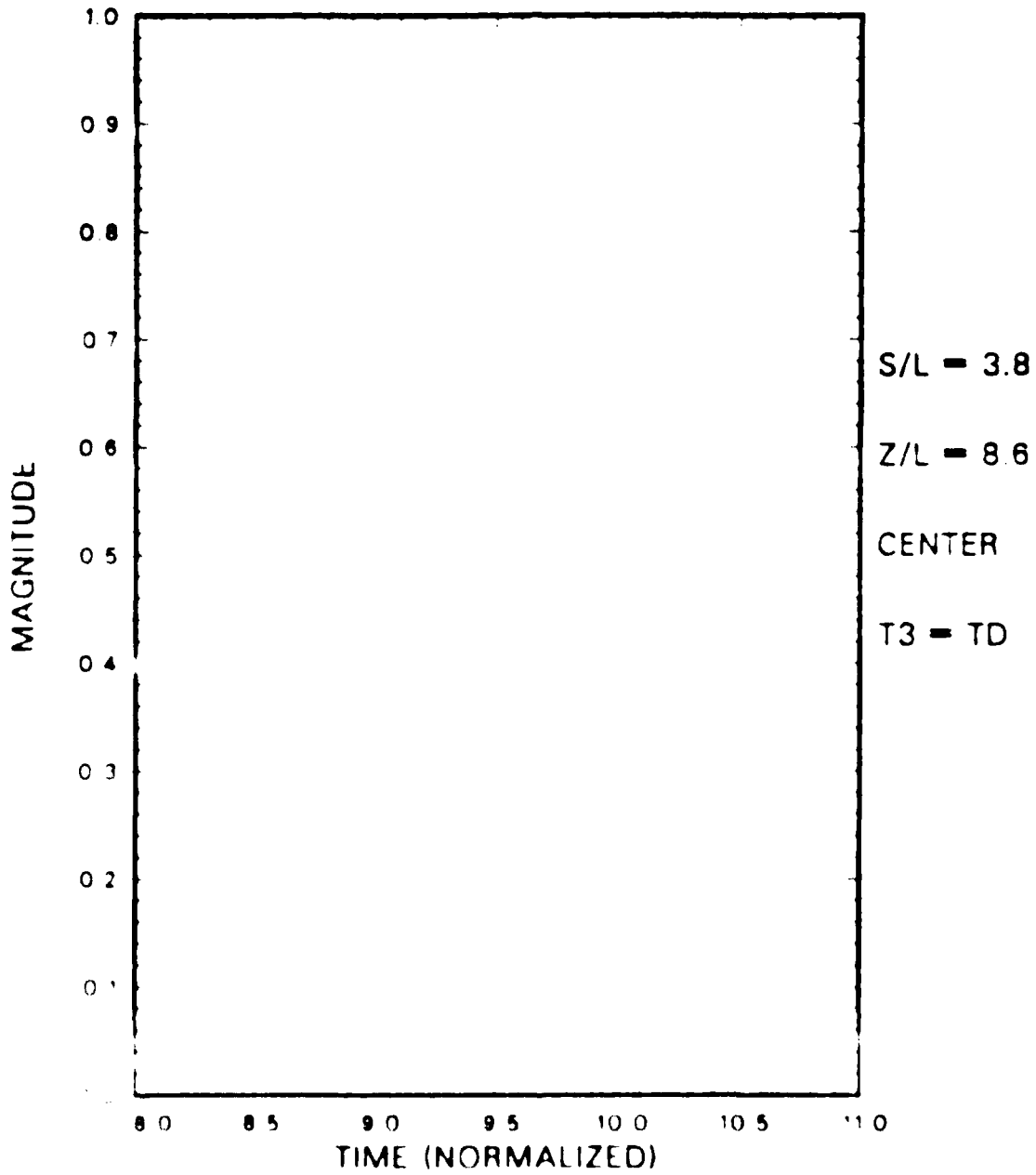


Figure 3.39. From Figure 3.22 Pulse 35

CERENKOV PULSE

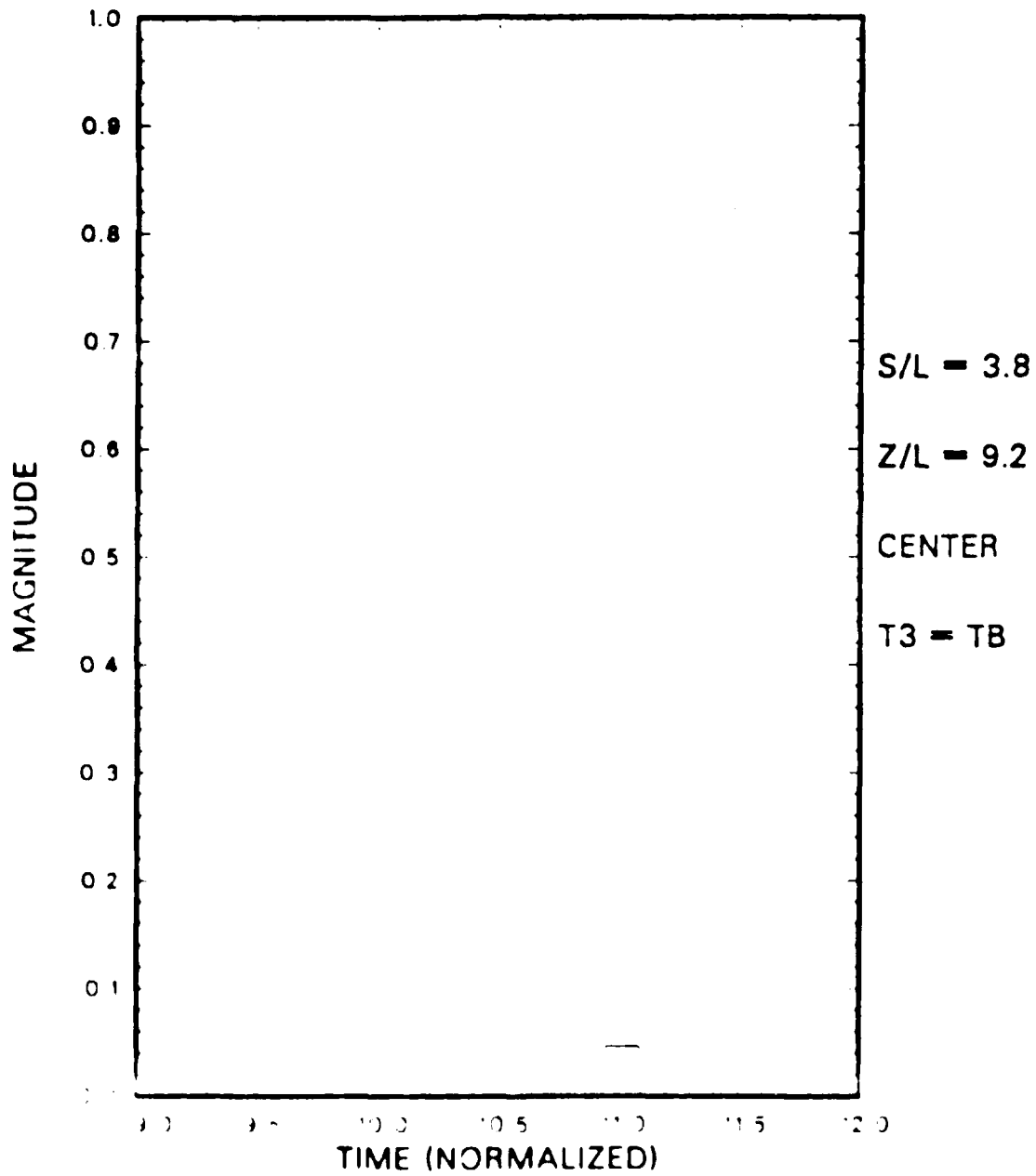


Figure 3.40 From Figure 3.22 Pulse 3c

CERENKOV PULSE

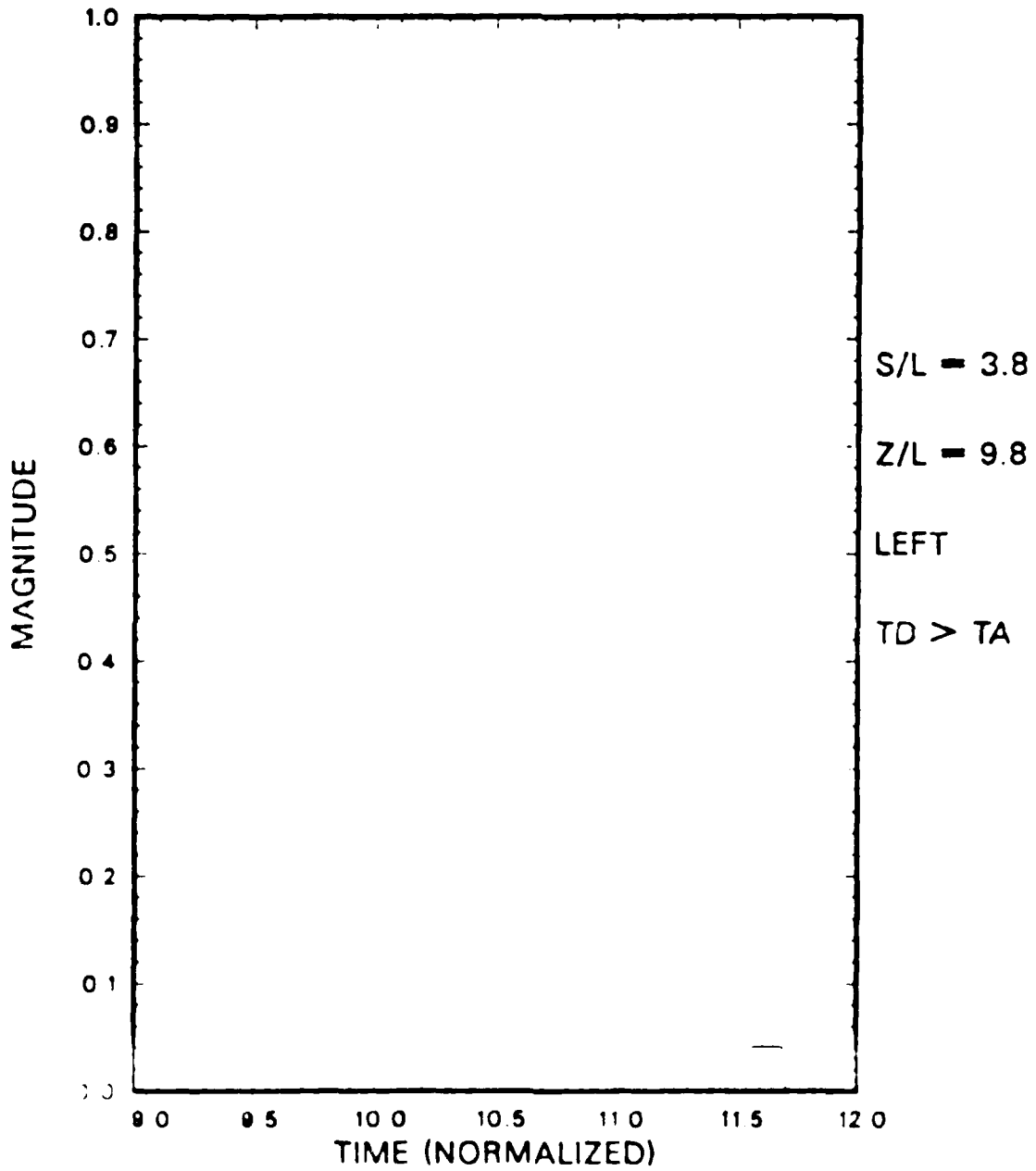


Figure 3-41 From Figure 3-22: Pulse 37.

TIME LINES

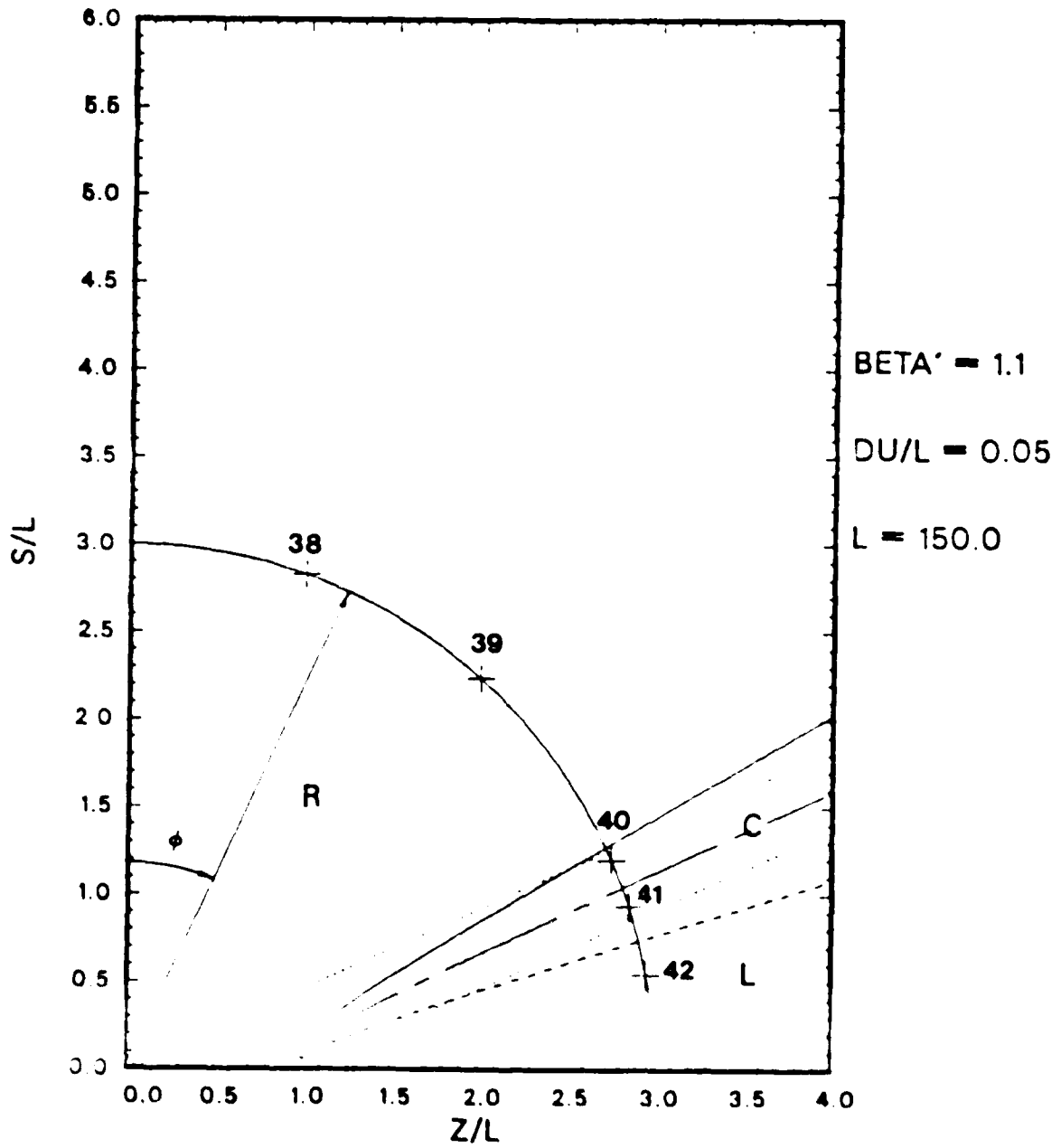


Figure 3.42 Equal Distance Points-Close Field.

TIME LINES

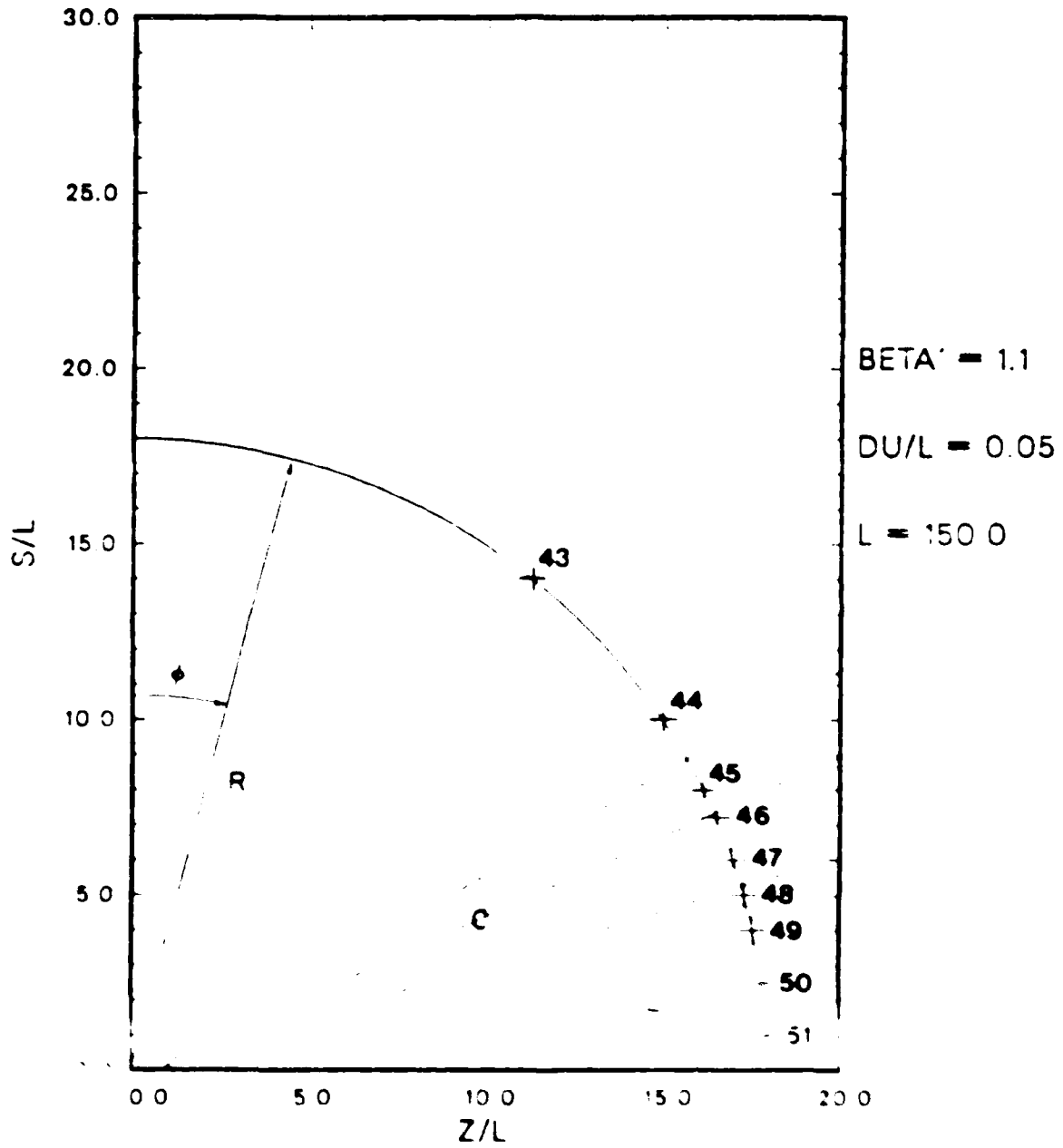


Figure 3-43: Equi-Dimensional Paths for $BETA' = 1.1$

CERENKOV PULSE

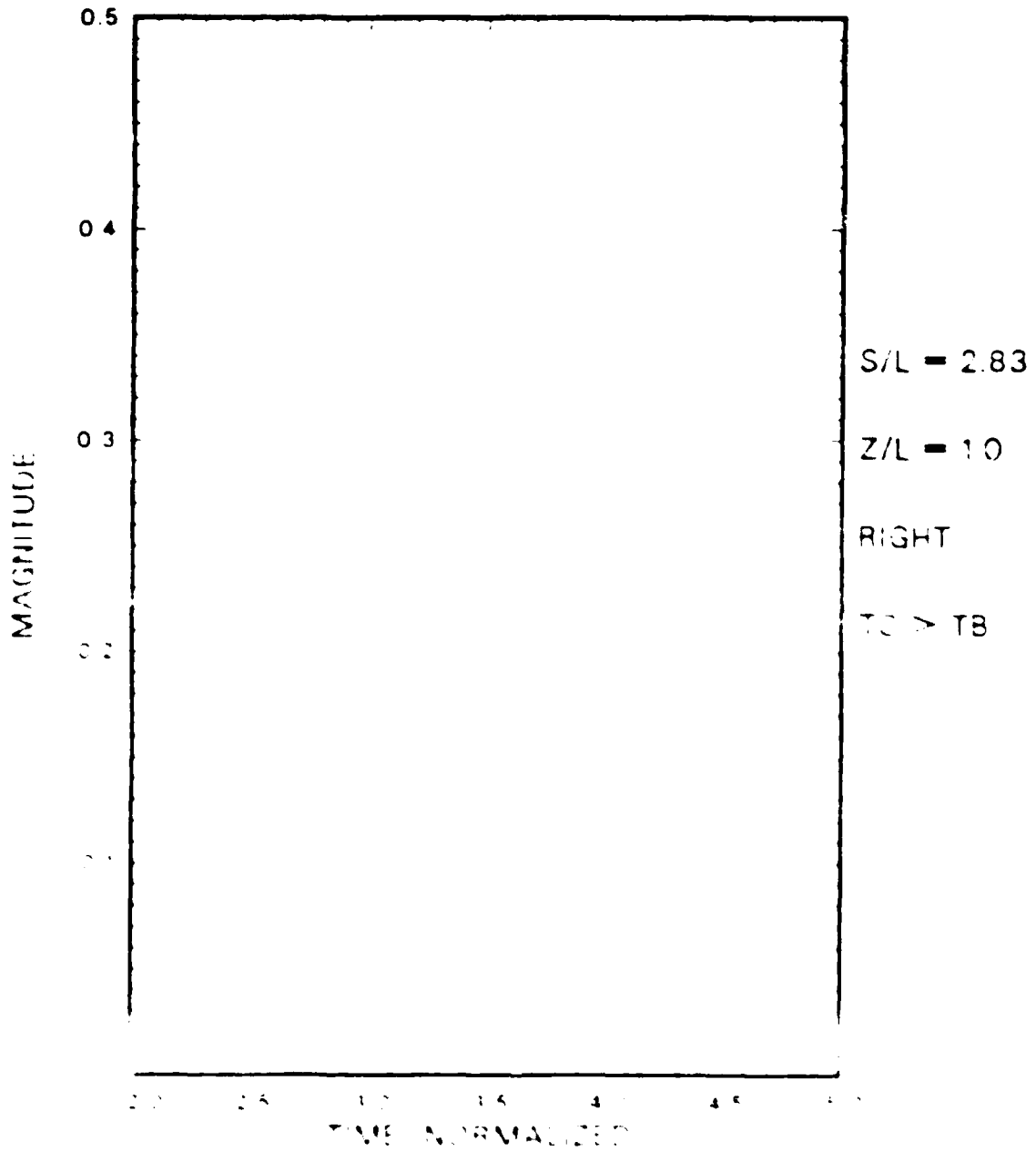
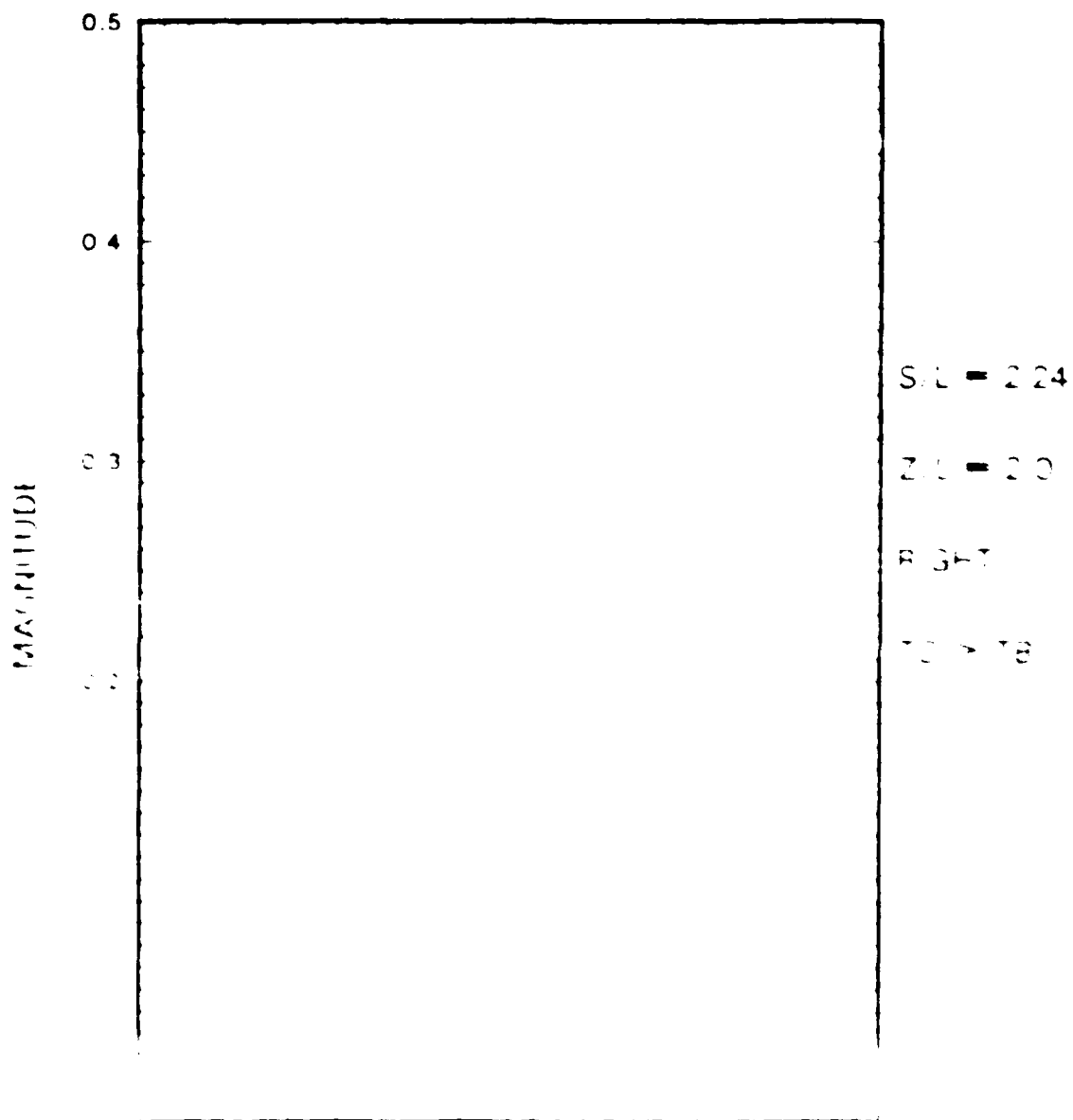


Figure 14. A Cerenkov Pulse

CERENKOV PULSE



45

CERENKOV PULSE

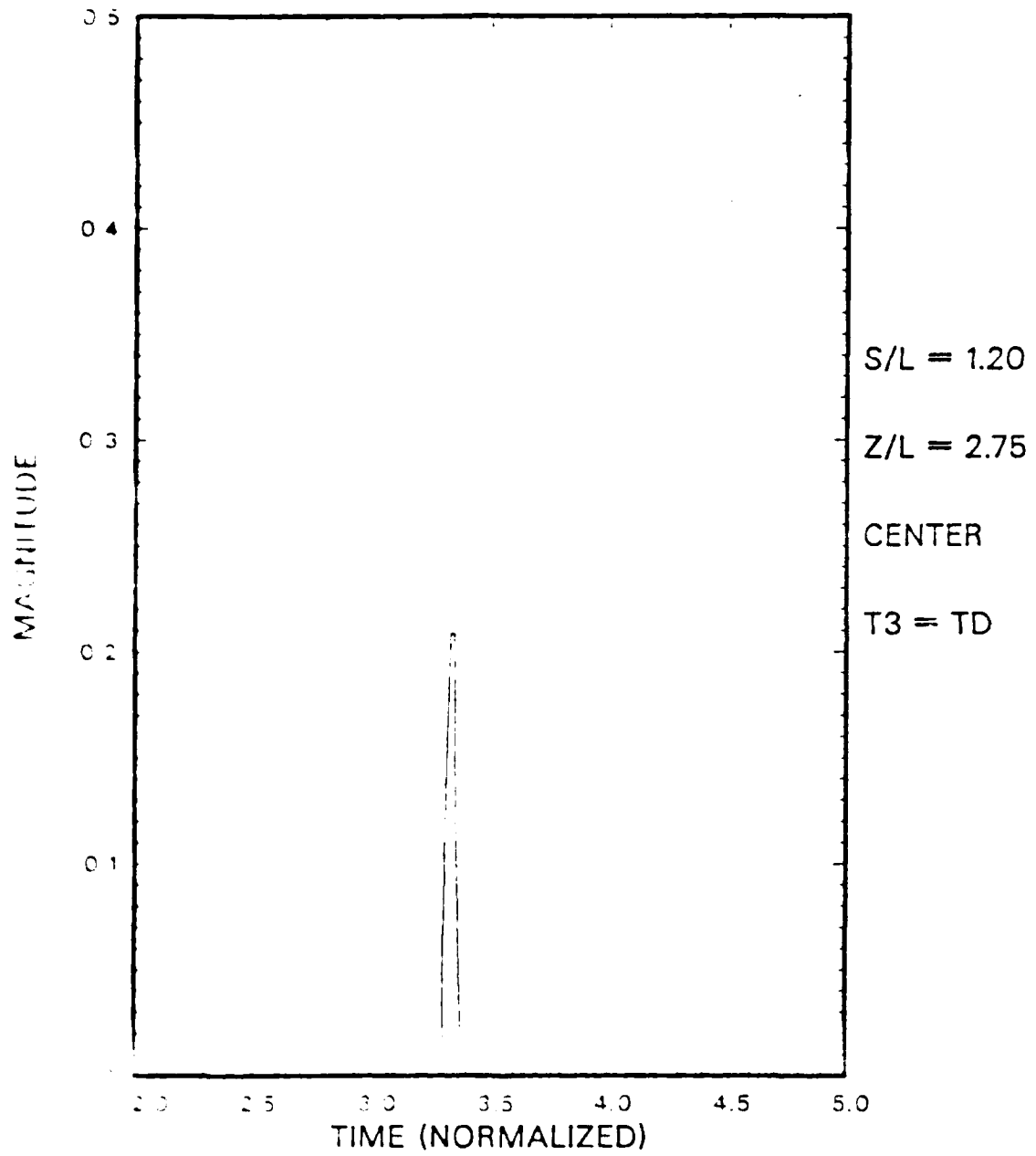


Figure 3.46 From Figure 3.42: Pulse 40.

CERENKOV PULSE

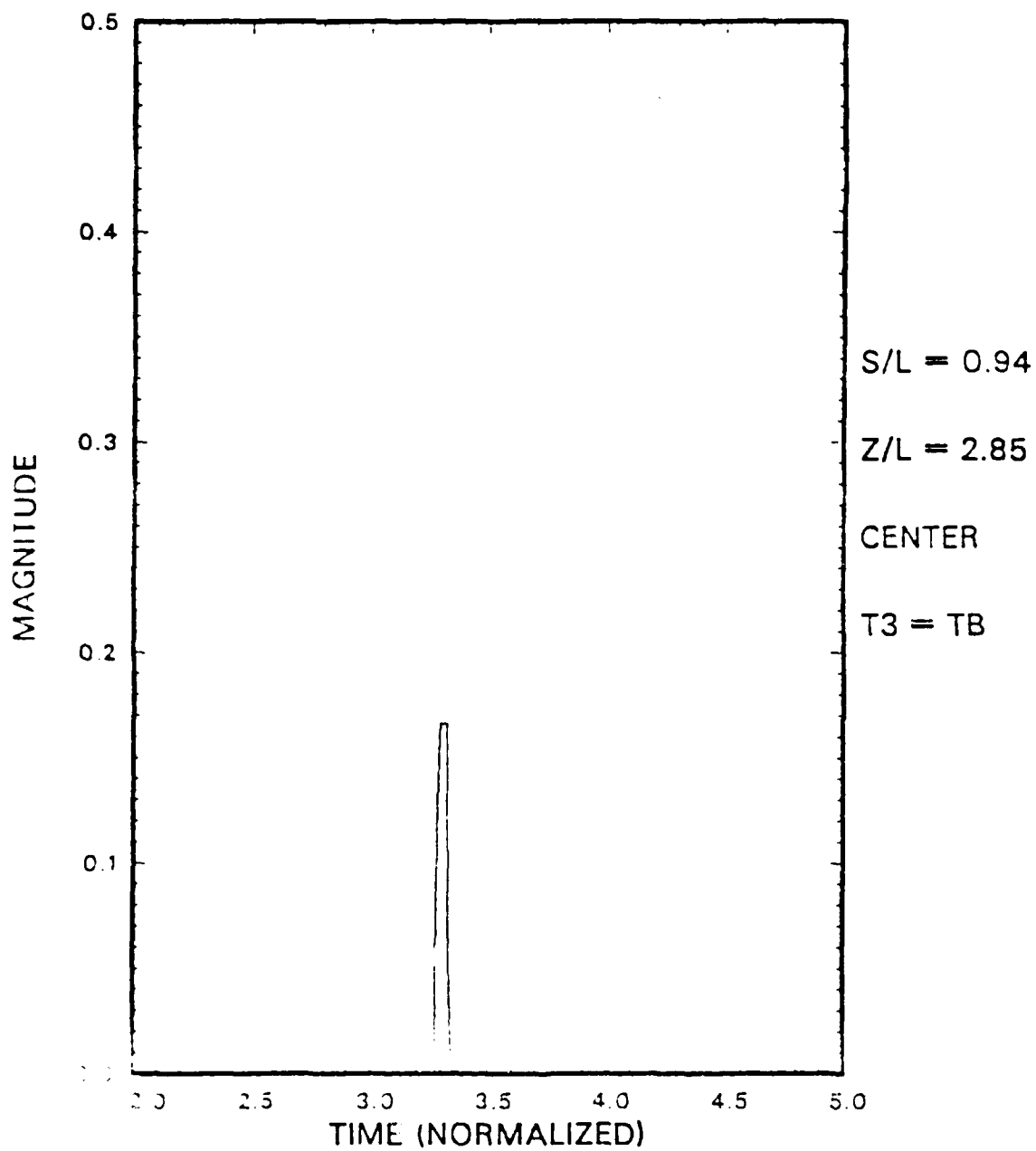


Figure 3.47 From Figure 3.42: Pulse 41.

CERENKOV PULSE

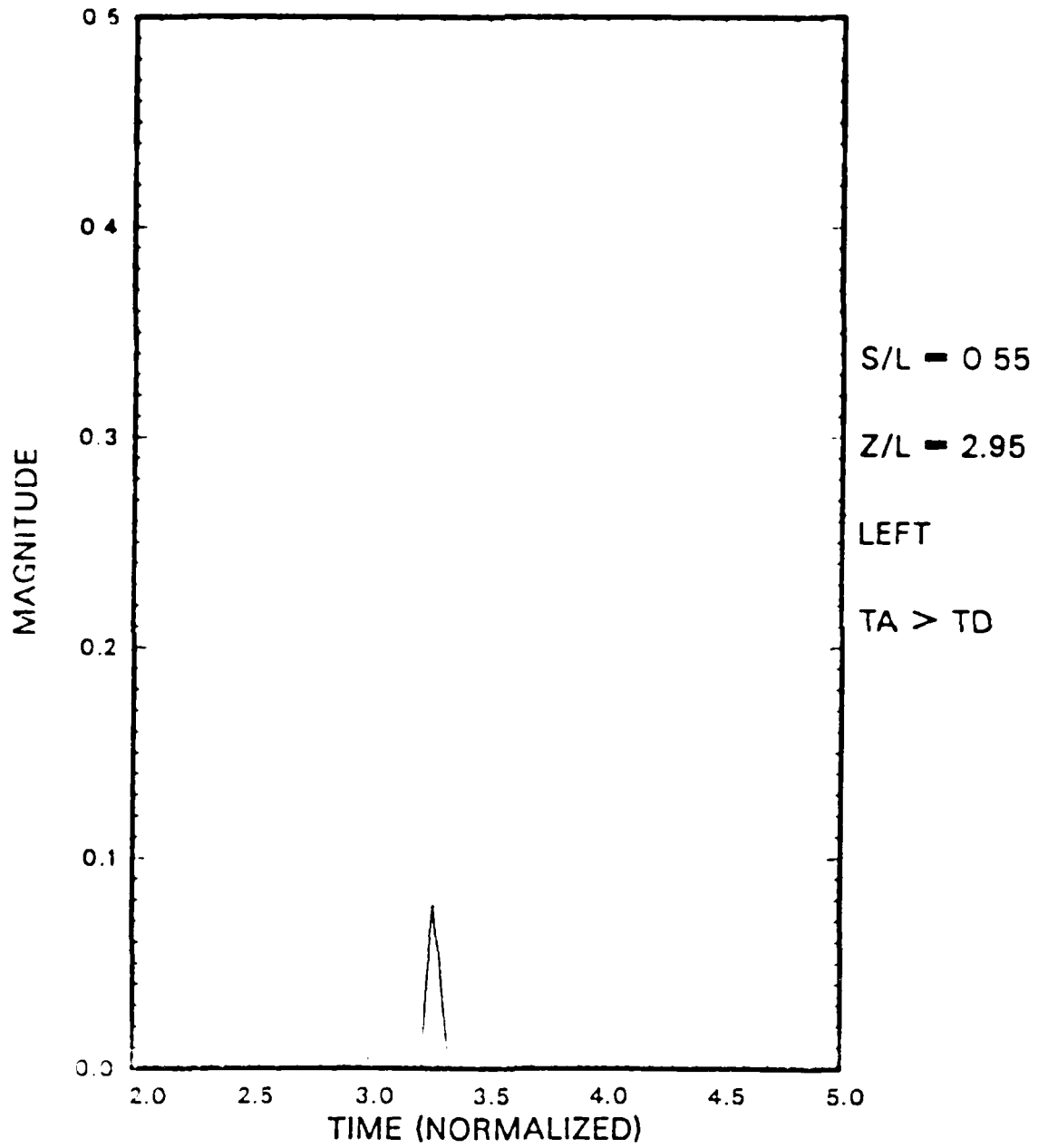


Figure 3.48 From Figure 3.42: Pulse 42.

CERENKOV PULSE

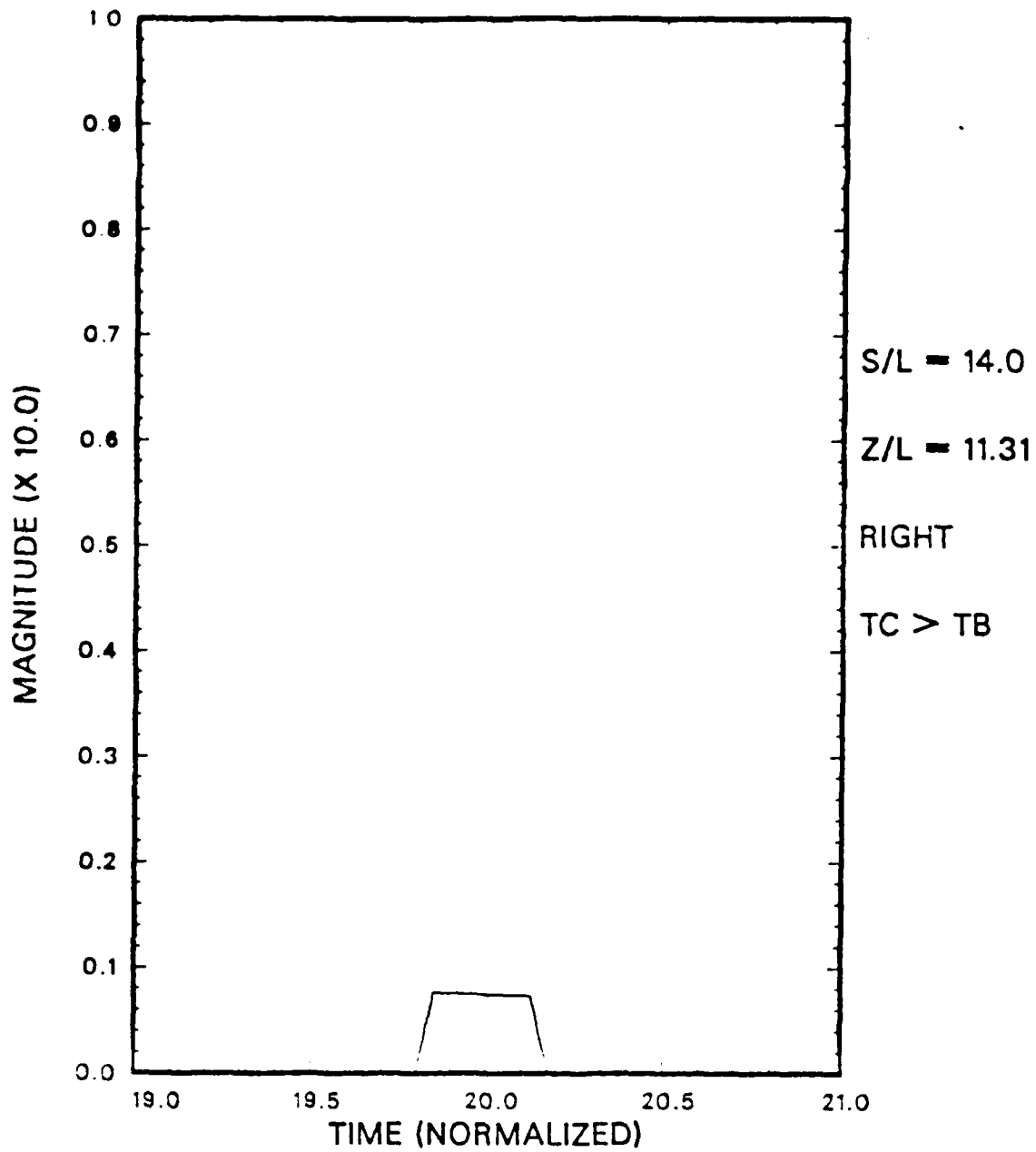


Figure 3.49 From Figure 3.43: Pulse 43.

CERENKOV PULSE

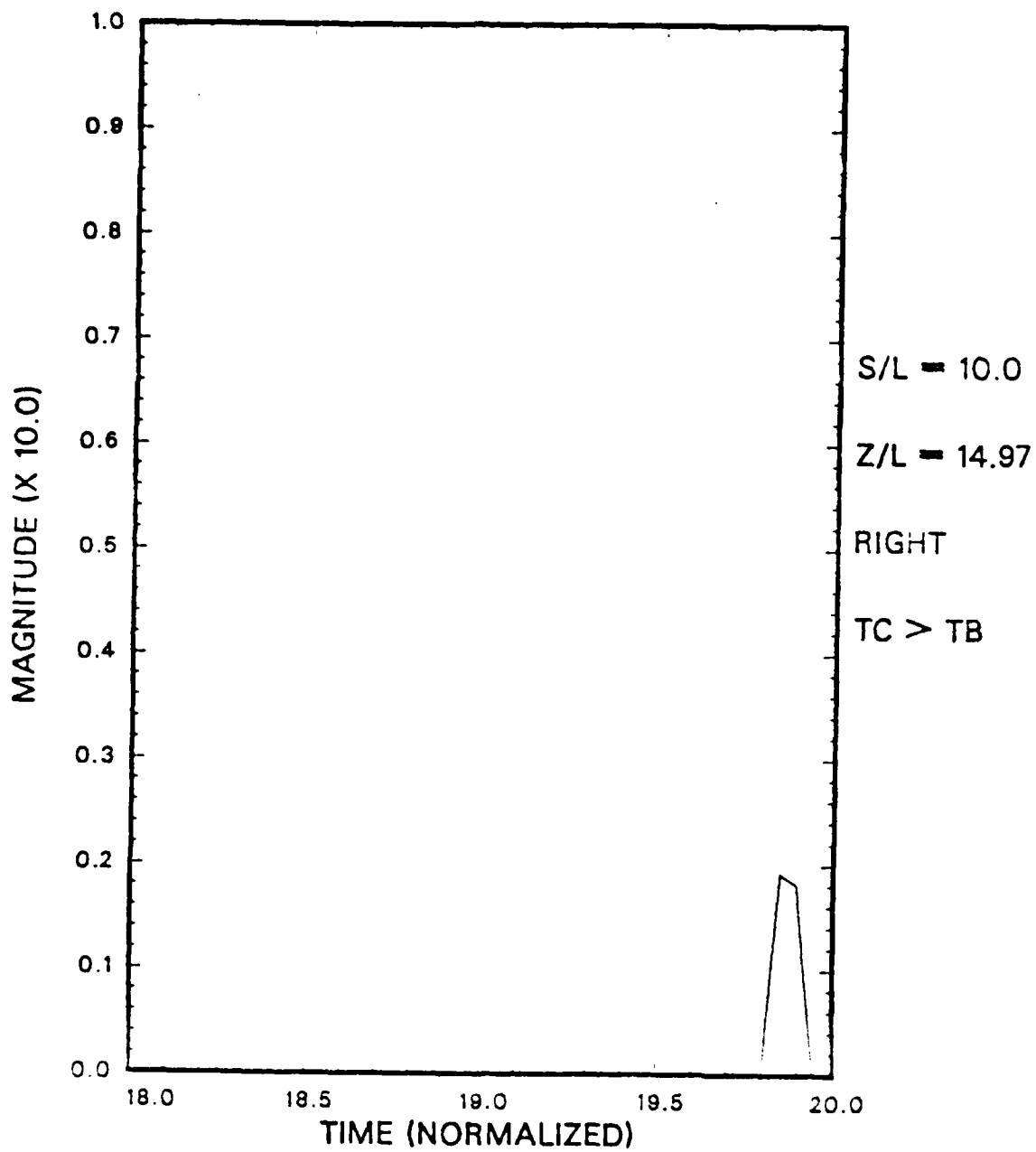


Figure 3.50 From Figure 3.43: Pulse 44.

CERENKOV PULSE

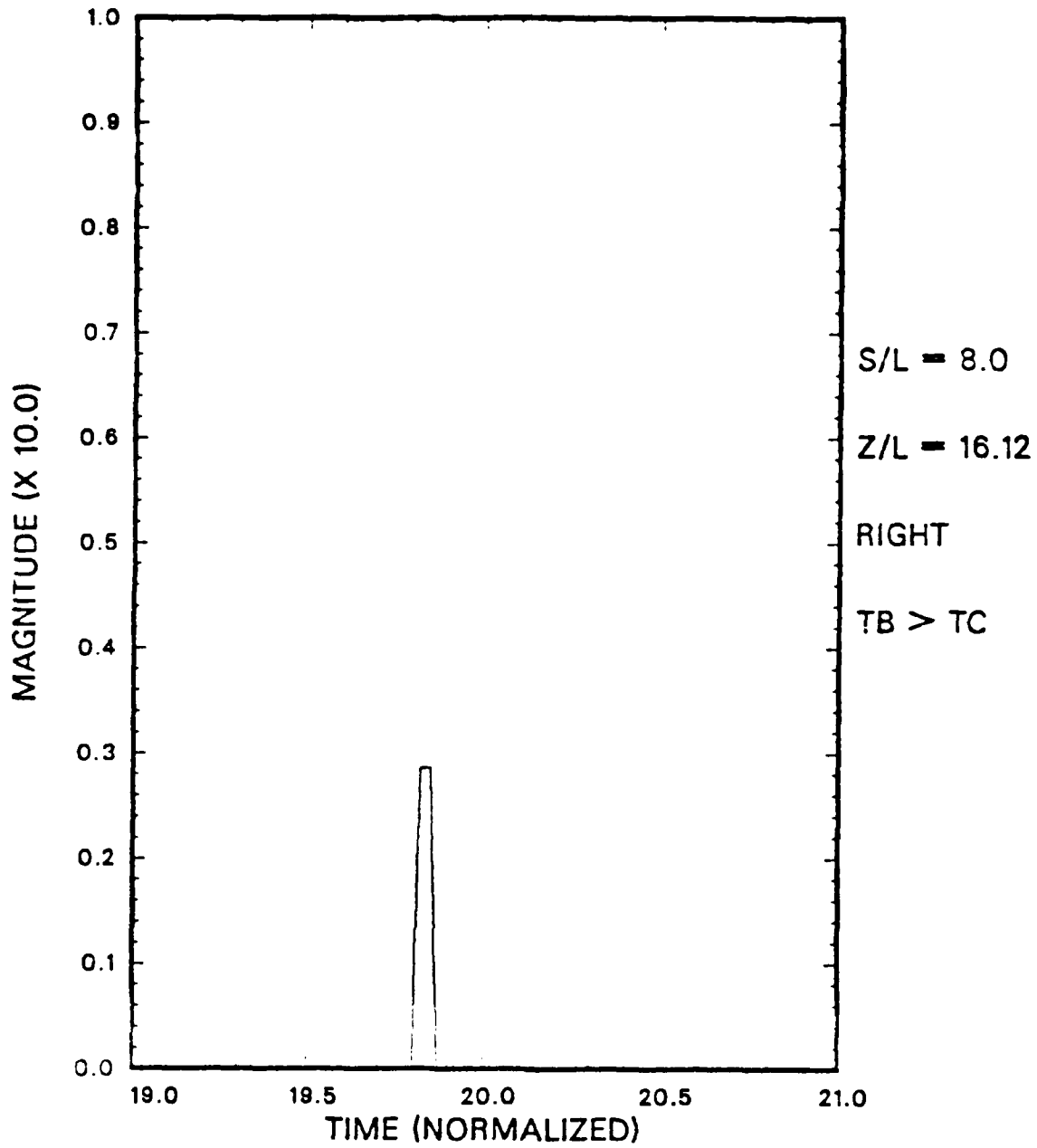


Figure 3.51 From Figure 3.43: Pulse 45.

CERENKOV PULSE

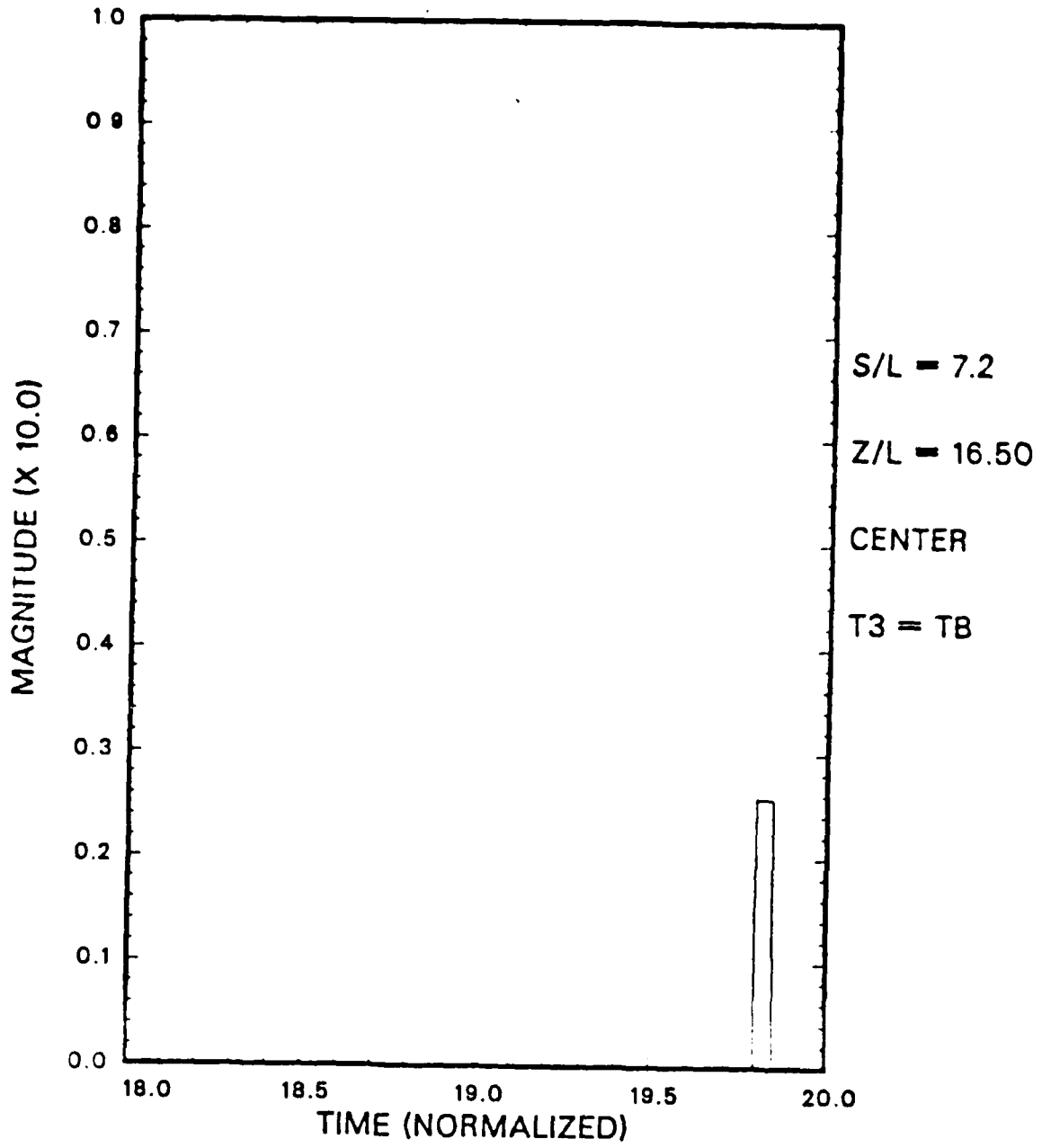


Figure 3.52 From Figure 3.43: Pulse 46.

CERENKOV PULSE

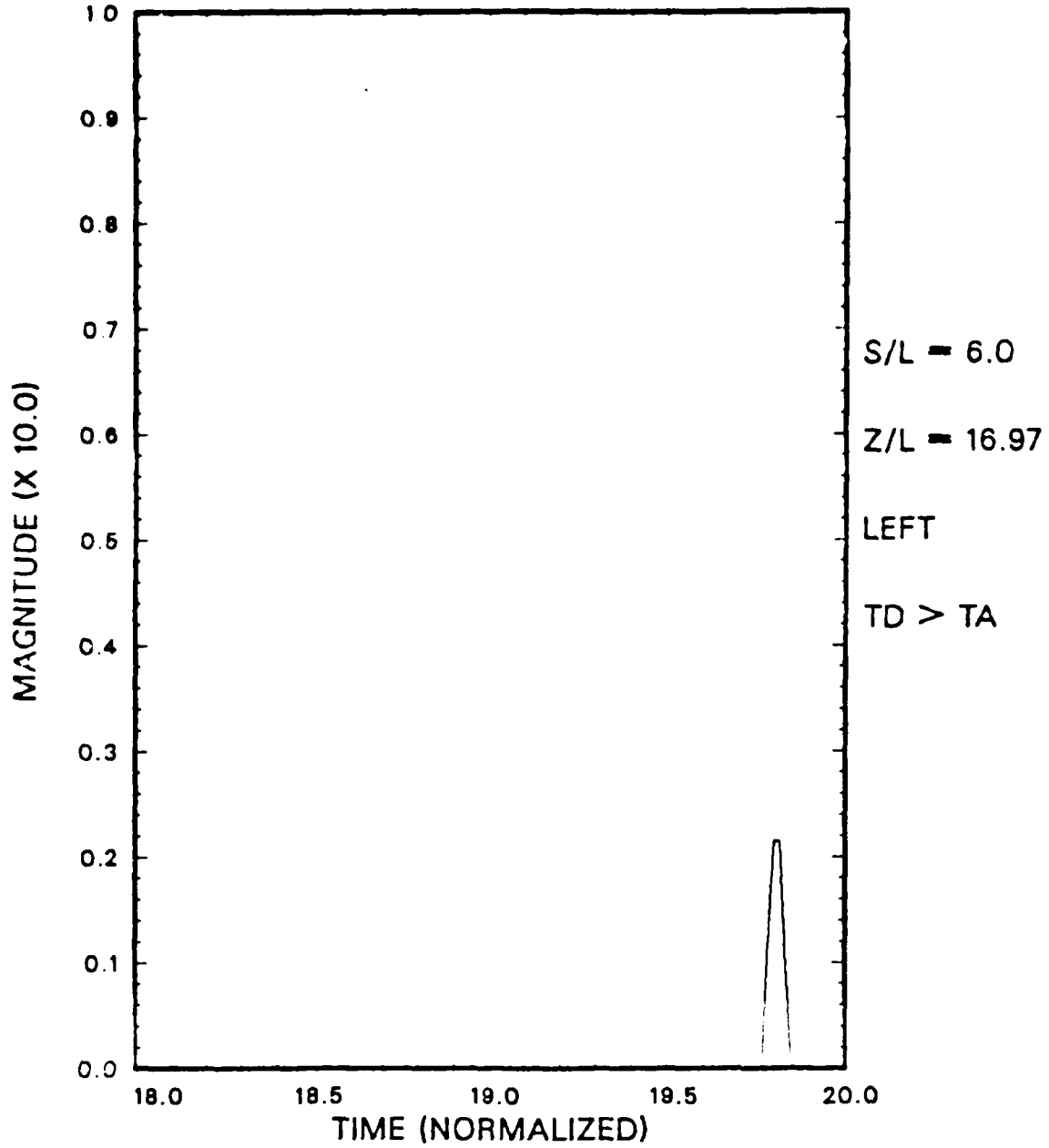


Figure 3.53 From Figure 3.43: Pulse 47.

CERENKOV PULSE

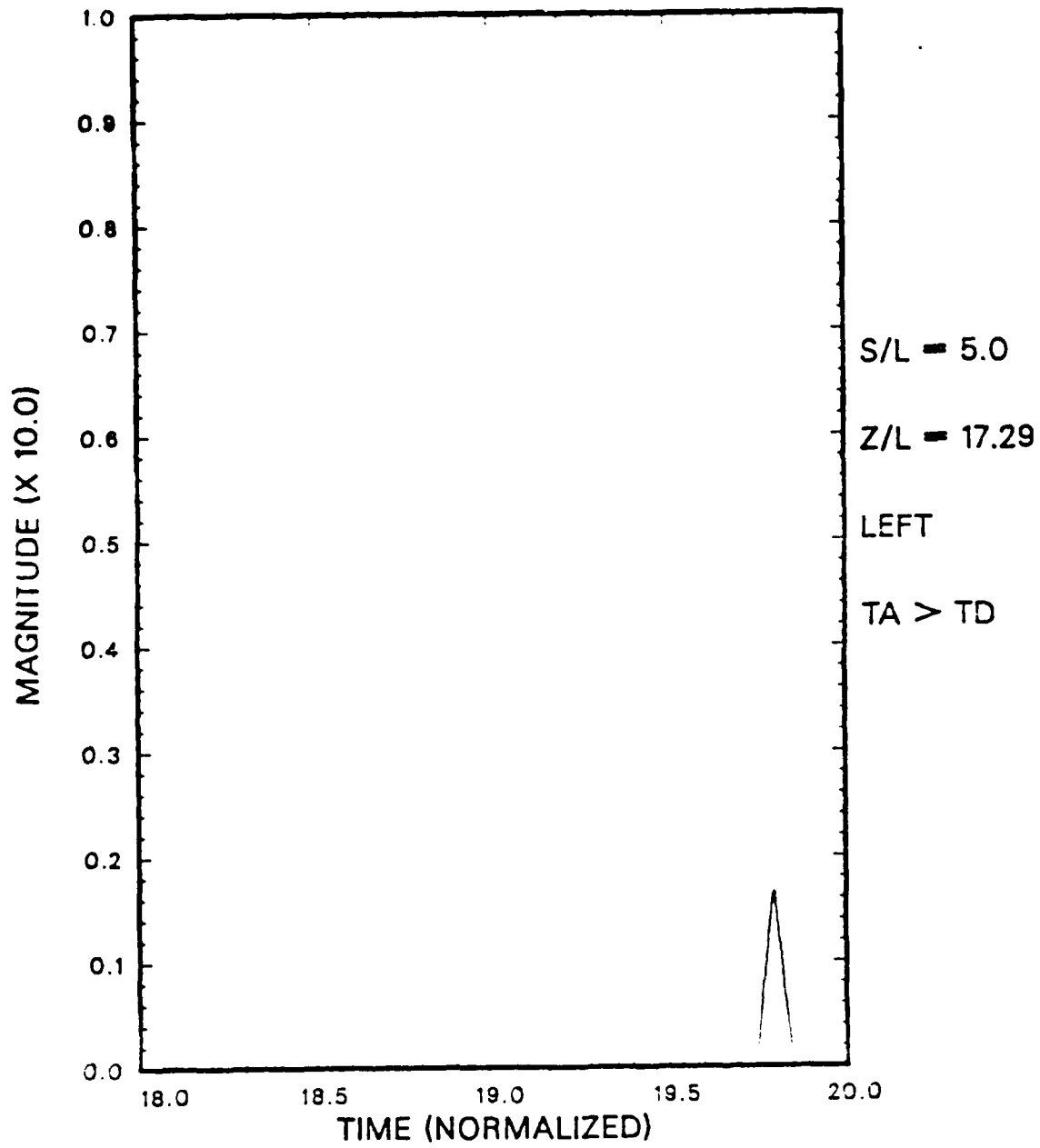


Figure 3.54 From Figure 3.43: Pulse 48.

CERENKOV PULSE

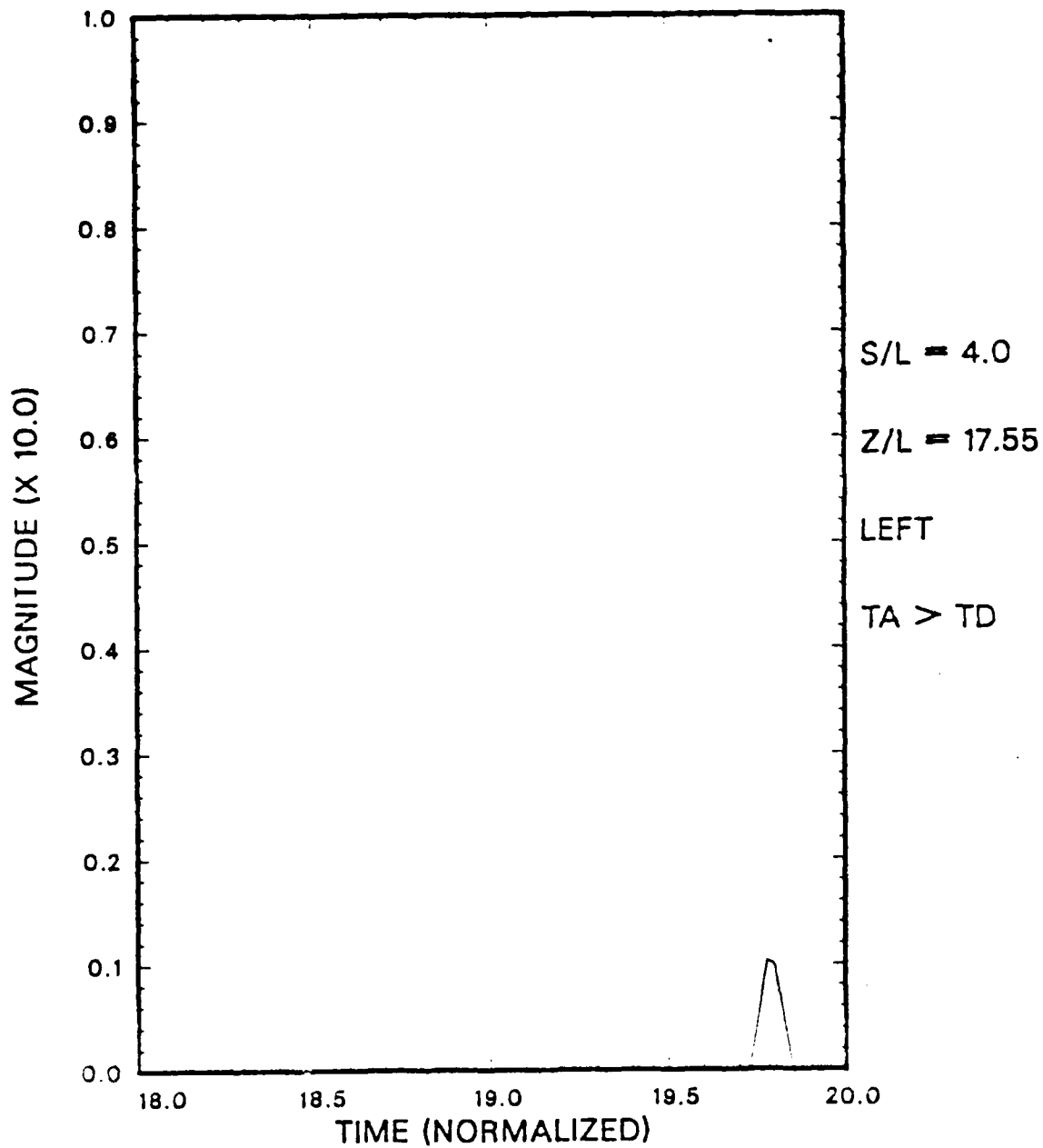


Figure 3.55 From Figure 3.43: Pulse 49.

CERENKOV PULSE

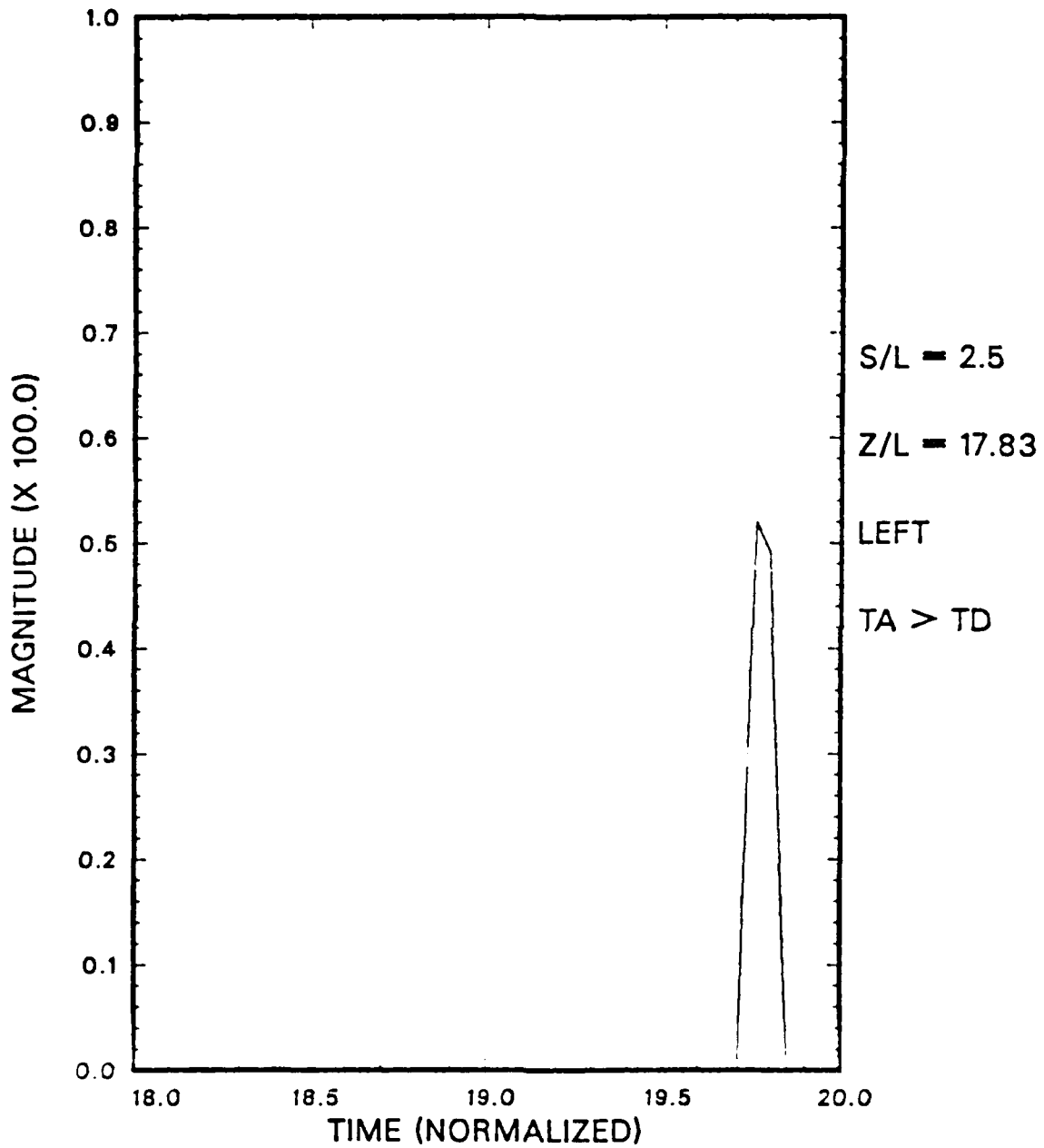


Figure 3.56 From Figure 3.43: Pulse 50.

CERENKOV PULSE

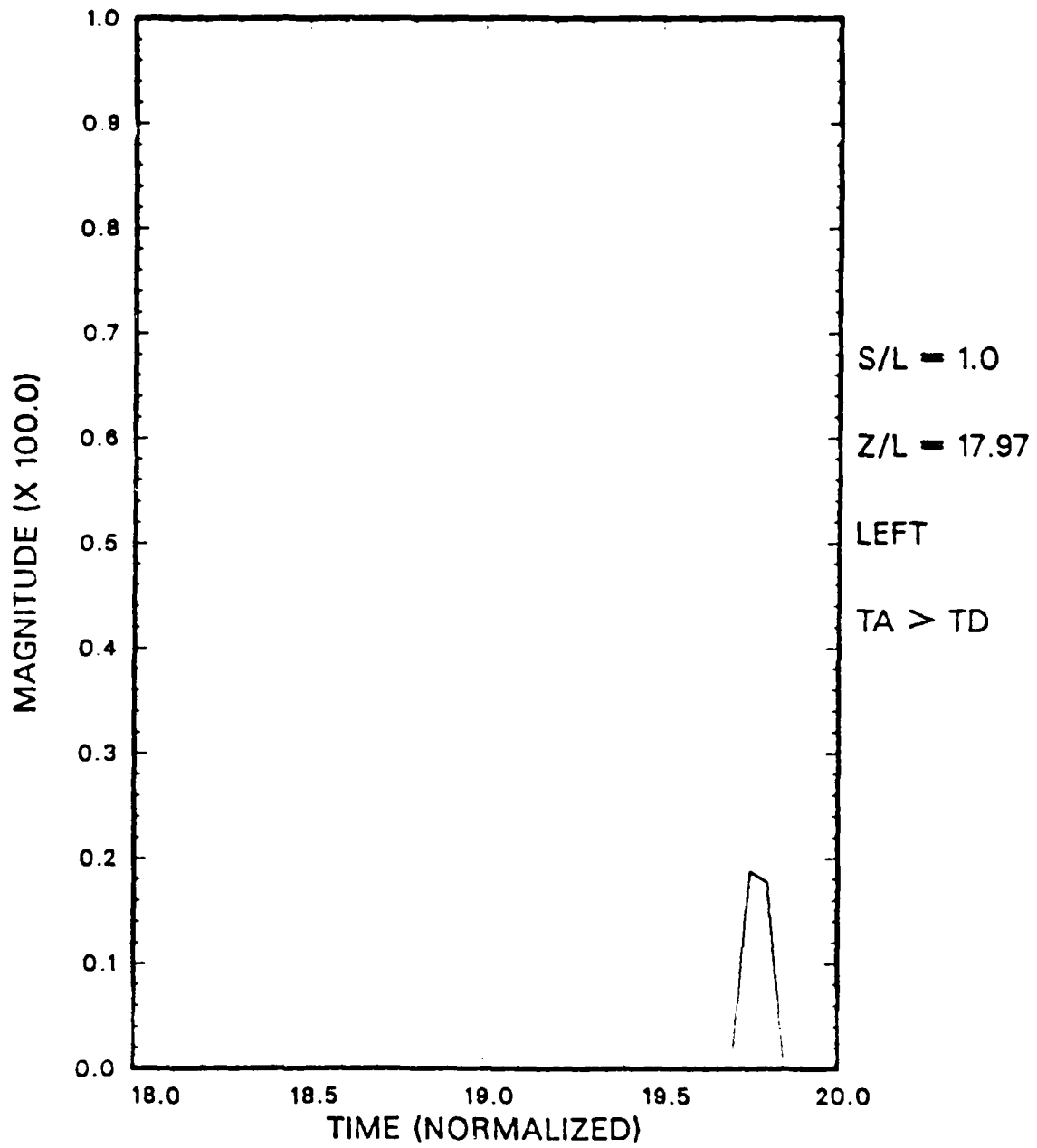


Figure 3.57 From Figure 3.43: Pulse 51.

IV. CONCLUSIONS

A. BACKGROUND

The shape of the B field (Cerenkov pulse) is known to be dependent on its position relative to the minimum of the function $u(z)$. However, based on the conclusions in [Ref. 2] p. 44], it was suspected that the pulse shape is also related to its position relative to the time boundary regions. Again, these regions are where $t_b = t_c$, $t_a = t_d$, and $t_c = t_a$. The recommendations that followed from this suspicion were to use different values for $\Delta u/L$ and to generate Cerenkov pulses at points close to these time boundaries. In the previous chapter, Figures 3.1 to 3.57 allows one to compare various shapes for different situations and $\Delta u/L$ values. These figures also aid in drawing conclusions about the pulse shapes and sizes.

B. OBSERVATIONS

1. General Trends

So far only a few brief remarks have been made with regard to the shapes and magnitudes of the Cerenkov pulses in the previous chapter. Here, more specific conclusions are drawn and some general observations are discussed. To make this easier, a useful way to study and compare the pulse shapes, and at the same time see where they fall with respect to the critical boundaries is to use Figures 4.1 to 4.4. The pulses are numbered in ascending order from left to right starting with the position closest to the origin and then moving out to greater distances. Figures 4.1 and 4.2 represent the close and far field regions respectively and correspond to the $\Delta u/L$ value of 0.05. They are simply Figures 3.1 and 3.2 with the Cerenkov pulses superimposed. The pulses are sketched to show relative magnitudes, shapes, and pulse widths. Figures 4.3 and 4.4 correspond to Figures 3.21 and 3.22. The pulse numbering continues where the last pulse number stops in Figure 4.2.

Starting with the pulse on the far left (number 1) in Figure 4.1 and proceeding in the positive Z/L direction, the pulses have the same basic shape. This means that the magnitude of the pulse goes from zero to a peak value, then declines to a smaller value before falling off to zero. Pulses 1 to 5 fall to the right of the path and do not cross a critical boundary. Each pulse begins at time t_a and then increases to a peak value at t_b . From here, the pulse declines in a non-linear fashion to a smaller value at t_c before

moving from left to right, the magnitudes of the peaks increase and the pulse widths decrease as the Cerenkov boundary is approached. Proceeding from pulse 6 to pulse 5, the pulse widths increase and the magnitudes decrease. The Cerenkov region is centered. These two pulses correspond to Figures 3.7 and 3.8. Once again the basic shapes are similar. From pulse 5 to pulse 7, the magnitudes increase. Moving right to pulse 7, yields the same trend in magnitudes and pulse widths. The value at t_c shows a relative increase and starts to blend into the decline from the peak magnitude to the end of the pulse. Since the observing position is approaching the $t_b = t_c$ boundary (see line 1), the integration process takes the value of the integral to the peak at t_b and then back down to zero. For reference, pulse 7 corresponds to Figure 3.9. Crossing the $t_b = t_c$ boundary to pulse 8, shows that the t_c value has vanished and the shape takes the form of a spike. Pulses 9, 10, and 11 on Figure 4.1, cross two time boundaries before leaving the Cerenkov region. The last pulse falls to the left of the path. There is no change in shape; the last three pulses are spikes. Their magnitudes decrease and the pulse widths increase with increasing Z/L . Pulses 8 to 11 correspond to Figures 3.10 to 3.13.

The above discussion considered Figure 4.1 and moved from left to right examining each pulse. Comments were made when a critical boundary was crossed and two pulses were compared when they were positioned on opposite sides of a boundary. This procedure for examining Figure 4.1 was necessary but, will not be repeated for Figures 4.2 to 4.4. Instead, only the general trends in shapes, magnitudes, and pulse widths will be noted.

Figure 4.2 illustrates the pulses that were generated at larger distances from the beam discharge point. The maximum value of the pulse increases from left to right up to pulse number 15 (Figure 3.17), and from there a decline begins. The pulse widths decrease and then increase in the same manner that the magnitudes increase and decrease. The shapes are similar to the close field observations with the exception of one minor difference. The smaller value at t_c is almost as large as the peak magnitude of the pulse. After the slightly rounded spike pulse (15) occurs, the remaining pulses are flat-tops as one proceeds to larger distances. From the maximum peak magnitude, the rest of the shapes show decreasing magnitudes and increasing pulse widths with increasing Z/L .

Figures 4.3 and 4.4 also show the close and far fields respectively. They are similar to Figures 4.1 and 4.2 with the exception that the value for $\Delta u/L$ is 0.15 vice

0.05. Again, the general trends in magnitudes and pulse widths are the same. However, the pulses further to the right take on flattop peaks where spikes were observed in the previous two figures. Other than this, analyzing Figures 4.3 and 4.4 would be repeating what was done earlier in Figures 4.1 and 4.2.

2. Specific Analysis

At this point, observations have been made by holding S/L constant and varying Z/L . This means that the distance from the beam discharge point is changing from one pulse to the next. Figures 3.42 and 3.43 illustrate the close and far observing positions respectively where the distance from the discharge point is constant. This allows one to see how the pulses change with respect to location in the S-Z plane without the effects of a varying range from the emission source. For reference, Figures 3.44 to 3.48 correspond to pulses 38 to 42 in the close positions, while Figures 3.49 to 3.57 correspond to pulses 43 to 51 in the far positions.

The pulses from Figures 3.42 and 3.43 yield no new information with regard to shape, but it is obvious that the peak magnitude occurs in the middle of the Cerenkov region as does the minimum pulse width. Without the aid of the equal distance analysis, this observation would be only a safe assumption. Figures 4.5 and 4.6 are plots of the peak magnitude and pulse width verses the angle measured from the vertical axis S/L . They both show that the angle at which the peak magnitude and minimum pulse width occur is the compliment of the Cerenkov angle. In other words, measuring the angle from the horizontal axis, would yield the peak magnitude and the minimum pulse width at the Cerenkov angle. This is consistent with Cerenkov radiation theory.

C. SUMMARY

One conclusion in [Ref. 2: p. 45], that can be reinforced after analyzing all the pulse shapes in this paper, is that a smaller $\Delta u/L$ value will yield more pointed pulse shapes. Still, there are some other points that need to be brought out. The more pointed pulse shapes, fall closer to a time boundary than the other pulses. This is true in the S-Z plane. Figures 3.10 (pulse 39), 3.20 (pulse 20), 3.30 (pulse 30) and 3.40 (pulse 40) are specific examples of this observation and applies to all cases with the exception to some of the cases involving the $t_a = t_b$ boundary. This is true in this sense because on the boundary there are only two angles that can be measured through during the integration process. For example, the pulses rise to a peak at t_a from t_b and then decay to zero.

AD-A184 870

CERENKOV RADIATION FIELD ANALYSIS DUE TO A PASSING
ELECTRON BEAM(U) NAVAL POSTGRADUATE SCHOOL MONTEREY CA
B K PRICE JUN 87

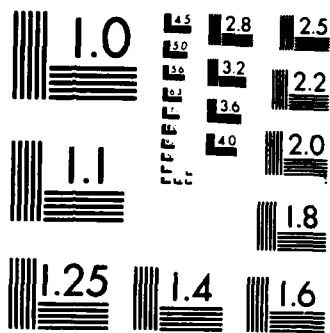
2/2

UNCLASSIFIED

F/G 20/8

NL





MICROCOPY RESOLUTION TEST CHART
NATIONAL BUREAU OF STANDARDS-1963-A

move away from the time boundary, there is enough distinction between the two times for the computer to notice two distinct magnitudes. This explains why the value at t_c continues to approach the magnitude of t_b , when the observing positions change from left to right on the S-Z plane when starting to the right of the path. In other words, if an observing position falls on a time boundary where two critical times are equal, then there exists a unique value for the magnitude of the pulse. In short, all this means that the general shape of the Cerenkov pulse depends on the location of the observer relative to a time boundary. In particular, for positions near or on a time boundary, the observed pulses are more spike-like. However, the magnitude and the pulse width are dependent on the observer's position relative to the Cerenkov region.

TIME LINES

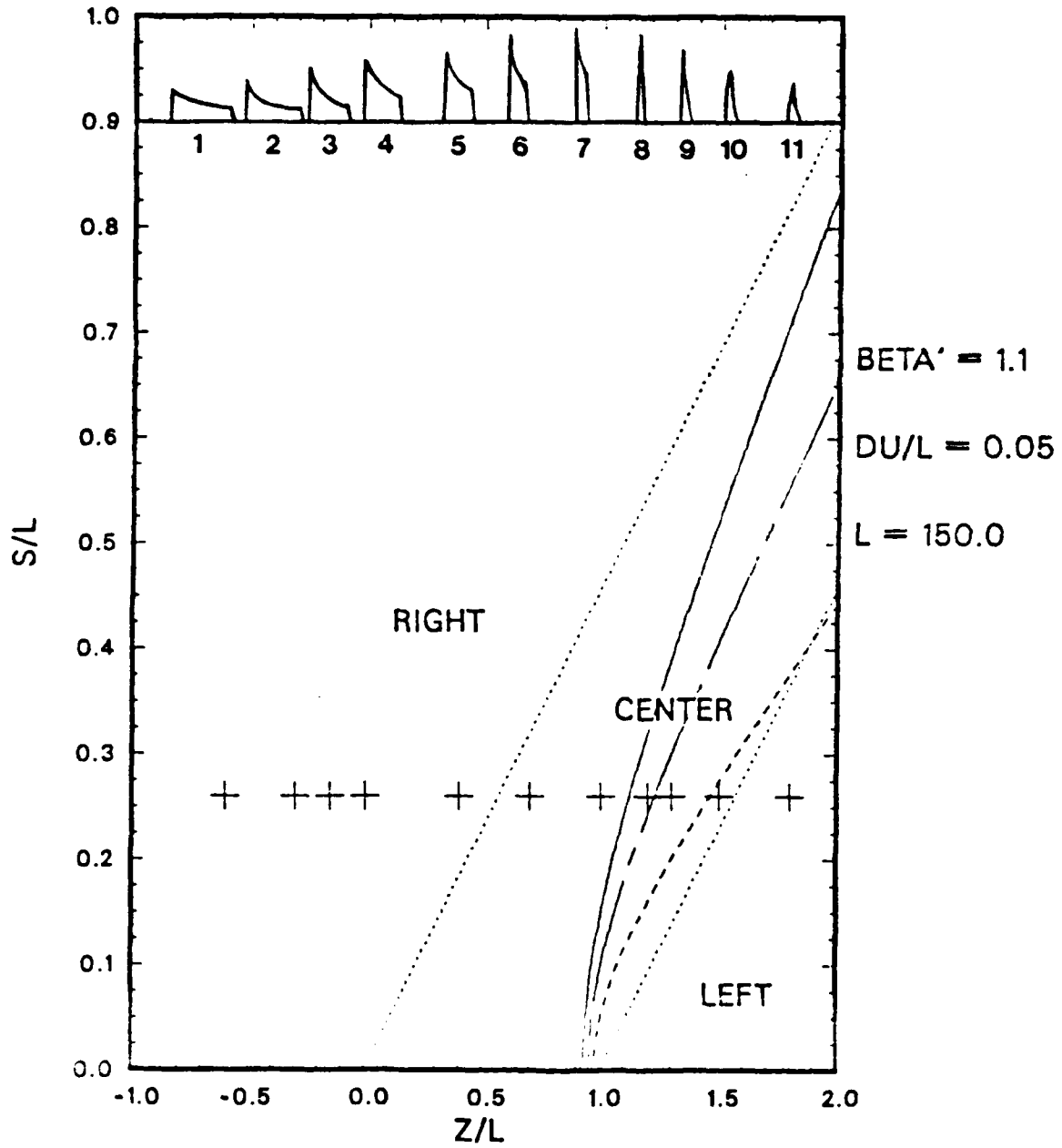


Figure 4.1 Pulse Shapes of Figure 3.1.

TIME LINES

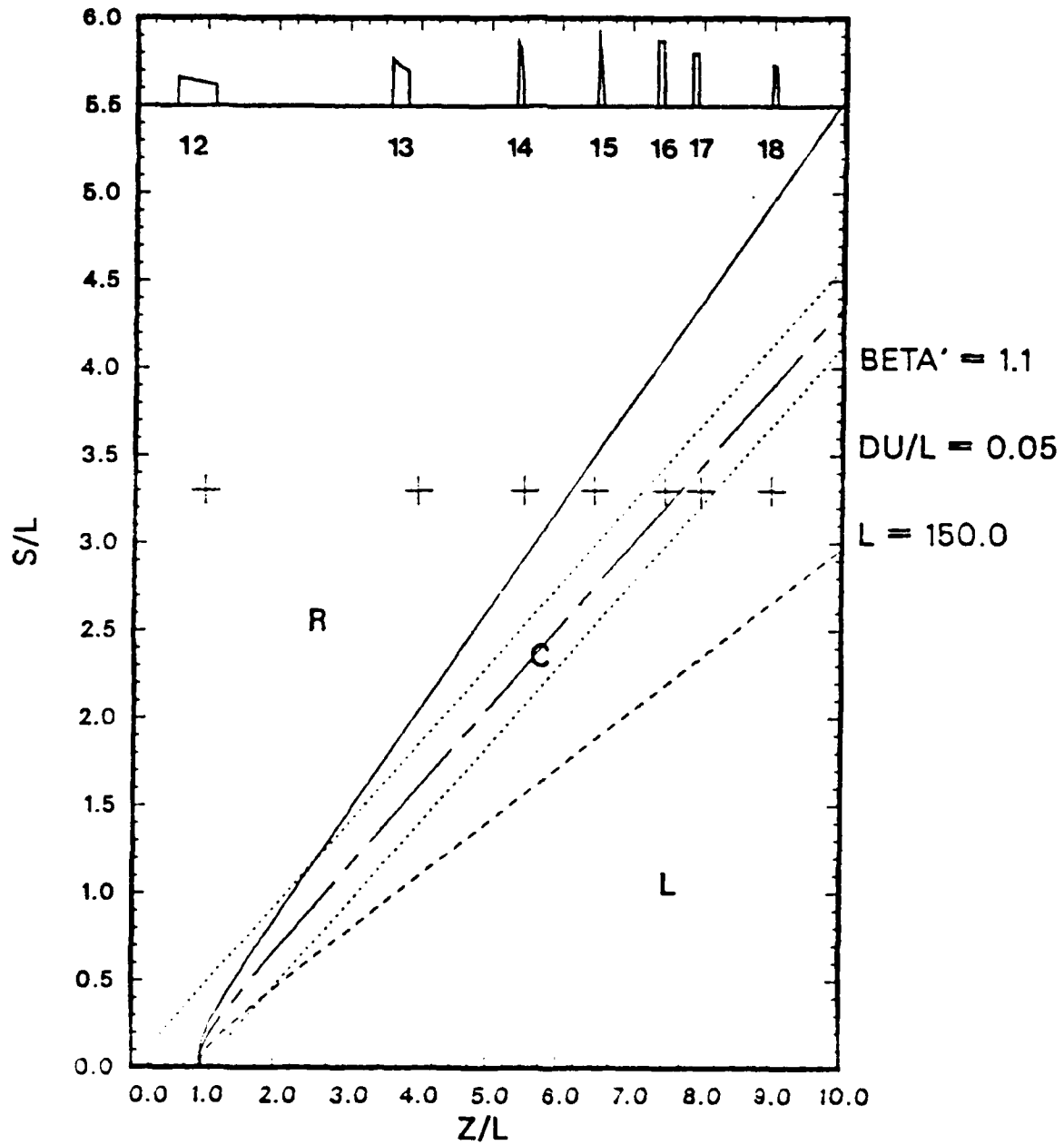


Figure 4.2 Pulse Shapes of Figure 3.2.

TIME LINES

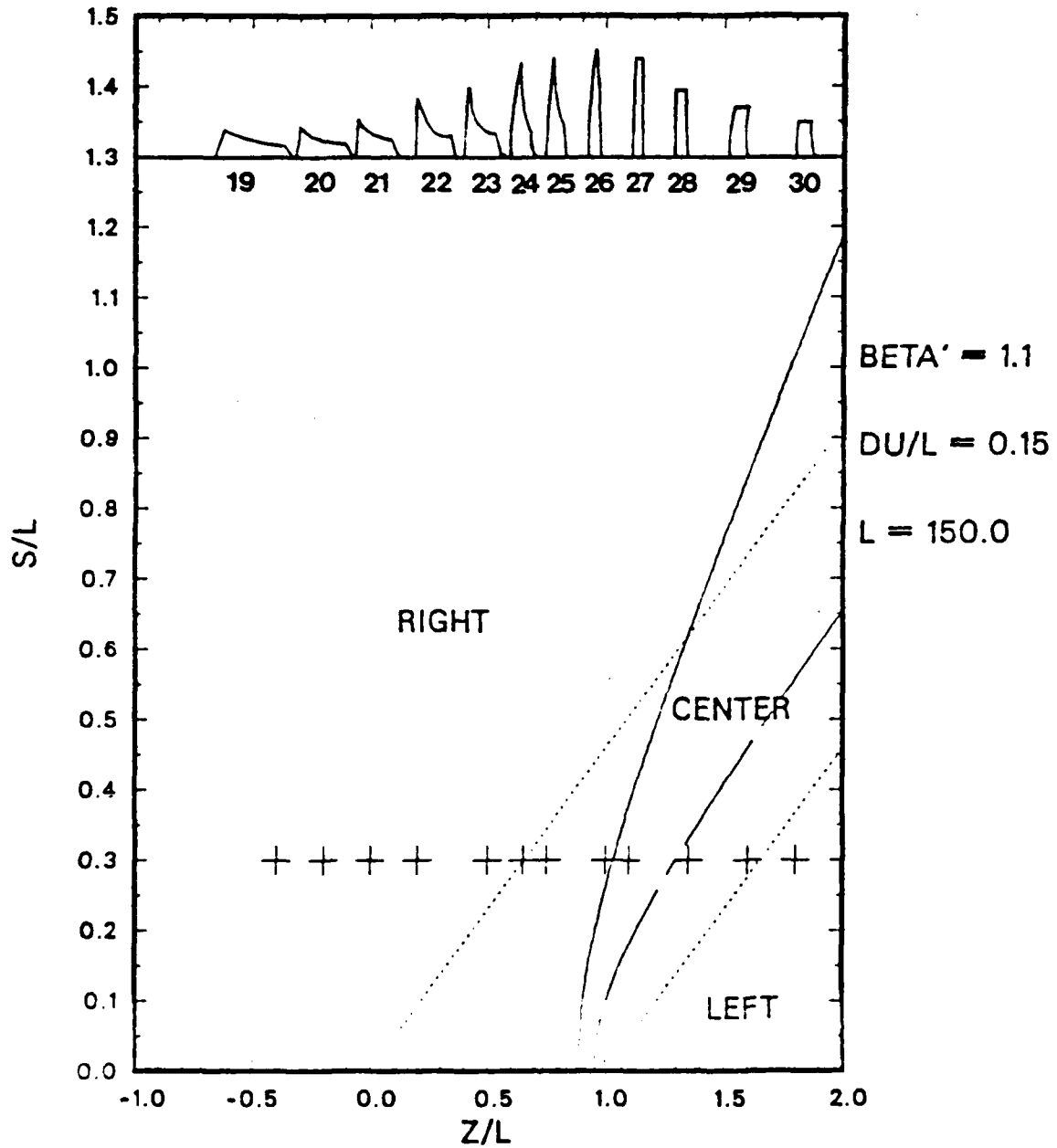


Figure 4.3 Pulse Shapes of Figure 3.21.

TIME LINES

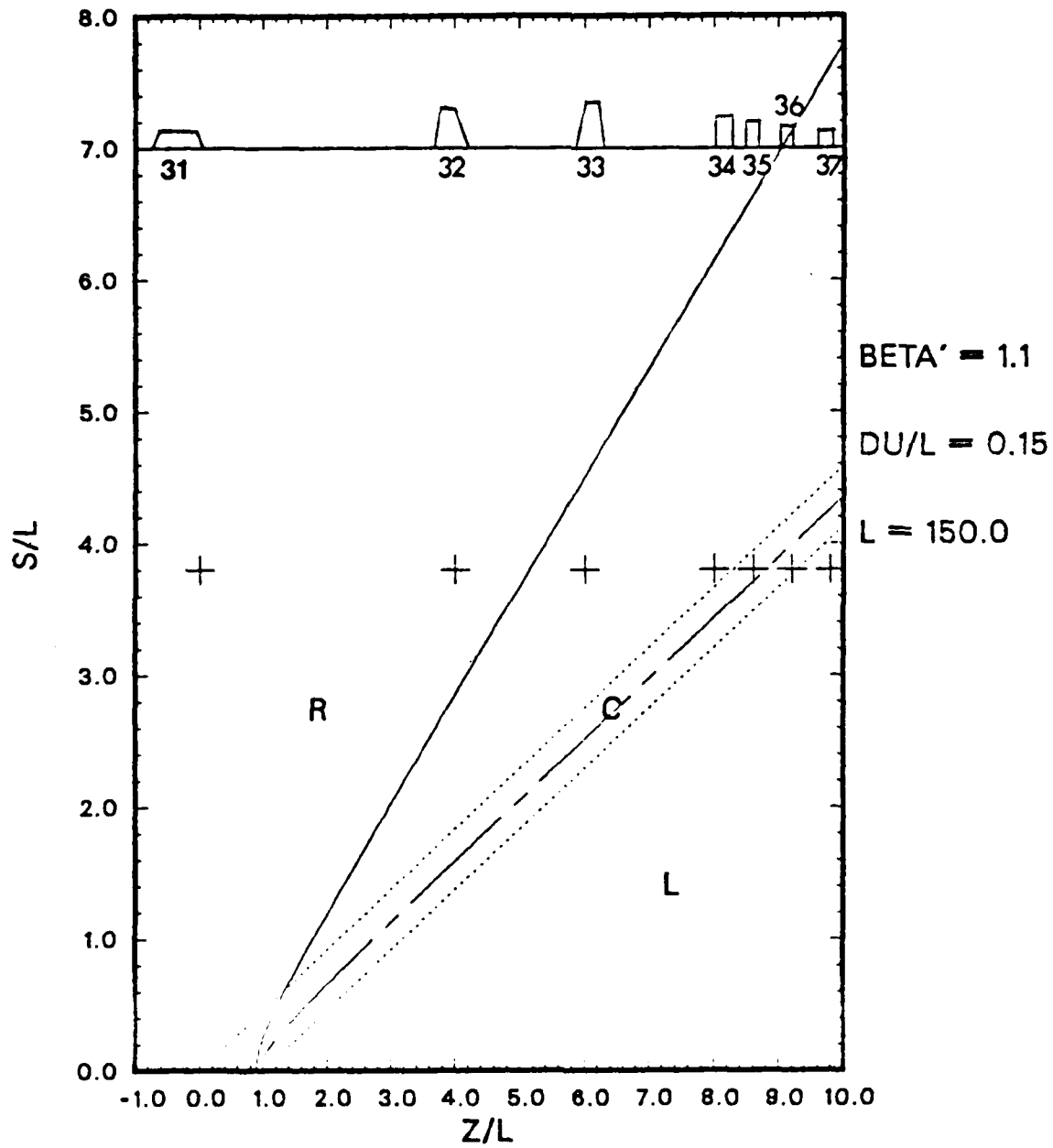


Figure 4.4 Pulse Shapes of Figure 3.22.

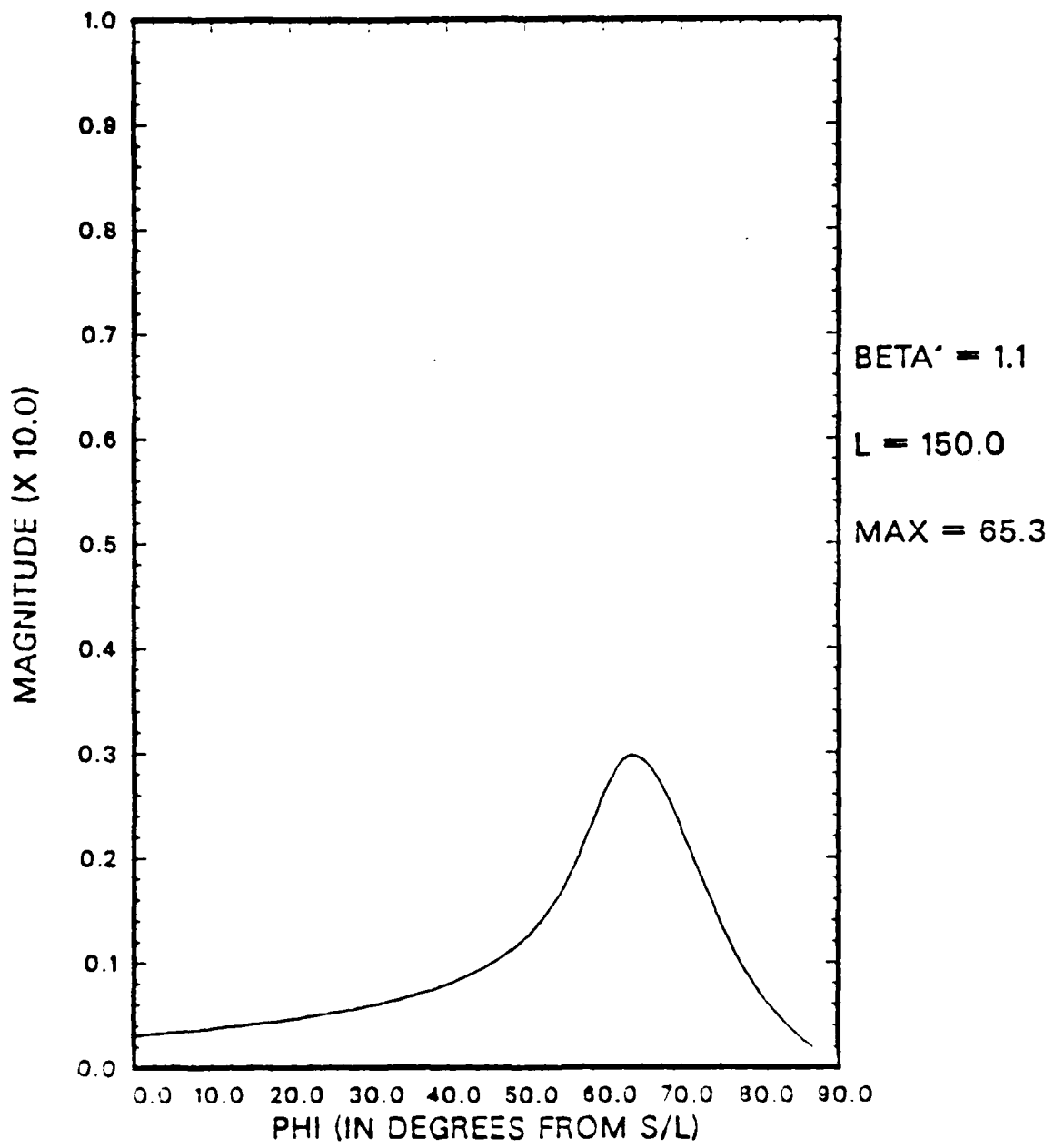


Figure 4.5 Peak Magnitude vs. Angle (ϕ).

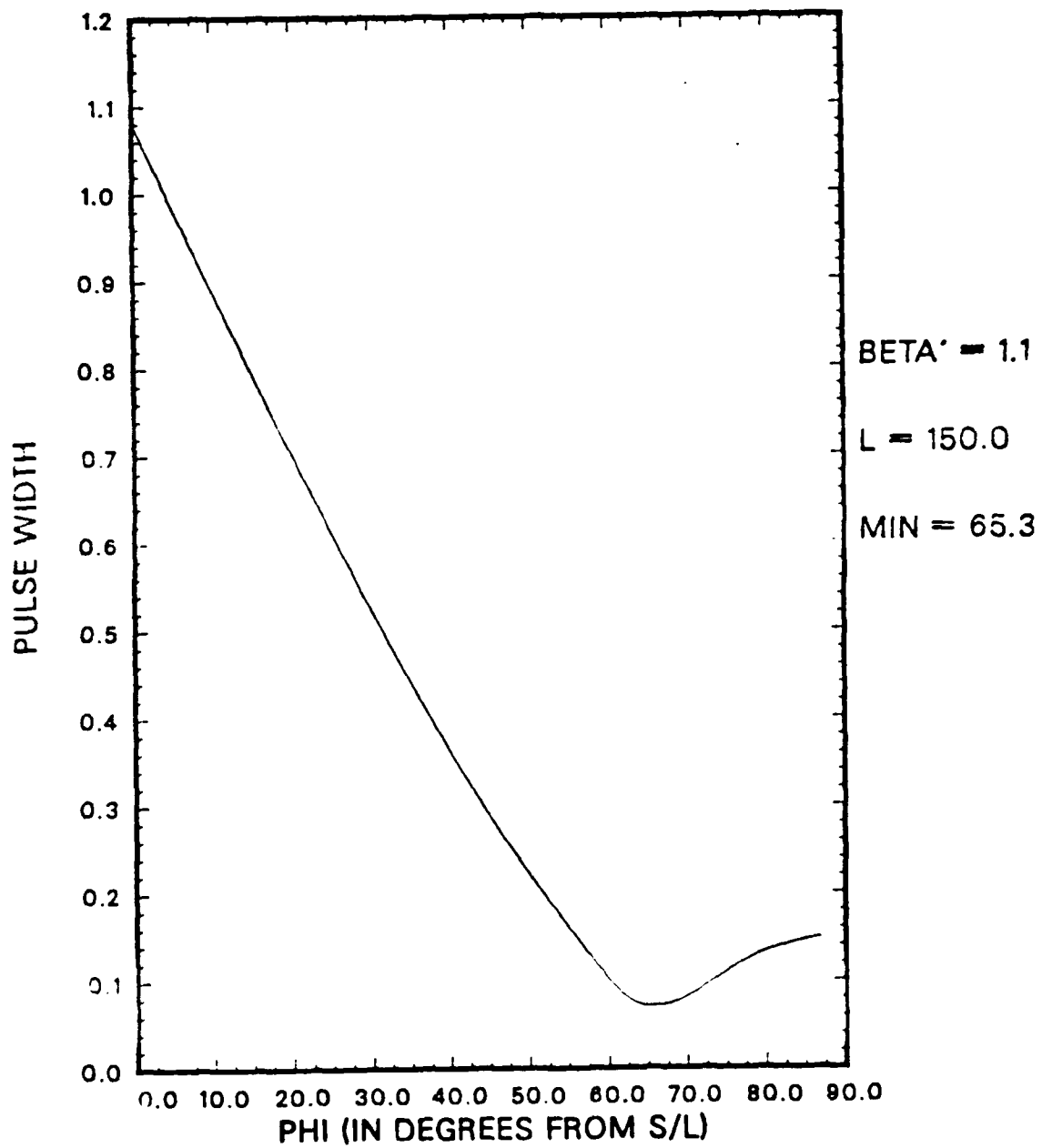


Figure 4.6 Pulse Width vs. Angle (ϕ).

APPENDIX A

CERENKOV PULSE PROGRAM

```

C *****
C *THIS PROGRAM IS LOCATED ON THE NPS MAIN FRAME UNDER THE FILENAME *
C *'CERENKV' AND IS WRITTEN USING WATFOR 77. AFTER ENTERING CERTAIN *
C *VALUES, DATA FOR THE MAGNITUDE OF THE CERENKOV PULSE IS GENERATED*
C *AND IS THEN PLOTTED BY ANY PLOTTING ROUTINE. THESE MAGNITUDES ARE*
C *PLOTTED AGAINST NORMALIZED TIME AND WHEN MULTIPLIED BY A CONSTANT*
C *YOU CAN GET ACTUAL B-FIELD OR E-FIELD. *
C *****

```

```

      DOUBLE PRECISION N, U1, U2, BETA, CO, ROE, A, G, CE, BPRME, POSZ
      DOUBLE PRECISION R1, R2, A1, RSETME, SRTE1, SRTE2, A2, D, E, DD
      DOUBLE PRECISION EE, Q, TA, TB, TC, TD, F, ZPI, ZPF, WPI, WPF
      DOUBLE PRECISION W1, W2, ZC, RC, ZPC, T1, T2, T3, DELR, ZPM, B1
      DOUBLE PRECISION B2, E1, E2, S1, XX, YY, S, L, Z, TPRME, B, BMAX
      DOUBLE PRECISION TMAX, TMIN, GPRME, THETA1, THETA2, TINC, TAU
      DIMENSION TPRME(9000), B(9000)
      INTEGER I, J, IMAX

```

```

C *****
C * ALL THE PERTINENT VARIABLES ARE ENTERED HERE AND SELF-EXPLAINS *
C * THE NEED FOR THE VARIABLE WITH TERMINAL INTERACTION. ONE POINT *
C * THAT NEEDS TO BE CLARIFIED, IS HOW TO ENTER U1 AND U2. U1 WILL *
C * BE ZERO AND U2 WILL BE A NEGATIVE VALUE. *
C *****

```

```

1  PRINT *, 'ENTER N'
    READ *, N
    PRINT *, 'ENTER ROE'
    READ *, ROE
    PRINT *, 'ENTER BETA'
    READ *, BETA
    PRINT *, 'ENTER BEAMLENGTH'
    READ *, L
    PRINT *, 'ENTER U1 SHOULD USUALLY BE ZERO'
    READ *, U1
    PRINT *, 'ENTER U2'
    READ *, U2
    PRINT *, 'ENTER S POSITION'
    READ *, S
    PRINT *, 'ENTER Z POSITION'
    READ *, Z
    PRINT *, 'ENTER CO IN M/NSEC'
    READ *, CO

```

```

      V = BETA*CO
      BPRME = N*BETA
      Q = (BPRME**2.0) - 1.0
      R1 = SORT((S**2.0) + (Z**2.0))
      R2 = SORT((S**2.0) + (Z - L)**2.0)
      S1 = (S**2.0)*Q
      TAU = L/V

```

```

C *****
C *THE BOUNDARY TIMES ARE COMPUTED AND USED THROUGHOUT THE PROGRAM *
C *DURING THE INTEGRATION PROCESS FOR CALCULATING THE MAGNITUDE OF *
C *THE CERENKOV PULSE. THE WRITE STATEMENT DISPLAYS THE NORMALIZED *
C *TIMES WHICH SERVES AS AN AID WHEN USING VARIOUS GRAPHICS ROUTINES*
C *FOR PLOTTING THE PULSES. *
C *****

```

```

      TA = ((BPRME*R1 - U1)/V)
      TB = ((BPRME*R1 - U2)/V)
      TC = ((L + (BPRME*R2) - U1)/V)
      TD = ((L + (BPRME*R2) - U2)/V)

```

```

110 WRITE(6,110) TA/TAU, TB/TAU, TC/TAU, TD/TAU
    FORMAT(4F10.5)

```

```

C *****
C *INITIALIZE THE DIMENSIONED VARIABLES FOR TIME AND MAGNITUDE - B *
C *****

```

```

    DO 10 I = 1,200
        TPRME(I) = 0.0
        B(I) = 0.0
10 CONTINUE

```

```

C *****
C *THE CERENKOV ANGLE CE IS CALCULATED AND BASED ON THE OBSERVING *
C *POSITIONS, THE VALUES OF THETA1 AND THETA2 ARE CALCULATED. FROM *
C *HERE WE CHECK TO SEE IF WE ARE TO THE LEFT, RIGHT, OR CENTER. *
C *****

```

```

    CE = DACOS(1.0/BPRME)
    IF (Z .LE. 0.0) THEN
        POSZ = ABS(Z)
        A = POSZ/S
        THETA1 = DATAN(A)
        THETA1 = THETA1 + 1.570796327
    ELSE

```

```

        A = S/Z
        THETA1 = DATAN(A)
    END IF
    IF (Z .LT. L) THEN
        GPRME = (L - Z)/S
        THETA2 = DATAN(GPRME) + 1.570796327
    END IF
    IF (Z .EQ. L) THEN
        THETA2 = 1.570796327
    END IF
    IF (Z .GT. L) THEN
        GPRME = S/(Z - L)
        THETA2 = DATAN(GPRME)
    END IF

```

```

C *****
C *THE CERENKOV ANGLE IS COMPARED TO THETA1. THE IF STATEMENT CHECKS*
C *TO SEE IF WE ARE TO THE RIGHT AND THUS DISPLAYS ON THE SCREEN. *
C *****

```

```

111 IF (THETA1 .GT. CE) THEN
    WRITE(6,111)
    FORMAT('PATH TO THE RIGHT')
    TINC = (TD - TA)/200.0
    DO 20 I = 1,200
        IF (I .EQ. 1.0) THEN
            TPRME(I) = TA
            B(I) = 0.0
        ELSE
            TPRME(I) = TA + (REAL(I)*TINC)
        END IF
        IF (TPRME(I) .GE. TD) THEN
            B(I) = 0.0
            GO TO 100
        END IF
        A1 = U1 + V*TPRME(I)
        A2 = U2 + V*TPRME(I)
        D = ((BPRME**2.0)*Z) - A1
        DD = ((BPRME**2.0)*Z) - A2
        E1 = ((Z - A1)**2.0) - S1
        E2 = ((Z - A2)**2.0) - S1
        IF (E1 .LT. 0.0) THEN
            E1 = 0.0
        END IF
        IF (E2 .LT. 0.0) THEN
            E2 = 0.0
        END IF
        SRTE1 = SQRT(E1)

```

```

SRTE2 = SORT(E2)
E = BPRME*SRTE1
EE = BPRME*SRTE2
ZPI = (DD + EE)/Q
ZPF = (D + E)/Q
IF (ZPI .LT. 0.0 ) THEN
  ZPI = 0.0
END IF
IF (ZPF .LE. 0.0) THEN
  ZPF = 0.0
END IF

```

```

C *****
C *WHEN TO THE RIGHT OF THE PATH TC > TB IS ONE OF THE CASES WE HAVE*
C *TO CHECK FOR AND THEN CARRY OUT THE INTEGRATION. *
C *****

```

```

IF (TC .GT. TB) THEN
  IF (TPRME(I) .GT. TA .AND. TPRME(I) .LT. TB) THEN
    WPI = Z - 0.0
    WPF = Z - ZPF
    W1 = WPI/S
    W2 = WPF/S
    YY = DATAN(W1)
    XX = DATAN(W2)
    B(I) = (ROE*N*(BETA**2.0))*(YY-XX)
  END IF
  IF (TPRME(I) .GT. TB .AND. TPRME(I) .LT. TC) THEN
    WPI = Z - ZPI
    WPF = Z - ZPF
    W1 = WPI/S
    W2 = WPF/S
    YY = DATAN(W1)
    XX = DATAN(W2)
    B(I) = ROE*N*(BETA**2.0)*(YY - XX)
  END IF
  IF (TPRME(I) .GT. TC .AND. TPRME(I) .LT. TD) THEN
    WPI = Z - ZPI
    WPF = Z - L
    W1 = WPI/S
    W2 = WPF/S
    YY = DATAN(W1)
    XX = DATAN(W2)
    B(I) = ROE*N*(BETA**2.0)*(YY - XX)
  END IF
END IF

```

```

C *****
C *ANOTHER CASE FOR THE PATH TO THE RIGHT IS TC LESS THAN TB. *
C *****

```

```

IF (TC .LT. TB) THEN
  IF (TPRME(I) .GT. TA .AND. TPRME(I) .LT. TC) THEN
    WPI = Z - 0.0
    WPF = Z - ZPF
    W1 = WPI/S
    W2 = WPF/S
    YY = DATAN(W1)
    XX = DATAN(W2)
    B(I) = ROE*N*(BETA**2.0)*(YY - XX)
  END IF
  IF (TPRME(I) .GT. TC .AND. TPRME(I) .LT. TB) THEN
    WPI = Z - 0.0
    WPF = Z - L
    W1 = WPI/S
    W2 = WPF/S
    YY = DATAN(W1)
    XX = DATAN(W2)
    B(I) = ROE*N*(BETA**2.0)*(YY - XX)
  END IF
  IF (TPRME(I) .GT. TB .AND. TPRME(I) .LT. TD) THEN
    WPI = Z - ZPI

```

```

          WPF = Z - L
          W1 = WPI/S
          W2 = WPF/S
          YY = DATAN(W1)
          XX = DATAN(W2)
          B(I) = ROE*N*(BETA**2.0)*(YY - XX)
        END IF
      END IF
C *****
C *FINALLY THE THIRD CASE FOR THE PATH TO THE RIGHT, TC = TB *
C *****
          IF (TB .EQ. TC) THEN
            IF (TPRME(I) .GT. TA .AND. TPRME(I) .LT. TB) THEN
              WPI = Z - 0.0
              WPF = Z - ZPF
              W1 = WPI/S
              W2 = WPF/S
              YY = DATAN(W1)
              XX = DATAN(W2)
              B(I) = ROE*N*(BETA**2.0)*(YY - XX)
            END IF
            IF (TPRME(I) .GT. TB .AND. TPRME(I) .LT. TD) THEN
              WPI = Z - ZPI
              WPF = Z - L
              W1 = WPI/S
              W2 = WPF/S
              YY = DATAN(W1)
              XX = DATAN(W2)
              B(I) = ROE*N*(BETA**2.0)*(YY - XX)
            END IF
          END IF
20      CONTINUE
          END IF
C *****
C *THE CERENKOV ANGLE IS COMPARED TO THETA2 TO SEE IF WE ARE TO THE *
C *LEFT OF THE PATH. THE 'WRITE' WILL INDICATE THIS ON THE SCREEN. *
C *****
          IF (THETA2 .LT. CE) THEN
112      WRITE(6,112)
          FORMAT('PATH TO THE LEFT')
          TINC = (TB - TC)/200.0
          DO 25 I = 1,200
            IF (I .EQ. 1.0) THEN
              TPRME(I) = TC
              B(I) = 0.0
            ELSE
              TPRME(I) = TC + (REAL(I)*TINC)
            END IF
            IF (TPRME(I) .GE. TB) THEN
              B(I) = 0.0
              GO TO 100
            END IF
            A1 = U1 + (V*TPRME(I))
            A2 = U2 - (V*TPRME(I))
            S1 = (BPRME**2.0)*Z - A1
            S2 = (BPRME**2.0)*Z - A2
            E1 = ((Z - A1)**2.0) - S1
            E2 = ((Z - A2)**2.0) - S1
            IF (E1 .LT. 0.0) THEN
              E1 = 0.0
            END IF
            IF (E2 .LT. 0.0) THEN
              E2 = 0.0
            END IF
            SRTE1 = SORT(E1)
            SRTE2 = SORT(E2)
            E = BPRME*SRTE1

```

```

EE = BPRME*SRTE2
ZPI = (D - E)/Q
ZPF = (DD - EE)/Q
IF (ZPI .LT. 0.0) THEN
  ZPI = 0.0
END IF
IF (ZPF .LT. 0.0) THEN
  ZPF = 0.0
END IF
C *****
C *CHECK FOR ONE OF THREE CASES THAT ONE CAN RUN INTO WHEN TO THE *
C *LEFT OF THE PATH. THIS PARTICULAR CASE IS TA < TD. *
C *****
IF (TA .LT. TD) THEN
  IF (TPRME(I) .GT. TC .AND. TPRME(I) .LT. TA) THEN
    WPI = Z - ZPI
    WPF = Z - L
    W1 = WPI/S
    W2 = WPF/S
    YY = DATAN(W1)
    XX = DATAN(W2)
    B(I) = ROE*N*(BETA**2.0)*(YY - XX)
  END IF
  IF (TPRME(I) .GT. TA .AND. TPRME(I) .LT. TD) THEN
    WPI = Z - 0.0
    WPF = Z - L
    W1 = WPI/S
    W2 = WPF/S
    YY = DATAN(W1)
    XX = DATAN(W2)
    B(I) = ROE*N*(BETA**2.0)*(YY - XX)
  END IF
  IF (TPRME(I) .GT. TD .AND. TPRME(I) .LT. TB) THEN
    WPI = Z - 0.0
    WPF = Z - ZPF
    W1 = WPI/S
    W2 = WPF/S
    YY = DATAN(W1)
    XX = DATAN(W2)
    B(I) = ROE*N*(BETA**2.0)*(YY - XX)
  END IF
END IF
C *****
C *THE SECOND CASE FOR THE PATH TO THE LEFT IS TA > TD. *
C *****
IF (TA .GT. TD) THEN
  IF (TPRME(I) .GT. TC .AND. TPRME(I) .LT. TD) THEN
    WPI = Z - ZPI
    WPF = Z - L
    W1 = WPI/S
    W2 = WPF/S
    YY = DATAN(W1)
    XX = DATAN(W2)
    B(I) = ROE*N*(BETA**2.0)*(YY - XX)
  END IF
  IF (TPRME(I) .GT. TD .AND. TPRME(I) .LT. TA) THEN
    WPI = Z - ZPI
    WPF = Z - ZPF
    W1 = WPI/S
    W2 = WPF/S
    YY = DATAN(W1)
    XX = DATAN(W2)
    B(I) = ROE*N*(BETA**2.0)*(YY - XX)
  END IF
  IF (TPRME(I) .GT. TA .AND. TPRME(I) .LT. TB) THEN
    WPI = Z - 0.0
    WPF = Z - ZPF
    W1 = WPI/S

```



```

                W2 = WPF/S
                YY = DATAN(W1)
                XX = DATAN(W2)
                B(I) = ROE*N*(BETA**2.0)*(YY - XX)
            END IF
        END IF
C *****
C *THE THIRD CASE FOR THE PATH TO THE LEFT IS TA = TD. *
C *****
        IF (TA .EQ. TD) THEN
            IF (TPRME(I) .GT. TC .AND. TPRME(I) .LT. TA) THEN
                WPI = Z - ZPI
                WPF = Z - L
                W1 = WPI/S
                W2 = WPF/S
                YY = DATAN(W1)
                XX = DATAN(W2)
                B(I) = ROE*N*(BETA**2.0)*(YY - XX)
            END IF
            IF (TPRME(I) .GT. TD .AND. TPRME(I) .LT. TB) THEN
                WPI = Z - 0.0
                WPF = Z - ZPF
                W1 = WPI/S
                W2 = WPF/S
                YY = DATAN(W1)
                XX = DATAN(W2)
                B(I) = ROE*N*(BETA**2.0)*(YY - XX)
            END IF
        END IF
25    CONTINUE
    END IF
C *****
C *IN THE EVENT THAT THE PREVIOUS TWO CONDITIONS DO NOT EXIST, THIS *
C *MEANS WE ARE CENTERED ON THE PATH. HOWEVER, THE FOLLOWING 'IF *
C *STATEMENT COMPARES CE WITH THETA1 AND THETA2 TOGETHER. THE WRITE *
C *STATEMENT INDICATES CENTER ON THE SCREEN. *
C *****
        IF (THETA1 .LT. CE .AND. THETA2 .GE. CE) THEN
            WRITE(6,113)
113    FORMAT('PATH ON CENTER')
            F = DTAN(CE)
            ZPC = Z - (S/F)
            RC = SQRT(S**2.0 + ((Z - ZPC)**2.0))
C *****
C *THE NEW VARIABLES T1 AND T2 ARE INTRODUCED. T1 IS WHERE THE *
C *MINIMUM OF THE U(Z') CURVE JUST TOUCHES THE TOP BOUNDARY OF THE *
C *U1 LINE. T2 CORRESPONDS TO THE U2 LINE. T1 IS WRITTEN ON THE *
C *SCREEN BY THE WRITE STATEMENT. *
C *****
            T1 = ((ZPC + (BPRME*RC) - U1)/V)
            T2 = ((ZPC + (BPRME*RC) - U2)/V)
            WRITE(6,333) T1/TAU
333    FORMAT(F10.4)
            DELR = R1 - R2
            IF (BPRME*DELR .GT. L) THEN
                T3 = TB
            END IF
            IF (BPRME*DELR .LE. L) THEN
                T3 = TD
            END IF
            TINC = (T3 - T1)/200.0
            DO 30 I = 1,200
                IF (I .EQ. 1.0) THEN
                    TPRME(I) = T1
                    B(I) = 0.0
                ELSE
                    TPRME(I) = T1 + (REAL(I)*TINC)
                END IF
            END DO

```

```

END IF
IF (TPRME(I) .GE. T3) THEN
  B(I) = 0.0
  GO TO 100
END IF
A1 = U1 + (V*TPRME(I))
A2 = U2 + (V*TPRME(I))
D = (BPRME**2.0)*Z - A1
DD = (BPRME**2.0)*Z - A2
E1 = ((Z - A1)**2.0) - S1
E2 = ((Z - A2)**2.0) - S1
IF (E1 .LT. 0.0) THEN
  E1 = 0.0
END IF
IF (E2 .LT. 0.0) THEN
  E2 = 0.0
END IF
SRTE1 = SORT(E1)
SRTE2 = SORT(E2)
E = BPRME*SRTE1
EE = BPRME*SRTE2
IF (TPRME(I) .GT. T1 .AND. TPRME(I) .LT. T2) THEN
  ZPM = (D - E)/Q
  ZPF = (D + E)/Q
  IF (ZPM .LE. 0.0) THEN
    ZPM = 0.0
    ZPI = ZPM
  END IF
  IF (ZPM .GT. 0.0) THEN
    ZPI = ZPM
  END IF
  IF (ZPF .GE. L) THEN
    ZPF = L
  END IF
  IF (ZPF .LT. L) THEN
    ZPF = (D + E)/Q
  END IF
  WPI = Z - ZPI
  WPF = Z - ZPF
  W1 = WPI/S
  W2 = WPF/S
  YY = DATAN(W1)
  XX = DATAN(W2)
  B(I) = ROE*N*(BETA**2.0)*(YY - XX)
END IF
IF (TPRME(I) .GT. T2 .AND. TPRME(I) .LT. T3) THEN
  ZPM = (D - E)/Q
  ZPM2 = (DD - EE)/Q
  IF (ZPM2 .LE. 0.0) THEN
    ZPF = 0.0
  END IF
  IF (ZPM2 .GT. 0.0) THEN
    ZPF = ZPM2
  END IF
  IF (ZPM .LE. 0.0) THEN
    ZPI = 0.0
  END IF
  IF (ZPM .GT. 0.0) THEN
    ZPI = ZPM
  END IF
  WPI = Z - ZPI
  WPF = Z - ZPF
  W1 = WPI/S
  W2 = WPF/S
  YY = DATAN(W1)
  XX = DATAN(W2)
  B1 = ROE*N*(BETA**2.0)*(YY - XX)
  ZPI = (DD + EE)/Q
  ZPF = (D + E)/Q

```

```

      IF (ZPI .GE. L) THEN
        ZPI = L
      END IF
      IF (ZPF .GE. L) THEN
        ZPF = L
      END IF
      IF (ZPF .LT. L) THEN
        ZPF = (D + E)/Q
      END IF
      WPI = Z - ZPI
      WPF = Z - ZPF
      W1 = WPI/S
      W2 = WPF/S
      YY = DATAN(W1)
      XX = DATAN(W2)
      B2 = ROE*N*(BETA**2.0)*(YY - XX)
      B(I) = B1 + B2
    END IF
30   CONTINUE
    END IF
C   *****
C   *ALL THROUGH THE PROGRAM THE VALUE 200 FOR THE DIMENSIONALIZED *
C   *VARIABLES TPRME AND B WAS USED BECAUSE IT BEST SUITED THE ROUTINE*
C   *USED BY THE GRAPHICS PROGRAM 'PLOT'. THIS GRAPHICS ROUTINE CAN BE*
C   *OBTAINED FROM PROFESSOR GLASS IN THE PHYSICS DEPARTMENT. *
C   *****
100 DO 50 I = 1,200
      TPRME(I) = TPRME(I)/TAU
      WRITE(26,500)TPRME(I),B(I)
500  FORMAT(F10.5,F10.5)
50   CONTINUE
      STOP
      END

```

APPENDIX B

S-Z PLANE PROGRAM

```

C *****
C *THIS PROGRAM TAKES THE DIFFERENT VARIABLES AVAILABLE SUCH AS BETA*
C *AND THE INDEX OF REFRACTION ETC. AND PRODUCES A S/L VS Z/L GRAPH *
C *(S-Z PLANE). AGAIN AS IN APPENDIX A, THE GRAPHICS ROUTINE USED *
C *CAN BE OBTAINED BY PROFESSOR GLASS OF THE PHYSICS DEPARTMENT. *
C *****
      DOUBLE PRECISION YL, YC, YR, X, Z, BETA, N, CO, RSETME, BPRME
      DOUBLE PRECISION DELU, L, OR, OL, OC, A, BR, BL, BC, C, ER, EL
      DOUBLE PRECISION EC, FR, FL, FC, HR, HL, HC, ZDIVL, MIN, INC
      INTEGER I
      DIMENSION X(200), YL(200), YC(200), YR(200)
C *****
C *THE VARIABLES FOR INPUT ARE DESCRIBED IN ORDER TO BETTER UNDER- *
C *STAND THIS PROGRAM. N IS THE INDEX OF REFRACTION. BETA IS EQUAL *
C *TO V/C AND IS DETERMINED FROM THE LORENTZ CONTRACTION FACTOR *
C *BASED ON THE ENERGY LEVEL OF THE BEAM. L IS THE APPROXIMATED BEAM*
C *LENGTH. ZDIVL IS THE MAXIMUM VALUE OF THE X AXIS AND MIN IS THE *
C *MINIMUM OF THE X AXIS. RSETME IS THE TIME IT TAKES FOR THE *
C *CURRENT TO REACH THE MAXIMUM LEVEL. *
C *****
      PRINT *, 'ENTER N'
      READ *, N
      PRINT *, 'ENTER BETA'
      READ *, BETA
      PRINT *, 'ENTER BEAMLENGTH'
      READ *, L
      PRINT *, 'ENTER MAX ZDIVL'
      READ *, ZDIVL
      PRINT *, 'ENTER MIN ZDIVL'
      READ *, MIN
      PRINT *, 'ENTER RISETIME IN NSEC'
      READ *, RSETME
      INC = (ZDIVL - MIN)/200.0
      DO 40 I = 1,200
        IF (I .EQ. 1.0) THEN
          X(I) = MIN
        ELSE
          X(I) = MIN + REAL(I)*INC
        END IF
        YR(I) = 0.0
        YL(I) = 0.0
        YC(I) = 0.0
40  CONTINUE
      BPRME = N*BETA
      DELU = RSETME*0.29979250*BETA
      ONEMIN = 1.0 - (DELU/L)
      ONEPLS = 1.0 + (DELU/L)
      OR = (1.0 - (DELU/L))/BPRME
      OL = (1.0 + (DELU/L))/BPRME
      OC = 1.0/BPRME
      DO 70 I = 1,200
        A = X(I)**2.0
        BR = OR**2.0
        BL = OL**2.0
        BC = OC**2.0
        C = (X(I) - 1.0)**2.0
        ER = (A - BR - C)**2.0
        EL = (A - BL - C)**2.0

```

```

EC = (A - BC - C)**2.0
FR = ER/(4.0*BR)
FL = EL/(4.0*BL)
FC = EC/(4.0*BC)
HR = FR - C
HL = FL - C
HC = FC - C
IF (HR .LT. 0.0) THEN
  HR = 0.0
END IF
IF (HL .LT. 0.0) THEN
  HL = 0.0
END IF
IF (HC .LT. 0.0) THEN
  HC = 0.0
END IF
IF (BPRME .GT. ONEMIN) THEN
  YR(I) = SQRT(HR)
ELSE
  YR(I) = 0.0
END IF
IF (BPRME .GT. ONEPLS) THEN
  YL(I) = SQRT(HL)
ELSE
  YL(I) = 0.0
END IF
IF (BPRME .GT. 1.0) THEN
  YC(I) = SQRT(HC)
ELSE
  YC(I) = 0.0
END IF
70 CONTINUE
C *****
C *THE DIMENSIONALIZED VARIABLES ARE USED AS FOLLOWS: X IS THE Z/L *
C *AXIS; YR IS OBTAINED FROM SETTING TB = TC; YL IS FROM TA = TD; *
C *YC IS FROM TA = TC OR TB = TD. *
C *****
      DO 80 I = 1,200
      WRITE(22,200) X(I), YR(I), YL(I), YC(I)
200   FORMAT(4F10.5)
80   CONTINUE
      STOP
      END

```

LIST OF REFERENCES

1. Buskirk, Fred R. and Neighbours, John R., *Time Development of Cerenkov Radiation*, Physical Review A, v. 31, Number 6, June 1985.
2. Lyman, Kathleen M., *Magnetic Fields from a Passing Charge Bunch*, Master's Thesis, Naval Postgraduate School, Monterey, California, September 1986.

INITIAL DISTRIBUTION LIST

	No. Copies
1. Defense Technical Information Center Cameron Station Alexandria, VA 22304-6145	2
2. Library, Code 0142 Naval Postgraduate School Monterey, CA 93943-5002	2
3. Professor J.R. Neighbours, Code 61 Nb Department of Physics Naval Postgraduate School Monterey, CA 93943-5000	4
4. Professor F.R. Buskirk, Code 61 Bs Department of Physics Naval Postgraduate School Monterey, CA 93943-5000	2
5. Professor K.E. Woehler, Code 61 Wo Department of Physics Naval Postgraduate School Monterey, CA 93943-5000	2
6. LT Byron K. Price, USN P.O. Box 1266 Owensboro, KY 42302	2

END

10-87

DTIC